

**A NUMERICAL STUDY OF HEAT TRANSFER AND
ENTROPY GENERATION IN POWELL-EYRING
NANOFLUID FLOWS**



A THESIS SUBMITTED TO THE UNIVERSITY OF KWAZULU-NATAL
FOR THE DEGREE OF DOCTOR OF PHILOSOPHY
IN THE COLLEGE OF AGRICULTURE, ENGINEERING & SCIENCE

By

Hammed Abiodun Ogunseye

School of Mathematics, Statistics & Computer Science

December 2020

Contents

Abstract	iii
Declaration	iv
Acknowledgments	vi
List of Publications	vii
1 Introduction	1
1.1 Nanofluids and hybrid nanofluids	1
1.2 The Powell-Eyring Nanofluid	3
1.3 Entropy generation	5
1.4 Lie group	7
1.5 Numerical methods of solution	7
1.5.1 Spectral quasilinearization method	8
1.5.2 Spectral local linearization method (SLLM)	13
1.6 Thesis objectives	15

1.7 Thesis Outline	16
2 On MHD mixed convective stagnation point flow of an Eyring-Powell nanofluid over a stretching cylinder with thermal slip conditions	18
3 Dynamical analysis of hydromagnetic Brownian and thermophoresis effects of squeezing Eyring–Powell nanofluid flow with variable thermal conductivity and chemical reactions	31
4 Lie group analysis of a Powell–Eyring nanofluid flow over a stretching surface with variable properties	53
5 A mathematical model for entropy generation in a Powell-Eyring nanofluid flow in a porous channel	66
6 Entropy generation in an unsteady Eyring-Powell hybrid nanofluid flow over a permeable surface: A Lie group analysis	79
7 Conclusion	97
References	100

Abstract

The heat transfer in non-Newtonian nanofluid flow through different geometries is an important research area due to the wide application of these fluids in biomedical, chemical and thermal engineering processes. The continuous generation of entropy leads to exergy loss which reduces the performance and efficiency of any physical system, therefore, the minimization of entropy generation becomes necessary. In this thesis, we present a numerical study of heat transfer and entropy generation in non-Newtonian nanofluid flows. We study the flow of a Powell-Eyring nanofluid, using models developed from experimental data. The equations that model the flow are, in each case, reduced to systems of nonlinear differential equations using Lie group theory scaling transformations. Accurate, efficient and rapidly converging spectral numerical techniques including the spectral quasilinearization, spectral local linearization and bivariate spectral quasilinearization methods are used to find the numerical solutions. The results show, among other findings, that increasing either the nanoparticle volume fraction or thermal radiation parameter enhances the nanofluid temperature, entropy generation and the Bejan number. In addition, we find that the Nusselt number increases with the temperature ratio parameter and thermal radiation. The results from this study may find use in the design of cooling devices to enhance and optimize the performance of thermal systems.

Declaration

The work presented in this dissertation is my original work under the supervision of Prof. P. Sibanda, School of Mathematics, Statistics, & Computer Science, University of KwaZulu-Natal, Pietermaritzburg campus, from April 2018 to December 2020.

No portion of this work has been submitted in any form to any university or institution of learning for any degree or qualification. Where use has been made of the work of others it is duly acknowledged.

Signature:..........

Hammed A. Ogunseye

December 11, 2020
.....

Date

Signature:..........

Prof. P. Sibanda

24-May-2021
.....

Date

This thesis is dedicated to the Almighty God, my father, and to my beloved wife.

Acknowledgments

I am most grateful to Almighty God for the gift of life, the endowment of knowledge and my journey so far. I acknowledge my supervisor Prof. P. Sibanda, for his good disposition, constructive criticisms, guidance, and advice, his encouragement and contribution to the overall success of this thesis.

I extend my profound gratitude to my caring parents, Alhaji and Mrs Ogunseye for their moral and financial support, words of encouragement throughout my program. My special thanks go to Dr Abdul Rasheed Adebayo, Mr Shina Oloniiju, Dr Ibukun S. Oyelakin, Dr Olumuyiwa Otegbeye and Dr Titi Agbaje for their wealth of ideas and suggestions during my research work. I appreciate you all.

Finally, I am indebted to my loving and wonderful wife, Maryam Abdulsalam for her love, support, sacrifice and understanding. You will always have a special place in my heart.

List of Publications

Ogunseye, H.A., Sibanda, P. and Mondal, H. MHD mixed convective stagnation-point flow of Eyring-Powell nanofluid over stretching cylinder with thermal slip conditions. *Journal of Central South University*, 26, 1172—1183, 2019.

I formulated the model, and provided the numerical solution of the flow equations using the spectral quasilinearization method.

Ogunseye, H.A., Salawu, S.O., Tijani, Y.O., Riliwan, M. and Sibanda, P. Dynamical analysis of hydromagnetic Brownian and thermophoresis effects of squeezing Eyring–Powell nanofluid flow with variable thermal conductivity and chemical reaction. *Multidiscipline Modeling in Materials and Structures*, 15(6), 1100–1120, 2019.

I modified an existing fluid model, solved the equations, interpreted the results and drafted the paper.

Ogunseye, H.A., Mondal, H., Sibanda, P. and Mamboundou H. Lie group analysis of a Powell–Eyring nanofluid flow over a stretching surface with variable properties. *SN Applied Sciences*, 2, 115, 2020.

I developed the model with discussion of the concept with my supervisor, carried out the numerical simulation and drafted the paper.

Ogunseye, H. A. and Sibanda, P. A mathematical model for entropy generation in a Powell-Eyring nanofluid flow in a porous channel. *Heliyon*, 5(5), 2019, e01662.

I conceptualized the work, formulated the model, solved the equations and drafted the paper.

Ogunseye, H.A, Tijani, Y.O, Sibanda, P. Entropy generation in an unsteady Eyring-Powell hybrid nanofluid flow over a permeable surface: A Lie group analysis. *Heat Transfer*. 1—17, 2020.

I formulated the fluid model, solved the conservation equations numerically using the bivariate spectral quasilinearization method and interpreted the results.

Signature:

Hammed. A. Ogunseye

Fe

.....

Date

Chapter 1

Introduction

The theoretical analysis of the flow of non-Newtonian fluids has, recently attracted increased attention from researchers. This is because most industrial and engineering fluids, such as polymer solutions, engine oils and greases, cannot be adequately modeled using Newton's law of viscosity. These non-Newtonian fluids find application in industrial and engineering processes such as in the food and polymer extrusion industries. Due to the multifarious nature of many non-Newtonian fluids, providing a single constitutive equation which adequately describes the flow of such fluids is still beyond the scope of present knowledge. Common constitutive models include, but are not limited to, those that describe the power-law fluid [1, 2], Casson fluid [3], viscoelastic fluid [4] and Powell-Eyring fluid [5]. The constitutive model of interest in this study is the Powell- Eyring fluid model, which has several advantages over other non-Newtonian fluid models. The Powell-Eyring model is derived from the molecular theory of fluids and not from empirical relations. The Powell-Eyring fluid has the same properties as a Newtonian fluid under low and high shear rates [6].

1.1 Nanofluids and hybrid nanofluids

The suspension of nanometre-sized particles in base fluids such as water and ethylene glycol has scientific support to enhance heat transfer, provided that the mixture is carefully made up in the correct proportions. A colloidal suspension of metals or their oxides (iron oxide, alumina, copper oxide, or zinc oxide), with particles having a diameter less than $100nm$ is called a nanofluid.

Nanofluids have many ubiquitous applications. To start with, in solar technology, nanofluids are used as a collector to enhance efficiency of a solar thermal system. In biomedical sciences, nanofluids find applications in cancer therapeutics and cryosurgery [7]. In engineering processes, they are used to enhance engineering operations, petrochemical applications and polymer processing [8]. Robert *et al.* [9], Devendiran and Amirtham [10], Wong and De Leon [11] and Munyalo and Zhang [12] all give a comprehensive survey of other applications of nanofluids. Buongiorno [13] proposed a mass, momentum, and heat transport model for a nanofluid. This model is a two-component four-equation nonhomogeneous equilibrium model. In that study, seven mechanisms for slip between a base fluid and nanoparticles were suggested, which included inertia, Brownian diffusion, thermophoresis, diffusiophoresis, the Magnetic effect, fluid drainage, and gravity, of which, thermophoresis and Brownian particle motion were observed to be the most important. In another study, Tiwari and Das [14] presented a different mathematical nanofluids model to further understand the thermal mechanism of nanofluids with interest on the effective fluid properties. They used the model is commonly referred to as the Tiwari-Das nanofluid model.

Khan and Pop [15] used the implicit finite difference method to studied the thermal behaviour of a nanofluid past a stretching surface with consideration of the effects of thermophoresis and Brownian motion. They found that the Nusselt number decreases with the thermophoresis parameter as well as the Brownian motion parameter. Bachok and his co-researchers [16] investigated the flow of a nanofluid over a shrinking or stretching plate in respect to stagnation-point using the Tiwari-Das nanofluid model. The Newton-Raphson shooting technique was used as the method of solution for the flow equations. They observed that nanoparticles inclusion enhanced the heat transfer and skin friction coefficients. The stagnation point flow of mixed convection transfer of heat and mass, radiative nanofluids over a stretchable surface was carried out by Pal and Mandal [17] using nanofluids of different kinds which include Al_2O_3 -water, TiO_2 -water and Cu-water. Their finding showed that Al_2O_3 -water has a higher heat transfer rate when compared to Cu-water nanofluid. Makinde and Aziz [18] probed the effect of convective heating in an impermeable stretching surface for a boundary layer nanofluid flow. The thermal boundary layer was reported to be strengthened with a rise in convective heating.

The majority of earlier studies cited above, assumed constant thermo-physical properties for the nanofluid. However, recent studies have shown that these properties can vary either as a function of temperature or nanoparticle size. Noghrehabadi and Behseresht [19] studied nanofluid flow over a vertical cone with variable properties. They accounted for the case where the nanofluid thermal conductivity and dynamic viscosity varied with the magnitude of the nanoparticles. They concluded that the variable thermophysical properties reduced the Nusselt number. In the work of Das *et al.* [20] they varied the nanofluid dynamic viscosity and thermal conductivity linearly with temperature, this study was conducted over a wedge. Recently, scientific study and investigation of nanofluid flow are now central on varying viscosity, thermal conductivity and some thermo-physical properties in respect to particle size and temperature. Of great interest, are the work of Masoud *et al.* [21], Hassani *et al.* [22], and Vajjha and Das [23]. These studies are worth mentioning.

In recent years, researchers have made further advances in new techniques for enhancing heat transfer rates in nanofluids. These efforts pave the way for what we now called hybrid nanofluid. The hybrid nanofluids are new kind of nanofluid, they are constituents of two (composite) nanoparticles in a base fluid. The hybrid nanofluids have been reported to have better thermal characteristics than the conventional nanofluids. These fluid gives superior performance in industrial, engineering and biomedical processes. Earlier research work on hybrid nanofluids include but not limited to the studies by Xuan and Lii [24], Botha *et al.* [25], Abbasi *et al.* [26] and Han *et al.* [27]. An exhaustive review of the work so far on hybrid nanofluids with recent trends was given by Sarkar *et al.* [28].

1.2 The Powell-Eyring Nanofluid

In 1944, Powell and Eyring [5] developed a fluid model to investigate the viscoelasticity of a non-Newtonian fluid. This model is now generally known as the Powell-Eyring (or Eyring-Powell) fluid model. The novelty of their model can be attributed to it being derived from the kinetic theory of the fluid and not simply empirical relations, as in the cases of other non-Newtonian fluid models.

The Eyring-Powell fluid model has also been shown to be very useful in the calculation of the fluid time scale for polymer concentrations (see Yoon and Ghajar [29]). One notable attribute of the Powell-Eyring fluid model include a zero shear rate and infinite shear rate viscosities. For an incompressible homogeneous Powell-Eyring fluid, the constitutive equation admit the mathematical expression (see Javed *et al.* [30])

$$\boldsymbol{\tau} = -p\mathbf{I} + \mu\mathbf{H}_1 + \left[\frac{1}{\beta|\mathbf{H}_1|} \sinh^{-1} \left(\frac{1}{\gamma} |\mathbf{H}_1| \right) \right] \mathbf{H}_1, \quad (1.1)$$

where p , \mathbf{I} , μ stands for the fluid pressure, identity tensor and dynamic viscosity respectively, β and γ are characteristics of the Eyring-Powell fluid, \mathbf{H}_1 represents the Rivlin-Ericksen tensor, defined as

$$\mathbf{H}_1 = (\nabla V) + (\nabla V)^{tr}, \quad (1.2)$$

and

$$|\mathbf{H}_1| = \sqrt{\frac{1}{2} \text{trace} (\mathbf{H}_1^2)}, \quad (1.3)$$

where the superscript tr indicates the transpose.

Javed and his collaborators [30] used the Keller box method to solve the emerging flow equations for the Powell-Eyring fluid flow over a stretchable plate. Their result shed light on enhancement of velocity profiles for a non-Newtonian fluid in comparison to the Newtonian fluid. Using the homotopy analysis method, Hayat *et al.* [31] obtained a semi-analytical solution for a Powell-Eyring fluid flow over an accelerating surface with a convective boundary condition. The findings that the resistance to flow increases with large magnetic field intensity were as a result of the work of Akbar *et al.* [32]. They investigated the flow of an electrical conducting Eyring-Powell fluid using the finite difference method.

The Eyring-Powell fluid model for non-Newtonian fluids can be modified to incorporate nanoparticles. An Eyring-Powell nanofluid is, thus, an Eyring-Powell fluid that contains a colloidal suspension of nanoparticles having a diameter less than $100nm$. The Eyring-Powell nanofluid has enhanced thermophysical properties such as thermal conductivity and the rate of heat transfer. There are several studies of the flow and properties of a Eyring-Powell nanofluid. These studies include

the analysis by Malik *et al.* [33] of a Eyring-Powell MHD convective nanofluid past an elongated sheet, which shows that the fluid flow increases with an increase in the Eyring-Powell and convective parameters. The study of Khan *et al.* [34] over a cone and a flat plate was performed for a mixed convection flow of a reactive Eyring-Powell nanofluid. Tanveer and his colleagues [35] investigated flow of a Powell-Eyring nanofluid in a bend channel. Agbaje *et al.*[36] examine the transient developing flow of an Eyring-Powell nanofluid over a shrinking plate. Hina [37] probed the importance of slip condition on the flow of an Eyring-Powell nanofluids. Hayat *et al.* [38] studied a radiative Eyring-Powell nanofluid with emphasis on heat transport and movement of fluid due to a stretching cylinder. However, to the best of our knowledge, there are limited attention of researchers to the flow of heat and mass transfer in Eyring-Powell hybrid nanofluids.

1.3 Entropy generation

Although enhancing the rate of heat transfer in a thermal system can be achieved by using a nanofluid, a major challenge in physical applications is the energy loss due to irreversibilities in the thermal processes. Recently, there have been a sizeable number of researchers working on the analysis of entropy generation in a nanofluid flow. Entropy generation is a measure of dissipated useful energy and degradation of the performance of engineering systems, such as transport and rate processes; and the dissipation depends on the extent of irreversibilities present during a process. Entropy generation is important as it continuous generation will reduce the efficiency of the system due to energy loss. A practical application is in thermal engineering processes. Optimum performance in engineering and industrial processes is possible by minimizing entropy generation [39]. The second law of thermodynamics proposed by Bejan [39] is the quantitative tool used to measure the degree of irreversibility through entropy generation. In this work, we analyze the irreversibility in the flow and heat transfer for an Eyring-Powell nanofluid flow using the statement of Bejan [39]. The irreversibility law of all real-life processes is the second law of thermodynamics. The rate of entropy generation per unit time and per unit volume is denoted by S'''_{gen} , given by Bejan

[40] as

$$S_{gen}''' = \frac{\kappa}{T^2} (\Delta T)^2 + \frac{\mu}{T} \Phi \geq 0, \quad (1.4)$$

where κ stands for the thermal conductivity, μ represent dynamic viscosity and Φ is the viscous dissipation function. The terms in equation (1.4) are non-negative.

Based on the approach proposed by Bejan [39], in recent years, many research work have emanated on minimizing irreversibilities effect which lead to efficient fluid flow process. Amongst these works include, the investigation of a third grade fluid flow by analysing its entropy generation by Pakdemirli and Yilbas [41]. Das *et al.* [42] probed the entropy generation of a pseudo-plastic nanofluid through a porous channel. From their findings, the entropy generation rate was reported to be directly proportional (increasing) to the Brinkman number. In a similar study to Das *et al.* [42], Jangili and his collaborators [43] used the homotopy analysis method to analyzed the entropy generation in a couple stress fluid flow. The study by Jangili *et al.* [43] confirms the findings of Das *et al.* [42]. The study of Tiew *et al.* [44] is central on entropy generation in a nanofluid flow through a channel with great interest on the viscous dissipation effect. Viscous dissipation is the main contributor to entropy generation in a system. Their analysis indicates that entropy generation rate can be minimized by reducing the viscous dissipation in the system. With entropy generation, Ibanez [45] obtained a closed form solution for a magnetohydrodynamic fluid flow. In a porous channel, López *et al.* [46] discussed the entropy production rate for a magnetohydrodynamic nanofluid flow. The study investigated the importance of nonlinear thermal radiation as well as convective-radiative boundary conditions. They proved linear relationship between aggregate entropy generation and thermal radiation parameter. Makinde and Eegunjobi [47] probed the effect of convective heating on the entropy production rate of a transient flow between two porous walls. Using the homotopy perturbation method on the governing flow equations, Nagaraju *et al.* [48] analysed suction and magnetic field effects on entropy production rate in a fluid flow through a cylindrical surface. Ishaq *et al.* [49] studied the entropy generation in an Eyring-Powell nanofluid as a film flow over a time dependent continuous permeable surface. Investigation on past literature show that work on entropy generation in hybrid nanofluid flow is still at an infancy stage. One of the few study in this subject area is the work of Das *et al.* [50], they study entropy generation in

a porous channel for Cu-Al₂O₃–water hybrid nanofluid flow. Afridi and his co-researchers [51] work on a curved surface by investigating the entropy production rate in a Cu-Al₂O₃–water hybrid nanofluid flow. Their results shed more light on the importance of the hybrid nanofluid over the regular nanofluid in minimizing entropy generation.

1.4 Lie group

A group is a set of elements together with an operation that combines two or more of its elements to form another element; the operation must satisfy the four axioms, of closure, associativity, identity and inverse. Groups share a basic affinity with the concept of symmetry. A symmetry group consists of set of a transformations that keep the object unchanged. A Lie group is a symmetry group that is differentiable manifold, with the characteristic that the group operations are well-defined with a smooth structure [52, 53]. Lie group theory is used to facilitate the solution of differential equations, for which there are two approaches; specifically, infinitesimal transformation and scaling transformation methods. In this study, these two methods are used in Chapters 4 and 6, respectively.

1.5 Numerical methods of solution

Partial differential equations are utilized in modeling flow and heat transfer problems. In practice, these equations are often reduced to a system of highly nonlinear ordinary differential equations or partial differential equations with a reduced number of independent variables using the Lie group symmetry method or by adopting existing similarity variables. Either way, the exact or closed form solution to these nonlinear equations does not exist, hence an approximate numerical solution would be sought. From the literature, the numerical methods available includes the finite elements methods [54], the Keller-box method [55], the Runge-Kutta shooting method [56] and the finite difference method [57, 58]. These methods may, however, require large computation times, give discontinuous solutions, or present difficulties when used to solve problems that contain singularities or multiple solutions. Over the last few decades, new numerical methods

that are robust and efficient have been developed for solving equations arising in boundary layer problems. These methods include the proposal by Motsa *et al.* [59] to combine the finite difference method with Chebyshev spectral methods. They used the method in solving equations for unsteady boundary layer flows and found that the spectral methods have potential as numerical tools for solving nonlinear differential equations arising from engineering problems. Compared to the Runge-Kutta shooting, Keller-box, finite element and finite differences methods, the spectral methods give higher accuracy and converge more rapidly. To demonstrate the effectiveness of the spectral based method, Motsa *et al.* [60] also used the bivariate spectral quasilinearization method to solve parabolic equations using Lagrange interpolation polynomials as the basis functions. Again, they showed that the performance of the bivariate spectral quasilinearization method was superior to that of the finite difference method in terms of convergence and accuracy. Using the spectral relaxation method, Oyelakin *et al.* [61] investigated the unsteady boundary layer flow of non-Newtonian fluid. The similarity equations were linearized and solved using the Chebyshev pseudo-spectral method. The spectral relaxation method was shown to be effective for boundary layer problems. In this study, the spectral quasilinearization method, bivariate spectral quasilinearization method and spectral local linearization method are used for the solution of fluid flow models.

1.5.1 Spectral quasilinearization method

In 1965 Bellman and Kalaba [62] generalized the Newton-Rhapson technique to find solutions of nonlinear ordinary and partial differential equation that arise when modelling in physical processes. This generalization was termed the quasilinearization method (QLM). The QLM converges quadratically to the exact solution. To illustrate the method, we consider a nonlinear n^{th} -order differential equation

$$L^n[y(x)] = f\left(x, y(x), y'(x), \dots, y^{(n-1)}(x)\right), \quad (1.5)$$

where L^n denotes a linear differential operator of n order. Applying the quasilinearization method to equation (1.5) yields

$$L^n[y_{r+1}(x)] = f\left(x, y_r(x), y_r'(x), \dots, y_r^{(n-1)}(x)\right) + \sum_{m=0}^{r-1} \left(y_{r+1}^{(m)}(x) - y_r^{(m)}(x)\right) f_{y^m} f\left(x, y_r(x), y_r'(x), \dots, y_r^{(n-1)}(x)\right), \quad (1.6)$$

with the initial and boundary conditions stated at the $(r+1)$ th iteration. As the linearized form of the equation (1.5), equation (1.6) can be solved recursively, using any iterative numerical method, so that where $y_r(x)$ is known, one can easily obtain $y_{r+1}(x)$ for $r = 0, 1, 2, \dots$

In 2014 Motsa *et al.* [59] introduced the spectral quasilinearization method (SQLM). This numerical method is a combination of the Chebyshev spectral collocation method and the Newton-Raphson linearization algorithm that had been proposed by Bellman and Kalaba [62]. The SQLM has been used by researchers to solve several flow-related problems. It has been shown that the method is efficient and robust. Dhlamini *et al.* [63] used the spectral quasilinearization method to study the fluid flow of a radiative fluid. RamReddy and Pradeepa [64] also utilized the spectral quasilinearization method in their study of the flow and heat transfer in a micropolar fluid. More references for the application of the spectral quasilinearization method to engineering problems can be found in [59, 65–67]. A general description of the spectral quasilinearization method as published by Motsa and Sibanda [68] is given below.

In general sense, we consider a system of n nonlinear ordinary differential equations of the form,

$$\Gamma_k[H_1, H_2, \dots, H_n] = 0, \quad k = 1, 2, \dots, n \quad (1.7)$$

where

$$H_i = \left\{ f_i, \frac{\partial f_i}{\partial \eta}, \frac{\partial^2 f_i}{\partial \eta^2}, \dots, \frac{\partial^p f_i}{\partial \eta^p} \right\}, \quad \text{with } i = 1, 2, \dots, n \quad (1.8)$$

The order of differentiation is denoted by p , the solution by $f_k(\eta)$ for $k = 1, 2, \dots, n$ and Γ_k for $k = 1, 2, \dots, n$ are nonlinear operators containing all the special derivatives of $f_k(\eta)$.

We assume that the solution can be approximated by a univariate Lagrange interpolation polynomial of the form

$$f_k(\boldsymbol{\eta}) \approx \sum_{i=0}^{N_n} f_k(\boldsymbol{\eta}_i) L_i(\boldsymbol{\eta}), \quad (1.9)$$

for $k = 1, 2, \dots, n$. The univariate Lagrange interpolation polynomial interpolates $f_k(\boldsymbol{\eta})$ at selected points $(\boldsymbol{\eta}_i)$ in the $(\boldsymbol{\eta})$ directions, for $k = 1, 2, \dots, N_n$. The Chebyshev-Gauss-Lobatto points [69, 70] for the selected grid points are defined by

$$\{\boldsymbol{\eta}_i\} = \left\{ \cos\left(\frac{\pi i}{N_n}\right) \right\}_{i=0}^{N_n}. \quad (1.10)$$

The characteristic Lagrange cardinal polynomial based on the Chebyshev-Gauss-Lobatto grid points (see [69, 70]) is the function $L_i(\boldsymbol{\eta})$ define as

$$L_i(\boldsymbol{\eta}) = \prod_{i=0, i \neq k}^{N_n} \frac{\boldsymbol{\eta} - \boldsymbol{\eta}_k}{\boldsymbol{\eta}_i - \boldsymbol{\eta}_k}, \quad (1.11)$$

where

$$L_i(\boldsymbol{\eta}) = \begin{cases} 1, & \text{if } i = k \\ 0, & \text{if } i \neq k \end{cases} \quad (1.12)$$

The nonlinear operators Γ_k , for $k = 1, 2, 3, \dots, n$ are first linearized using the quasilinearization technique [62]. The quasilinearization method uses the Taylor's approximation of Γ_k about some previous iteration. We assume infinitesimal difference between past and currents solution and all their derivatives. Applying the quasilinearization method, we obtain

$$\begin{aligned} \Gamma_k[H_1, H_2, \dots, H_n] &\approx (H_{1,r+1} - H_{1,r}, H_{2,r+1} - H_{2,r}, \dots, H_{N,r+1} - H_{N,r}) \cdot \nabla \Gamma_k[H_{1,r}, H_{2,r}, \dots, H_{n,r}] \\ &\quad + [H_{1,r}, H_{2,r}, \dots, H_{n,r}], \end{aligned} \quad (1.13)$$

r and $r + 1$ denote past and current iterations respectively and ∇ is a vector of the partial derivatives given as

$$\nabla = \{\nabla_{f_1}, \nabla_{f_2}, \dots, \nabla_{f_n}\}. \quad (1.14)$$

We express

$$\nabla_{f_n} = \left\{ \frac{\partial}{\partial f_n'}, \frac{\partial}{\partial f_n''}, \frac{\partial}{\partial f_n'''}, \dots, \frac{\partial}{\partial f_n^{(p)}} \right\}, \quad n = 1, 2, \dots \quad (1.15)$$

where the prime denotes differentiation with respect to η . The linearised equation (1.13) can be expressed in a compact form as

$$\begin{aligned} \sum_{s=1}^n H_{s,r+1} \cdot \nabla_{f_s} \Gamma_k[H_{1,r}, H_{2,r}, \dots, H_{n,r}] &= \sum_{s=1}^n H_{s,r} \cdot \nabla_{f_s} \Gamma_k[H_{1,r}, H_{2,r}, \dots, H_{n,r}] \\ &- \Gamma_k[H_{1,r}, H_{2,r}, \dots, H_{n,r}], \end{aligned} \quad (1.16)$$

for $k = 1, 2, \dots, n$. Equation (1.16) forms a system of n coupled linear differentiation equations. They are solved iteratively for $f_1(\eta), f_2(\eta), \dots, f_n(\eta)$. Equation (1.16) can further be expressed as follows:

$$\sum_{s=0}^p \alpha_{1,s,r}^{(1)}(\eta) f_{1,r+1}^{(s)} + \sum_{s=0}^p \alpha_{2,s,r}^{(1)}(\eta) f_{2,r+1}^{(s)} + \dots + \sum_{s=0}^p \alpha_{n,s,r}^{(1)}(\eta) f_{n,r+1}^{(s)} = R_1(\eta), \quad (1.17)$$

$$\sum_{s=0}^p \alpha_{1,s,r}^{(2)}(\eta) f_{1,r+1}^{(s)} + \sum_{s=0}^p \alpha_{2,s,r}^{(2)}(\eta) f_{2,r+1}^{(s)} + \dots + \sum_{s=0}^p \alpha_{n,s,r}^{(2)}(\eta) f_{n,r+1}^{(s)} = R_2(\eta), \quad (1.18)$$

$$\sum_{s=0}^p \alpha_{1,s,r}^{(3)}(\eta) f_{1,r+1}^{(s)} + \sum_{s=0}^p \alpha_{2,s,r}^{(3)}(\eta) f_{2,r+1}^{(s)} + \dots + \sum_{s=0}^p \alpha_{n,s,r}^{(3)}(\eta) f_{n,r+1}^{(s)} = R_3(\eta), \quad (1.19)$$

\vdots

$$\sum_{s=0}^p \alpha_{1,s,r}^{(n)}(\eta) f_{1,r+1}^{(s)} + \sum_{s=0}^p \alpha_{2,s,r}^{(n)}(\eta) f_{2,r+1}^{(s)} + \dots + \sum_{s=0}^p \alpha_{n,s,r}^{(n)}(\eta) f_{n,r+1}^{(s)} = R_n(\eta), \quad (1.20)$$

where $\alpha_{n,p,r}^{(k)}(\eta)$, is the variable of $f_{n,r+1}^{(p)}$. The variable coefficient corresponds to the k^{th} equation, for $k = 1, 2, \dots, n$. p is the order of differentiation. We obtain

$$\alpha_{n,p,r}^{(k)}(\eta) = \frac{\partial \Gamma_k}{\partial f_{n,r}^{(p)}},$$

The right-hand side of the k^{th} equation is given by

$$R_k(\eta) = \sum_{s=0}^p \alpha_{1,s,r}^{(k)}(\eta) f_{1,r}^{(s)} + \sum_{s=0}^p \alpha_{2,s,r}^{(k)}(\eta) f_{2,r}^{(s)} + \dots + \sum_{s=0}^p \alpha_{n,s,r}^{(k)}(\eta) f_{n,r}^{(s)} - \Gamma_k[H_{1,r}, H_{2,r}, \dots, H_{n,r}].$$

Equations (1.17) – (1.20) are evaluated at the Chebychev-Gauss-Lobatto grid points

$\eta_1(i = 0, 1, \dots, N_n)$. The values of the derivatives at the Chebychev-Gauss-Lobatto points (η_i) (for

$i = 0, 1, \dots, N_n$) are computed as

$$\left. \frac{df_n}{d\eta} \right|_{(\eta_i)} = \sum_{\omega=0}^{N_n} f_n(\eta_\omega) \frac{dL_{\omega}(\eta)}{d\eta} \quad (1.21)$$

$$= \sum_{\omega=0}^{N_n} f_n(\eta_\omega) D_{i,\omega} = \sum_{\omega=0}^{N_n} D_{i,\omega} f_n(\eta_\omega), \quad (1.22)$$

where $D_{i\omega} = \frac{dL_{\omega}(\eta_i)}{d\eta}$ is the i th and ω th entry of the standard first derivative Chebyshev differentiation matrix of size $(N_n + 1) \times (N_n + 1)$ as defined in [[62],[69],[70]]. Higher, p th order derivatives are defined as

$$\left. \frac{d^p f_n}{d\eta^p} \right|_{(\eta_i)} = \sum_{\omega=0}^{N_n} D_{i,\omega}^p f_n(\eta_\omega) = D^p F_n, i = 1, 2, \dots, N_n \quad (1.23)$$

where the vector \mathbf{F}_n defined as

$$\mathbf{F}_n = [f_n(\eta_0), f_n(\eta_1), \dots, f_n(\eta_{N_n})]^T, \quad (1.24)$$

and the subscript T denotes matrix transpose. Substituting equations (1.23) and (1.23) into equations (1.17)– (1.20) yields

$$\sum_{k=1}^n A_{1,k} \mathbf{F}_k = \mathbf{R}_1, \quad (1.25)$$

$$\sum_{k=1}^n A_{2,k} \mathbf{F}_k = \mathbf{R}_2, \quad (1.26)$$

⋮

$$\sum_{k=1}^n A_{n,k} \mathbf{F}_k = \mathbf{R}_n, \quad (1.27)$$

where

$$A_{1,1} = \sum_{s=0}^p \alpha_{1,s,r}^{(1)} \mathbf{D}^{(s)}, \quad A_{1,2} = \sum_{s=0}^p \alpha_{2,s,r}^{(1)} \mathbf{D}^{(s)}, \quad \dots \quad A_{1,n} = \sum_{s=0}^p \alpha_{n,s,r}^{(1)} \mathbf{D}^{(s)}, \quad (1.28)$$

$$A_{2,1} = \sum_{s=0}^p \alpha_{2,s,r}^{(2)} \mathbf{D}^{(s)}, \quad A_{2,2} = \sum_{s=0}^p \alpha_{2,s,r}^{(2)} \mathbf{D}^{(s)}, \quad \dots \quad A_{2,n} = \sum_{s=0}^p \alpha_{n,s,r}^{(2)} \mathbf{D}^{(s)}, \quad (1.29)$$

⋮

$$A_{n,1} = \sum_{s=0}^p \alpha_{1,s,r}^{(n)} \mathbf{D}^{(s)}, \quad A_{n,2} = \sum_{s=0}^p \alpha_{2,s,r}^{(n)} \mathbf{D}^{(s)}, \quad \dots \quad A_{n,n} = \sum_{s=0}^p \alpha_{n,s,r}^{(n)} \mathbf{D}^{(s)}, \quad (1.30)$$

and

$$\alpha_{n,s,r}^{(n)} = \begin{vmatrix} \alpha_{n,s,r}^{(n)}(\eta_0) & & & & \\ & \alpha_{n,s,r}^{(n)}(\eta_0) & & & \\ & & \ddots & & \\ & & & & \alpha_{n,s,r}^{(n)}(\eta_0) \end{vmatrix} \quad (1.31)$$

1.5.2 Spectral local linearization method (SLLM)

Spectral local linearization method is an iterative method that decouples a nonlinear system of differential equations, using the single term Taylor series expansion, to give a linear system of differential equations. The method is fully described in Motsa [71], where it is used to solve a selection of fluid flow problems. Recently, the spectral local linearization method was used in the study of entropy generation in a second grade fluid flow with nonlinear thermal radiation by Sithole *et al.* [72]. Without loss of generality, we consider the same system of n nonlinear ordinary differential equations considered in equation (1.7) and (1.8)

The method uses an assumption that the solution is possible via a Lagrange interpolation polynomial, given as

$$f_k(\eta) \approx \sum_{i=0}^{N_n} f_k(\eta_i) L_i(\eta), \quad (1.32)$$

for $k = 1, 2, \dots, n$. The grid points are given by (η) direction, for $i = 0, 1, 2, \dots, N_n$. These selected grid points are called Chebyshev-Gauss-Lobatto points ([69]) and are given by

$$\{\eta_i\} = \left\{ \cos\left(\frac{\pi i}{N_n}\right) \right\}_{i=0}^{N_n} \quad (1.33)$$

and

$$L_i(\eta) = \prod_{i=0, i \neq k}^{N_n} \frac{\eta - \eta_k}{\eta_i - \eta_k}, \quad (1.34)$$

where

$$L_i(\eta_k) = \delta_{ik} = \begin{cases} 0 & \text{if } i \neq k, \\ 1 & \text{if } i = k. \end{cases} \quad (1.35)$$

Applying the quasilinearization method independently in each equation, we get a system of n decoupled linear differential equations of the form:

$$\sum_{s=0}^p \alpha_{s,r}^{(1)}(\eta) f_{1,r+1}^{(s)} = R_1(\eta), \quad (1.36)$$

$$\sum_{s=0}^p \alpha_{s,r}^{(2)}(\eta) f_{2,r+1}^{(s)} = R_2(\eta), \quad (1.37)$$

\vdots

$$\sum_{s=0}^p \alpha_{s,r}^{(n)}(\eta) f_{n,r+1}^{(s)} = R_n(\eta), \quad (1.38)$$

where $\alpha_{s,r}^k(\eta)$, are the variable coefficients of $f_{k,r+1}^{(s)}(\eta)$, respectively, for $k = 1, 2, \dots, n$ and $s = 0, 1, 2, \dots, p$. These coefficients correspond to the k^{th} equation, for $k = 1, 2, \dots, n$. Since the constant p denotes the order of differentiation, then

$$\alpha_{s,r}^{(k)}(\eta) = \frac{d\Gamma_k}{df_{k,r}^{(s)}} \quad (1.39)$$

In general, the k th righthand side is given by

$$R_k(\eta) = \sum_{s=0}^p \alpha_{s,r}^{(k)}(\eta) f_{k,r}^{(s)}(\eta) - \Gamma_k(\eta). \quad (1.40)$$

The equations (1.32) are evaluated at the Chebychev-Gauss-Lobatto grid points $\eta_i (i = 0, 1, \dots, N_n)$.

Substituting equations (1.32) into equations (1.40) yields

$$A_{1,1} \mathbf{F}_1 = \mathbf{R}_1, \quad (1.41)$$

$$A_{2,2} \mathbf{F}_2 = \mathbf{R}_2, \quad (1.42)$$

\vdots

$$A_{n,n} \mathbf{F}_n = \mathbf{R}_n, \quad (1.43)$$

where

$$A_{1,1} = \sum_{s=0}^p \alpha_{s,r}^{(1)} \mathbf{D}^{(s)}, \quad A_{2,2} = \sum_{s=0}^p \alpha_{s,r}^{(2)} \mathbf{D}^{(s)}, \quad \dots, \quad A_{n,n} = \sum_{s=0}^p \alpha_{s,r}^{(n)} \mathbf{D}^{(s)}. \quad (1.44)$$

The diagonal matrices of the corresponding variable coefficients are given by

$$\alpha_{s,r}^{(k)} = \begin{vmatrix} \alpha_{s,r}^{(k)}(\eta_0) & & & \\ & \alpha_{s,r}^{(k)}(\eta_1) & & \\ & & \ddots & \\ & & & \alpha_{s,r}^{(k)}(\eta_{N_n}) \end{vmatrix}, \quad (1.45)$$

the boundary conditions for equations (1.44) can be expressed as the following $(N_n + 1) \times (N_n + 1)$ matrix system

$$\begin{bmatrix} G_{0,0}^{(k)} & G_{0,1}^{(k)} & \cdots & G_{0,N_\eta}^{(k)} \\ G_{1,0}^{(k)} & G_{1,1}^{(k)} & \cdots & G_{1,N_\eta}^{(k)} \\ \vdots & \vdots & \ddots & \vdots \\ G_{N_\eta,0}^{(k)} & G_{N_\eta,1}^{(k)} & \cdots & G_{N_\eta,N_\eta}^{(k)} \end{bmatrix} \begin{bmatrix} \mathbf{F}_k \\ \mathbf{F}_k \\ \vdots \\ \mathbf{F}_k \end{bmatrix} = \begin{bmatrix} R_k \\ R_k \\ \vdots \\ R_k \end{bmatrix}, \quad (1.46)$$

where

$$G_{(i,j)}^{(k)} = \sum_{s=0}^p \alpha_{s,r}^{(k)} \mathbf{D}^{(s)}, \quad \text{for } k = 1, 2, \dots, n. \quad (1.47)$$

The vector R_k is defined as

$$R_{k,i} = \mathbf{R}_k,$$

for $k = 1, 2, \dots, n$.

1.6 Thesis objectives

This study may be divided into two parts. Part I is concerned with the numerical solution of Powell-Eyring nanofluid flows in various geometries, and Part II is an investigation of the entropy generation in the flow of a Powell-Eyring nanofluid. To attain these aims, in Part I, we study the flow of a Powell-Eyring nanofluid along vertical cylindrical and flat surfaces. We use Lie group symmetry to convert the coupled partial differential equations that model the flow problems into a set of coupled ordinary differential equations, which are then solved using the spectral quasilinearization and spectral local linearization methods. In Part II, we investigate entropy generation in the flow of a steady and unsteady Powell-Eyring nanofluid and hybrid nanofluid using the bivariate spectral quasilinearization and spectral quasilinearization methods.

1.7 Thesis Outline

In Chapter 2, we use the spectral quasilinearization method to analyze the mixed convective stagnation-point flow of an electrically conducting Eyring-Powell nanofluid flow over a stretching cylinder. The Tiwari-Das nanofluid model is used to model the flow problem. We study the significant effect of the nonlinear Rosseland approximation, heat generation and the thermal slip boundary condition.

The effect of temperature-dependent thermal conductivity on the fluid flow and heat transfer of an Eyring-Powell nanofluid is studied in Chapter 3. Here channel flow is considered, represented by two parallel infinite plates. The non-Fourier heat flux and Buongiorno nanofluid models are used in the problem formulation. The reduced nonlinear differential equation is solved using the spectral local linearization method.

In Chapter 4, we study the impact of variable thermo-physical properties, which depend on both temperature and nanoparticle size, on the fluid flow of an Eyring-Powell nanofluid past a stretching plate using the spectral local linearization method. The nanofluid model utilized in our study here is adapted from an experimental study. The Lie group symmetry method is used in finding the similarity solution to the formulated model.

In Chapter 5, we focus our attention on how to minimize heat loss in a nanofluid flow. We investigated entropy generation rate and magnetic effect of aluminum oxide-water Powell-Eyring nanofluid flow through a vertical channel. Using the experimental data of the nanofluid dynamic viscosity model, we analyze the combined effects of convective cooling on the heat transfer, suction/injection, viscous dissipation and entropy generation rate. The contents in this chapter are published in Heliyon Journal (2019).

In Chapter 6, we study the Eyring-Powell viscous hybrid nanofluid model, with great emphasis on the entropy generation. The similarity solution was obtained using the Lie group symmetry approach. Afterward, we used the bivariate spectral quasilinearization method to obtain solution

to the emerging similarity equations. Our study also investigated the effect of viscous dissipation on the hybrid nanofluid flow.

Finally, an overview of the results from this study and concluding remarks are given in Chapter 7.

Chapter 2

On MHD mixed convective stagnation point flow of an Eyring-Powell nanofluid over a stretching cylinder with thermal slip conditions

In this chapter, we report on the impact of both nonlinear thermal radiation and a thermal slip condition on the mixed convection in a magnetohydrodynamics Eyring-Powell copper-water nanofluid over a stretching cylinder. The traditional Eyring-Powell nanofluid model is revised to account for nonlinear thermal radiation and heat generation with a thermal slip boundary condition. The spectral quasilinearization method is used to solve the self-similar flow equations. The findings from this chapter show that the skin friction and the heat transfer coefficients are enhanced by increasing the values of the curvature parameter. Increasing the thermal slip parameter leads to a decrease in the heat transfer rate.



MHD mixed convective stagnation-point flow of Eyring-Powell nanofluid over stretching cylinder with thermal slip conditions

Hammed Abiodun OGUNSEYE, Precious SIBANDA, Hiranmoy MONDAL

School of Mathematics, Statistics and Computer Science, University of KwaZulu-Natal,
Private Bag X01, Scottsville, Pietermaritzburg 3209, South Africa

© Central South University Press and Springer-Verlag GmbH Germany, part of Springer Nature 2019

Abstract: The optimal design of heating and cooling systems must take into account heat radiation which is a non-linear process. In this study, the mixed convection in a radiative magnetohydrodynamic Eyring-Powell copper-water nanofluid over a stretching cylinder was investigated. The energy balance is modeled, taking into account the non-linear thermal radiation and a thermal slip condition. The effects of the embedded flow parameters on the fluid properties, as well as on the skin friction coefficient and heat transfer rate, are analyzed. Unlike in many existing studies, the recent spectral quasi-linearization method is used to solve the coupled nonlinear boundary-value problem. The computational result shows that increasing the nanoparticle volume fraction, thermal radiation parameter and heat generation parameter enhances temperature profile. We found that the velocity slip parameter and the fluid material parameter enhance the skin friction. A comparison of the current numerical results with existing literature for some limiting cases shows excellent agreement.

Key words: Eyring-Powell model; stretching cylinder; nanofluid; thermal radiation; slip effects; spectral quasi-linearization method

Cite this article as: Hammed Abiodun OGUNSEYE, Precious SIBANDA, Hiranmoy MONDAL. MHD mixed convective stagnation-point flow of Eyring-Powell nanofluid over stretching cylinder with thermal slip conditions [J]. Journal of Central South University, 2019, 26(5): 1172–1183. DOI: <https://doi.org/10.1007/s11771-019-4079-6>.

1 Introduction

The term of nanofluid refers to a colloidal suspension of tiny particles having a diameter less than 100 nm. CHOI [1] reported that nanofluids have remarkably enhanced thermal conductivity relative to conventional heat transfer fluids. These fluids now have several applications in engineering and biomedical sciences. SAID et al [2] observed that the heating and cooling of a system using solar energy is enhanced when the collector is a nanofluid. Gold nanoparticles were discovered to have therapeutic properties for cancer treatment either as drug carriers or in photothermal therapy (see JAIN et al [3]). BUONGIORNO [4] proposed

a mathematical model for convective transport in a nanofluid. He presented an analysis of the influences of Brownian motion and thermophoretic diffusion in his model. To further understand the thermal behaviour of nanofluids, DAS et al [5] presented another nanofluid model with more emphasis placed on the effective fluid properties.

In recent years, several researchers have given attention to stagnation-point flow due to its relevance in many industrial and engineering processes. Some of the areas of interest include the cooling of electronic devices and nuclear reactors, polymer processes and the flow of ground water. BACHOK et al [6] studied the stagnation-point flow of a nanofluid over a stretching or shrinking plate and observed in their research that the skin

Received date: 2018-08-30; Accepted date: 2018-10-19

Corresponding author: Hiranmoy MONDAL, PhD; Tel: +27731529463; E-mail: hiranmoymondal@yahoo.co.in; ORCID: 0000-0002-9153-300X

friction and heat transfer coefficients are enhanced with nanofluid. RAMZAN et al [7] investigated the stagnation-point flow of a electrically conducting fluid with a generalized slip condition. HAYAT et al [8] investigated the stagnation-point flow of carbon nanotubes over a stretchable cylinder with partial slip. ISHAK et al [9] analyzed the heat transfer of mixed convection stagnation-point flow over a vertical linear stretching sheet. The mixed convection stagnation-point flow of nanofluid over a stretching or shrinking sheet with internal heat generation or absorption in a porous medium was explored by PAL et al [10]. The results of their investigation showed among others, that in a situation of large value of the heat generation or absorption parameter the copper-water temperature increases. ABBAS et al [11] studied stagnation-point flow on a permeable stretching cylinder with heat generation or absorption. The influence of variable viscosity and thermal radiation on stagnation-point flow past a porous stretching sheet was addressed by MUKHOPADHYAY [12]. It was shown that an increase in the thermal parameter led to a significant increase in the thermal boundary layer thickness. Other related studies of nanofluid flow with different geometries can be found in the studies [13–17] and the references therein.

Practically, most industrial and technological real fluids are non-Newtonian. Hence, the Newtonian constitutive relation based on linear shear stress and strain can not be used to study such fluids. For the study of non-Newtonian fluids, several models have been proposed, such as the Casson fluid model, power law model, Maxwell fluid, Jeffrey fluid, Eyring-Powell fluid. In this study, we assume the Eyring-Powell fluid model proposed by EYRING and POWELL [18]. The choice of this model is due to the fact that the constitutive model is derived from the molecular theory of fluid and not based on an empirical relation. JAVED et al [19] studied Eyring-Powell fluid flow over a stretchable plate using the Keller box method to solve the flow equations. They showed that the velocity profiles are enhanced for a non-Newtonian fluid, as against the use of a Newtonian fluid. HAYAT et al [20] obtained a series solution for heat transfer in an Eyring-Powell fluid flow over a continuously moving surface with a convective boundary condition using the homotopy analysis method. AKBAR et al [21]

studied the magnetohydrodynamic (MHD) flow of an Eyring-Powell fluid using the implicit finite difference method. It was shown that for large magnetic field intensity, the resistance to flow increases. BABU et al [22] analyzed MHD mass transfer of Eyring-Powell nanofluid over a permeable cone with buoyancy forces and suction or injection effects. HAYAT et al [23] considered the effects of heat generation or absorption on MHD Eyring-Powell nanofluid over an impermeable stretched cylinder. In the work of RAMZAN et al [24] reactive Eyring-Powell nanofluid with variable properties was investigated. MALIK et al [25] reported the mixed convection flow of MHD Eyring-Powell nanofluid past a plate. KHAN et al [26] investigated mixed convection flow of reactive Eyring-Powell nanofluid over a cone and plate.

The thermal properties and flow structure of a copper-water nanofluid using the Eyring-Powell model has not been studied, with most studies limited to the Buongiorno model [4]. The objective of this study is to investigate the thermal properties of a water based Eyring-Powell nanofluid flow past a vertical stretching cylinder under heat generation, velocity and thermal slip boundary conditions. To the best of the authors knowledge, the problem analysis has not been investigated. The transformed equations are solved numerically using the spectral quasi-linearization method proposed by MOTSA [27]. To validate the accuracy and convergence of the numerical method, a comparison of the skin friction coefficient and the Nusselt number for limiting cases with existing literature is presented.

2 Mathematical formulation

Consider the steady two-dimensional, laminar and incompressible mixed convective magnetohydrodynamic flow and heat transfer in a radiative Eyring-Powell nanofluid past a vertical stretching cylinder of radius, a . It is assumed that a uniform magnetic field strength, B_0 , is applied along the radial direction, r , and the stretching velocity of the cylinder is given by $u_w(z)=U_0z/l$, where $U_0>0$ is the stretching constant, z is the co-ordinate measured along the axial direction and l is the characteristic length (see Figure 1).

The nanofluid is composed of copper

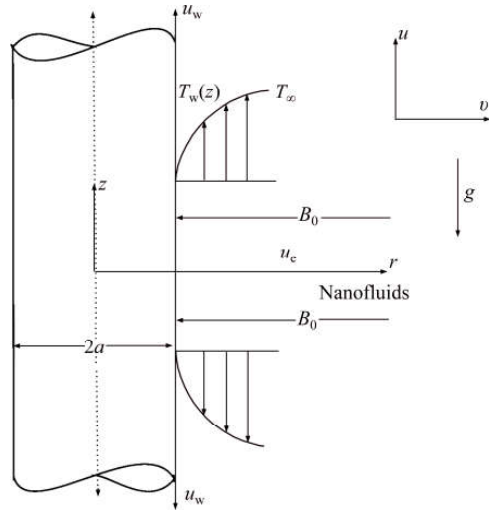


Figure 1 Geometry of problem

nanoparticles suspended in water. The base fluid and the suspended nanoparticles are assumed to be in thermal equilibrium. Under the usual boundary layer and Oberbeck-Boussinesq approximations, the equations of conservation of mass, momentum and energy balance describing the Eyring-Powell nanofluid can be written as follows [23]:

$$\frac{\partial(ru)}{\partial z} + \frac{\partial(rv)}{\partial r} = 0 \tag{1}$$

$$u \frac{\partial u}{\partial z} + v \frac{\partial u}{\partial r} = u_e(z) \frac{du_e(z)}{dz} + \frac{\sigma_{nf} B_0^2}{\rho_{nf}} (u_e(z) - u) + \left(\nu_{np} + \frac{1}{\rho_{np} bc} \right) \left(\frac{\partial^2 u}{\partial r^2} + \frac{1}{r} \frac{\partial u}{\partial r} \right) - \frac{1}{6 \rho_{nf} bc^3} \left[\frac{1}{r} \left(\frac{\partial u}{\partial r} \right)^3 + 3 \left(\frac{\partial u}{\partial r} \right)^2 \frac{\partial^2 u}{\partial r^2} \right] + \frac{\sigma_{nf} B_0^2}{\rho_{nf}} (u_e(z) - u) + \frac{g(\rho\beta)_{nf}(T - T_\infty)}{\rho_{nf}} \tag{2}$$

$$u \frac{\partial T}{\partial z} + v \frac{\partial T}{\partial r} = \frac{\kappa_{nf}}{(\rho C_p)_{nf}} \left(\frac{\partial^2 T}{\partial r^2} + \frac{1}{r} \frac{\partial T}{\partial r} \right) - \frac{1}{(\rho C_p)_{np}} \frac{1}{r} \frac{\partial}{\partial r} (r q_r) + \frac{Q_0(T - T_\infty)}{(\rho C_p)_{nf}} \tag{3}$$

subjected to the boundary conditions:

$$v = v_w(z), \quad u = u_w(z) + e_1 \frac{\partial u}{\partial r},$$

$$T = T_w(z) + e_2 \frac{\partial T}{\partial r} \quad \text{on } r = a,$$

$$u \rightarrow u_e(z) = \frac{U_\infty z}{l}, \quad T \rightarrow T_\infty \quad \text{when } r \rightarrow \infty \tag{4}$$

where u and v are the velocity components in the z and r directions, respectively; b and c are fluid parameters; g is the gravitational acceleration; T is the fluid temperature; q_r is the radiative heat flux; $u_e(z)$ is the free stream velocity; Q_0 denotes the uniform volumetric heat generation or absorption coefficient; $v_w(z) > 0$ signifies fluid suction while $v_w(z) < 0$ indicates fluid injection; e_1 and e_2 stand for the velocity and thermal slip coefficients, respectively; $T_w(z) = T_\infty + \frac{\Delta z}{l}$, denotes the prescribed wall temperature; U_∞ and T_∞ are the reference velocity and temperature, respectively; ν_{np} , ρ_{np} , β_{np} , σ_{np} , κ_{np} and $(\rho C_p)_{np}$ denote the kinematic viscosity, density, thermal expansion coefficient, electrical conductivity, thermal conductivity and heat capacity, respectively. For a spherical-shaped nanoparticles, the physical properties of the nanofluid are defined by [5]

$$\left\{ \begin{aligned} \mu_{nf} &= \frac{\mu_f}{(1-\phi)^{2.5}} \\ \rho_{nf} &= (1-\phi)\rho_f + \phi\rho_s \\ (g\beta)_{nf} &= (1-\phi)(g\beta)_f + \phi(g\beta)_s \\ (\rho C_p)_{nf} &= (1-\phi)(\rho C_p)_f + \phi(\rho C_p)_s \\ \sigma_{nf} &= \sigma_f \left[1 + \frac{3 \left(\frac{\sigma_s}{\sigma_f} - 1 \right) \phi}{\left(\frac{\sigma_s}{\sigma_f} + 2 \right) - \left(\frac{\sigma_s}{\sigma_f} - 1 \right) \phi} \right] \\ \frac{\kappa_{nf}}{\kappa_f} &= \frac{k_s + 2k_f - 2(k_f - k_s)\phi}{k_s + 2k_f + (k_f - k_s)\phi} \end{aligned} \right. \tag{5}$$

where the subscripts f and s stand for the base fluid and nanoparticles; ϕ is the solid volume fraction of the nanoparticle; μ , ρ , β , (ρC_p) , σ and κ respectively represent the viscosity, density, thermal expansion coefficient, heat capacity, electrical conductivity and thermal conductivity, respectively. The thermo-physical properties of water and nanoparticles are given in Table 1.

Using the Rosseland approximation [28], the radiative heat flux can be expressed as follows:

Table 1 Thermo-physical properties of water and nanoparticles [5]

Fluid	ρ' ($\text{kg}\cdot\text{m}^{-3}$)	c_p' ($\text{J}\cdot\text{kg}^{-1}\cdot\text{K}^{-1}$)	k' ($\text{W}\cdot\text{m}^{-1}\cdot\text{K}^{-1}$)	β' 10^{-3}K^{-1}	σ' ($\text{S}\cdot\text{m}^{-1}$)
Water	997.1	4179	0.613	21	5.5×10^{-6}
Cu	8933	385	401	1.67	59.5×10^{-6}

$$q_r = -\frac{16\sigma^*T^3}{3k^*} \frac{\partial T}{\partial r} \tag{6}$$

where σ^* is the Steffan-Boltzman constant and k^* is the Rosseland mean absorption coefficient.

Substituting Eqs. (6) into the energy balance Eq. (3) yields

$$u \frac{\partial T}{\partial z} + v \frac{\partial T}{\partial r} = \frac{\kappa_{nf}}{(\rho C_p)_{nf}} \left(\frac{\partial^2 T}{\partial r^2} + \frac{1}{r} \frac{\partial T}{\partial r} \right) + \frac{16\sigma^*}{3\kappa^*(\rho C_p)_{np}} \frac{1}{r} \frac{\partial}{\partial r} \left(rT^3 \frac{\partial T}{\partial r} \right) + \frac{Q_0(T - T_\infty)}{(\rho C_p)_{nf}} \tag{7}$$

To transform Eqs. (1), (2) and (7) into ordinary differential equation, we introduce the following stream function and similarity variables (see HAYAT et al [23] and MUKHOPADHYAY [12]):

$$\begin{aligned} \psi &= az \sqrt{\left(\frac{v_f U_0}{l} \right)}, \\ \eta &= \frac{r^2 - a^2}{2a} \sqrt{\frac{U_0}{v_f l}}, \\ \theta(\eta) &= \frac{T - T_\infty}{T_w - T_\infty} \end{aligned} \tag{8}$$

where ψ is the stream function such that $u = \frac{1}{r} \frac{\partial \psi}{\partial r}$ and $v = -\frac{1}{r} \frac{\partial \psi}{\partial z}$ and η is the similarity variable.

Using Eq. (8), Eq. (1) is identically satisfied while Eqs. (2) and (7) reduce to the following coupled nonlinear ordinary differential equations:

$$\begin{aligned} (1 + 2\gamma\eta) \left(\frac{1}{(1-\phi)^{2.5}} + \Gamma \right) f''' - \frac{4}{3} \Gamma \delta \gamma (1 + 2\gamma\eta) (f'')^3 + \\ 2\gamma \left(\frac{1}{(1-\phi)^{2.5}} + \Gamma \right) f'' + M_1 (ff'' - f'^2) + M_1 \varepsilon^2 - \\ \Gamma \delta (1 + 2\gamma\eta)^2 f'' (f'')^2 - M_2 Ha^2 (f' - \varepsilon) + \\ M_3 \lambda \theta = 0 \end{aligned} \tag{9}$$

$$\begin{aligned} \left(M_4 + \frac{4}{3} R_d (1 + \theta(\theta_w - 1))^3 \right) ((1 + 2\gamma\eta)\theta'' + 2\gamma\theta') + \\ M_5 Pr (f\theta' - f'\theta) + Pr Q \theta + \\ 4R_d (\theta_w - 1) (1 + 2\gamma\eta) (1 + \theta(\theta_w - 1))^2 \theta'^2 = 0 \end{aligned} \tag{10}$$

subjected to the boundary conditions:

$$\begin{aligned} f(0) = f_w, \quad f'(0) = 1 + A_1 f''(0), \quad f'(\infty) = \varepsilon, \\ \theta(0) = 1 + A_2 \theta'(0), \quad \theta(\infty) = 0 \end{aligned} \tag{11}$$

where the prime denotes differentiation with respect to η ; γ is the curvature parameter; Γ and δ is the

fluid parameter, respectively; Ha is the Hartman number; ε is the velocity ratio of the free stream velocity to that of stretching cylinder wall; λ represents the mixed convection parameter; R_d stands for the thermal radiation parameter; θ_w is the temperature ratio parameter; Pr is the Prandtl number; Q denotes the heat generation ($Q > 0$) or absorption ($Q < 0$) parameter; f_w stands for suction ($f_w < 0$) or injection ($f_w > 0$); A_1 and A_2 are the dimensionless velocity slip and thermal slip parameter, respectively. These parameters are expressed as follows:

$$\begin{aligned} \gamma &= \sqrt{\frac{vl}{U_0 a^2}}, \quad \Gamma = \frac{1}{\mu_f bc}, \quad \delta = \frac{U_0^3 z^2}{2v_f l^3 c^2}, \quad \varepsilon = \frac{U_\infty}{U_0}, \\ Ha &= \frac{\sigma_f B_0^2 l}{\rho_f U_0}, \quad \lambda = \frac{Gr}{Re_z}, \quad Gr = \frac{g\beta_f \Delta T z^3}{v_f^2}, \\ Re_z &= \frac{U_0 z^2}{v_f l}, \quad R_d = \frac{4\sigma^* T_\infty^3}{k^* \kappa_f}, \quad Pr = \frac{(\mu C_p)_f}{\kappa_f}, \\ \theta_w &= \frac{T_w}{T_\infty}, \quad Q = \frac{Q_0 l}{U_0 (C_p)_f}, \quad f_w = -v_w \sqrt{\frac{l}{v_f U_0}}, \\ M_1 &= 1 - \phi + \phi \left(\frac{\rho_s}{\rho_f} \right), \quad A_1 = e_1 \sqrt{\frac{U_0}{v_f l}}, \\ M_2 &= \left[1 + \frac{3 \left(\frac{\sigma_s}{\sigma_f} - 1 \right) \phi}{\frac{\sigma_s}{\sigma_f} + 2 - \left(\frac{\sigma_s}{\sigma_f} - 1 \right) \phi} \right], \quad A_2 = e_2 \sqrt{\frac{U_0}{v_f l}}, \\ M_3 &= 1 - \phi + \phi \left(\frac{(\rho\beta)_s}{(\rho\beta)_f} \right), \quad M_5 = 1 - \phi + \phi \left(\frac{(\rho C_p)_s}{(\rho C_p)_f} \right), \\ M_4 &= \frac{k_s + 2k_f - 2(k_f - k_s)\phi}{k_s + 2k_f + (k_f - k_s)\phi} \end{aligned} \tag{12}$$

here Gr is the local Grashof number and Re_z is the local Reynold number. Furthermore, the skin friction coefficient, C_f and the local Nusselt number, Nu_z are defined as follows (see HAYAT et al [23] and JAVED et al [19]):

$$C_f = \frac{\tau_w}{\rho_f U_w^2}, \quad Nu_z = \frac{z q_w}{\kappa_f (T_w - T_\infty)} \tag{13}$$

The wall shear stress, τ_w and the wall heat flux, q_w at $r=a$ are expressed as:

$$\tau_w = \left[\mu_{nf} \left(\frac{\partial u}{\partial r} \right) + \frac{1}{bc} \left(\frac{\partial u}{\partial r} \right) - \frac{1}{6bc^3} \left(\frac{\partial u}{\partial r} \right)^3 \right]_{r=a} \tag{14}$$

$$q_w = - \left[\left[\kappa_{nf} + \frac{16\sigma^* T^3}{3k^*} \right] \left(\frac{\partial T}{\partial r} \right) \right]_{r=a} \tag{15}$$

In dimensionless forms, the skin friction

coefficient, C_f and the local Nusselt number, Nu_z are:

$$C_f Re_z^{\frac{1}{2}} = \left(\frac{1}{(1-\varphi)^{2.5}} + \Gamma \right) f''(0) - \frac{\Gamma \delta}{3} (f''(0))^3 \quad (16)$$

$$Nu_z Re_z^{-\frac{1}{2}} = - \left(M_4 + \frac{4}{3} R_d (\theta(0)(\theta_w - 1) + 1)^3 \right) \theta'(0) \quad (17)$$

3 Spectral quasi-linearization method of solution

The system of coupled, nonlinear differential equations given in Eqs. (9)–(11) are solved numerically using the SQLM. The principle of the SQLM is derived from the pioneering work of Ref. [29]. The nonlinear system is linearized using the Newton-Raphson algorithm. The linearized equations are integrated using Chebyshev spectral collocation method. With the appropriate initial guesses, the SQLM converges rapidly and gives an accurate solution. Studies on the accuracy and convergence of SQLM are reported in Refs. [27] and [30].

Equations (9)–(10) can be rewritten in decomposed form as a sum of both linear and nonlinear components. Linearizing using one term Taylor’s series for multiple variables, gives the iterative scheme:

$$\alpha_{1,n} f_{n+1}'' + \alpha_{2,n} f_{n+1}'' + \alpha_{3,n} f_{n+1}' + \alpha_{4,n} f_{n+1} + \alpha_{5,n} \theta_{n+1} = R_n^f \quad (18)$$

$$\alpha_{6,n} \theta_{n+1}'' + \alpha_{7,n} \theta_{n+1}' + \alpha_{8,n} \theta_{n+1} + \alpha_{9,n} f_{n+1}' + \alpha_{10,n} f_{n+1} = R_n^\theta \quad (19)$$

with corresponding boundary conditions:

$$\begin{aligned} f_{n+1}(0) &= f_w, \quad f_{n+1}'(0) = 1 + A_1 f_{n+1}''(0), \\ f_{n+1}'(\infty) &= \varepsilon, \quad \theta_{n+1}(0) = 1 + A_2 \theta_{n+1}'(0), \\ \theta_{n+1}(\infty) &= 0 \end{aligned} \quad (20)$$

where the coefficients $\alpha_{i,n}$ ($i=1, \dots, 10$), are known functions from previous iterations and are given by:

$$\alpha_{1,n} = (1 + 2\gamma\eta) \left(\frac{1}{(1-\varphi)^{2.5}} + \Gamma \right) - \Gamma \delta (1 + 2\gamma\eta)^2 (f_n'')^2,$$

$$\begin{aligned} \alpha_{2,n} &= 2\gamma(1 + 2\gamma\eta) \left(\frac{1}{(1-\varphi)^{2.5}} + \Gamma \right) + \\ &M_1 f_n - 2\Gamma \delta (1 + 2\gamma\eta) f_n'' (2\gamma f_n'' + (1 + 2\gamma\eta) f_n'''), \end{aligned}$$

$$\begin{aligned} \alpha_{3,n} &= -M_1 (Ha^2 M_2 + 2f_n'), \\ \alpha_{4,n} &= M_1 f_n'', \\ \alpha_{5,n} &= M_3 \lambda, \\ \alpha_{6,n} &= \left(M_4 + \frac{4}{3} R_d (1 + \theta_n (\theta_w - 1))^3 \right) \times (1 + 2\gamma\eta) \\ \alpha_{7,n} &= 2\gamma \left(M_4 + \frac{4}{3} R_d (1 + \theta_n (\theta_w - 1))^3 \right) + \\ &8R_d (1 + 2\gamma\eta) (1 + \theta_n (\theta_w - 1))^2 \theta_n' + M_5 Pr f_n', \\ \alpha_{8,n} &= Pr(Q - M_3 f_n') + 4R_d (\theta_w - 1) (1 + \theta (\theta_w - 1))^2 \times \\ &((2\eta\gamma + 1)\theta'' + 2\gamma\theta') + 8R_d (\theta_w - 1)^2 (2\eta\gamma + 1) \times \\ &(1 + \theta (\theta_w - 1)) \theta'^2, \\ \alpha_{9,n} &= -M_5 Pr \theta_n, \\ \alpha_{10,n} &= M_5 Pr \theta_n', \\ R_n^f &= \alpha_{1,n} f_n'' + \alpha_{2,n} f_n'' + \alpha_{3,n} f_n' + \alpha_{4,n} f_n + \alpha_{5,n} \theta_n - \Phi_f, \\ R_n^\theta &= \alpha_{6,n} \theta_n'' + \alpha_{7,n} \theta_n' + \alpha_{8,n} \theta_n + \alpha_{9,n} f_n' + \alpha_{10,n} f_n - \Phi_\theta \\ \Phi_f &= (1 + 2\gamma\eta) \left(\frac{1}{(1-\varphi)^{2.5}} + \Gamma \right) f_n''' - M_2 Ha^2 (f_n' - \varepsilon) + \\ &2\gamma \left(\frac{1}{(1-\varphi)^{2.5}} + \Gamma \right) f_n'' + M_1 (f_n f_n'' - f_n'^2) + M_3 \lambda \theta_n - \\ &\frac{4}{3} \Gamma \delta \gamma (1 + 2\gamma\eta) (f_n'')^3 - \Gamma \delta (1 + 2\gamma\eta)^2 f_n'' (f_n'')^2 + M_1 \varepsilon^2, \\ \Phi_\theta &= \left(M_4 + \frac{4}{3} R_d (1 + \theta_n (\theta_w - 1))^3 \right) [(1 + 2\gamma\eta) \theta_n'' + \\ &2\gamma \theta_n'] + M_5 Pr (f_n \theta_n' - f_n' \theta_n) + Pr Q \theta + \\ &4R_d (\theta_w - 1) (1 + 2\gamma\eta) (1 + \theta_n (\theta_w - 1))^2 \theta_n'^2 \end{aligned} \quad (21)$$

Equations (18)–(20) constitute the SQLM iterative scheme. The equations are solved numerically using the Chebyshev pseudo-spectral technique as described in Ref. [31]. Initializing the algorithm with appropriate initial approximations, the results for f_{n+1} and θ_{n+1} , when $n=1, 2, \dots$ are computed iteratively.

We discretize Eqs. (18) and (19) using the Chebyshev pseudo-spectral collocation method. Firstly, the semi-infinite domain, $\eta \in [0, \infty)$ is truncated by replacing it with $\eta \in [0, \varpi_\infty]$, where $\varpi_\infty \in \mathbb{Z}^+$.

Secondly, we transform the interval $[0, \varpi_\infty] \mapsto [-1, 1]$, using the transformation $\eta = \frac{1}{2}(\xi + 1)\varpi_\infty$. The derivatives of the unknown variables $f(\eta)$ and $\theta(\eta)$ are computed using the Chebyshev differentiation matrix D (see [32]), at the collocation points as a matrix vector product:

$$\frac{df}{d\eta} = \sum_{i=0}^{\bar{N}} D_{ij} f(\xi_i) = DF, \quad j = 0, 1, 2, \dots, \bar{N} \quad (22)$$

where $\bar{N} + 1$ is the number of collocation points, $D = 2D/\varpi_\infty$ and $F = [f(\xi_0), f(\xi_1), \dots, f(\xi_{\bar{N}})]^T$ is a vector function at the collocation point. The Gauss-Lobatto points are selected to define the nodes in $[-1, 1]$ as:

$$\xi_k = \cos\left(\frac{\pi k}{\bar{N}}\right), \quad k = 0, 1, \dots, \bar{N}; \quad -1 \leq \xi \leq 1 \quad (23)$$

Let θ be a similar vector function representing θ . Higher order derivatives of f and θ are evaluated as powers of D , that is

$$f^s(\eta) = D^s F, \quad \theta^s(\eta) = D^s \theta \quad (24)$$

Substituting Eqs. (22)–(24) into Eqs. (18) and (19), we obtain the following SQLM scheme in a matrix form:

$$\begin{bmatrix} A_{11} & A_{12} \\ A_{21} & A_{22} \end{bmatrix} \begin{bmatrix} F_{r+1} \\ \theta_{r+1} \end{bmatrix} = \begin{bmatrix} R_n^f \\ R_n^\theta \end{bmatrix} \quad (25)$$

where A_{ij} ($i, j=1, \dots, 2$) are $(\bar{N} + 1) \times (\bar{N} + 1)$ matrices and R_n^f and R_n^θ are $(\bar{N} + 1) \times 1$ vectors, defined as:

$$\begin{cases} A_{11} = \text{diag}[\alpha_{1,n}]D^3 + \text{diag}[\alpha_{2,n}]D^2 + \text{diag}[\alpha_{3,n}]D + \text{diag}[\alpha_{4,n}]I \\ A_{12} = \text{diag}[\alpha_{5,r}]I \\ A_{21} = \text{diag}[\alpha_{9,n}]D + \text{diag}[\alpha_{10,n}]I \\ A_{22} = \text{diag}[\alpha_{6,n}]D^2 + \text{diag}[\alpha_{7,n}]D + \text{diag}[\alpha_{8,n}]I \end{cases} \quad (26)$$

subjected to the boundary conditions

$$\begin{aligned} F_{n+1}(\xi_{\bar{N}}) &= f_w, \quad \sum_{i=0}^{\bar{N}} [D_{Ni}^2 - A_1 D_{Ni}] F_{n+1}(\xi_{\bar{N}}) = 1, \\ \sum_{i=0}^{\bar{N}} D_{0i} F_{n+1}(\xi_0) &= \varepsilon, \quad \sum_{i=0}^{\bar{N}} [I_{Ni} - A_2 D_{Ni}] \theta_{n+1}(\xi_{\bar{N}}) = 1, \\ \theta_{n+1}(\xi_0) &= 0 \end{aligned} \quad (27)$$

A suitable initial approximation for the SQLM scheme is

$$\begin{cases} f_0(\eta) = f_w + \eta\varepsilon + \left(\frac{1-\varepsilon}{1+A_1}\right)(1-\exp(-\eta)) \\ \theta_0(\eta) = \frac{1}{1+A_2} \exp(-\eta) \end{cases} \quad (28)$$

4 Results and discussion

In this section, the computational results showing the effect of flow parameters on the

velocity profiles, $f(\eta)$, temperature profiles $\theta(\eta)$, skin friction coefficient and Nusselt number are discussed. To validate the correctness of the numerical results obtained from the iterative scheme given by Eqs. (18)–(20), the skin friction coefficient, $f''(0)$ is compared with result of MAHAPATRA et al [33] in Table 2, and in Table 3; the values of the local Nusselt number $-\theta'(0)$ are compared with those of ZAIMI et al [34]. Thus, Tables 2 and 3 show the accuracy and convergence of SQLM.

Table 2 Comparison of SQLM results for $f''(0)$ with MAHAPATRA et al [33] for distinct values of ε when $\gamma=1, Ha=f_w=\lambda=0$ and $A_1=0$

ε	$f''(0)$		
	MAHAPATRA et al [33]	SQLM	Error
0.1	-0.9694	-0.9694	0
0.2	-0.9181	-0.9181	0
0.5	-0.6673	-0.6673	0
2	2.0175	2.0175	0
3	4.7293	4.7293	0

Table 3 Comparison of SQLM results for $-\theta'(0)$ with ZAIMI et al [34] for different values of Pr by setting $\varepsilon=\lambda=1, \varphi=\gamma=1, Ha=Ra=Q=A_1=0$ and $A_2=0$

Pr	$-\theta'(0)$		
	ZAIMI et al [34]	SQLM	Error
0.72	1.09310	1.09310	0
6.8	3.28957	3.28957	0
10	3.98240	3.98240	0
20	5.62013	5.62013	0
30	6.87771	6.87771	0
40	7.93830	7.93830	0
50	8.87292	8.87292	0
60	9.71801	9.71801	0
70	10.49524	10.49524	0
80	11.21874	11.21874	0
90	11.89831	11.89831	0
100	12.54109	12.54109	0

The following ranges of values are used; $0 \leq \gamma \leq 1.2, 0 \leq \varphi \leq 0.2, 0 \leq I \leq 1.0, 0 \leq Ha \leq 3.0, 0.8 \leq \varepsilon \leq 1.2, 0 \leq f_w \leq 0.7, 0 \leq A_1 \leq 0.7, 0 \leq R_d \leq 0.9$ and $0 \leq A_2 \leq 0.6$.

The impact of the curvature parameter γ on the velocity profile is shown in Figure 2. It is observed that very close to the surface of the cylinder for $\eta \in [0, 0.7]$, the velocity profiles diminish with an

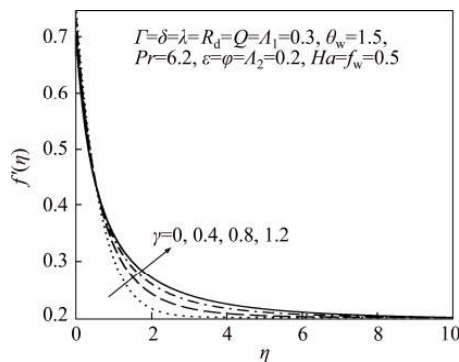


Figure 2 Effect of γ on $f'(\eta)$

increase in the curvature parameter, while the velocity profiles are seen to be enhanced far away from the surface. Physically, higher values of the curvature parameter reduces the radius of the cylinder, thus, the contact area of the nanofluid with the cylinder is reduced. Hence, the momentum boundary layer thickness is improved. Similar outcome was reported by HAYAT et al [8]. In Figure 3, the influence of the nanoparticle volume fraction φ on the velocity distribution is illustrated. The velocity profile and momentum boundary layer thickness retard with an increase in the nanoparticle volume fraction. The influence of the fluid parameter Γ on the velocity profile is presented in Figure 4. It is seen that with the increase in the fluid parameter, the velocity profile and the momentum boundary layer thickness are enhanced. Physically, it is correct since the fluid parameter has an inverse relation with the nanofluid dynamic viscosity, thus, the fluid becomes less viscous with large value of the fluid parameter. Hence, the velocity profile is enhanced. This finding is consistent with JAVED et al [19]. Figure 5 presents the velocity profiles for distinct values of the Hartmann number Ha . A decreasing trend is observed in the velocity profile as the Hartmann number increases. This is physically consistent due to the damping influence of the Lorentzian hydromagnetic drag. The impact of the velocity ratio parameter ε on the velocity profile is presented in Figure 6. The result shows that for $\varepsilon > 1$, that is, when the free stream velocity is greater than the stretching velocity, the boundary layer thickness decreases with an increase in the velocity ratio parameter and the opposite phenomenon is observed for $\varepsilon < 1$. However, the boundary layer breaks down for $\varepsilon = 1$, as the free

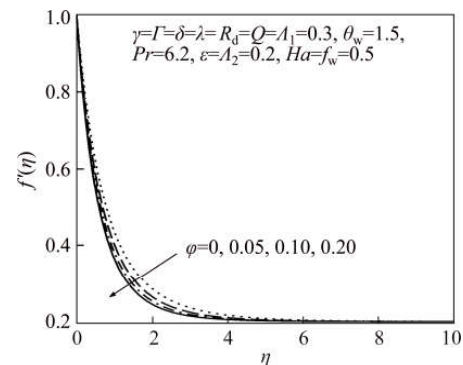


Figure 3 Effect of φ on $f'(\eta)$

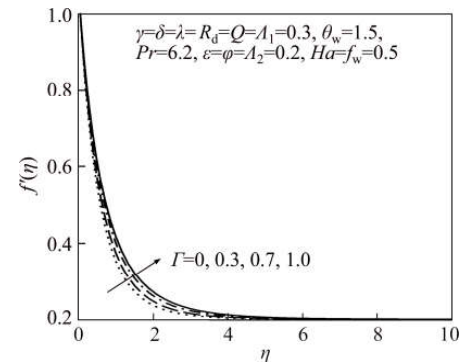


Figure 4 Effect of Γ on $f'(\eta)$

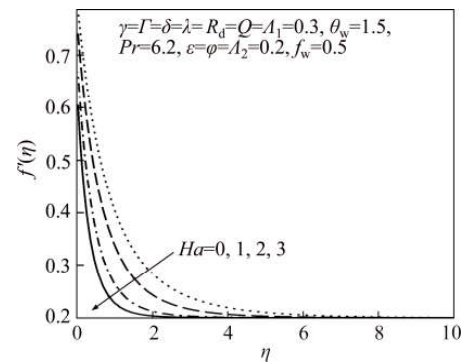


Figure 5 Effect of Ha on $f'(\eta)$

stream velocity coincides with the stretching velocity. Figure 7 illustrates the effect of the mixed convection parameter λ on the velocity profile. This plot shows that the velocity profile and momentum boundary layer thickness are enhanced for higher values of the mixed convection parameter. Physically, an increase in the mixed convection parameter leads to an increment in the buoyancy force, hence, the velocity profile is improved. Figure 8 depicts the effect of the suction/injection

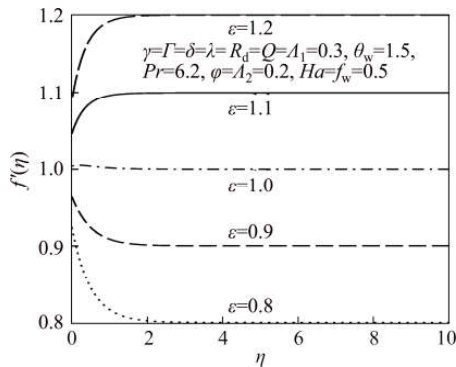


Figure 6 Effect of ε on $f'(\eta)$

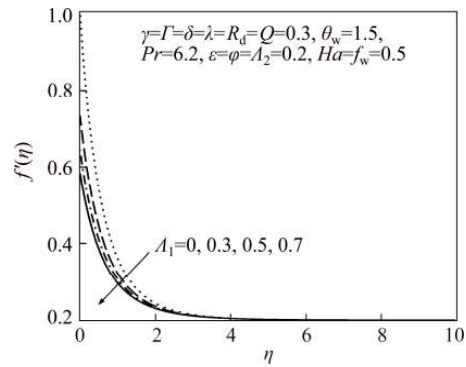


Figure 9 Effect of A_1 on $f'(\eta)$

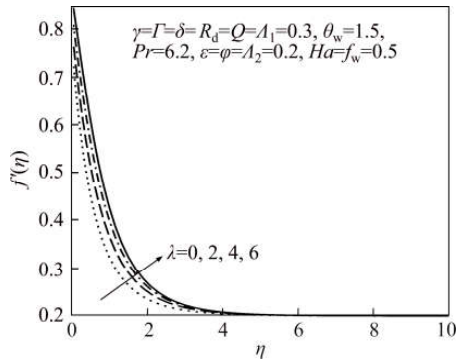


Figure 7 Effect λ on $f'(\eta)$

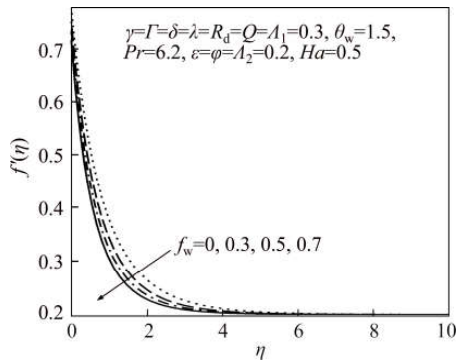


Figure 8 Effect f_w on $f'(\eta)$

parameter f_w on the velocity profile. The thickness of the momentum boundary layer is reduced with an increase in the suction parameter ($f_w > 0$). Similar trend was reported by MUKHOPADHYAY [13]. In Figure 9, the effect of the velocity slip parameter A_1 on the velocity profile is presented. Similar to the effects of the Hartmann number Ha , the velocity profile and momentum boundary layer thickness retard for higher values of the velocity slip parameter. Physically, the adhesive force between

the wall and the nanofluid decreases with higher velocity slip parameter, which results in the partial transfer of stretching velocity to the nanofluid. Hence, the velocity profile decreases. This outcome is similar to the report of HAYAT et al [8].

Figures 10–15 show the temperature profiles in the flow. The response of the temperature to the curvature parameter is presented in Figure 10. The temperature profile and the thermal boundary layer thickness are enhanced with an increase in curvature parameter. Figure 11 shows the temperature profiles for different nanoparticle volume fraction ϕ . An increase in the nanoparticle fraction is seen to increase the nanofluid temperature. This is physically correct due to the fact that as the nanoparticle volume fraction increases, the thermal conductivity of the nanofluid is enhanced, hence, improving the thermal distribution. This observation is similar to the result of DAS et al [5]. In Figure 12, the influence of Hartmann number on the temperature distribution is displayed. From the figure, it is seen that the thermal boundary layer thickness is enhanced for large Hartmann number. Figure 13 depicts the impact of the thermal radiation parameter R_d on the nanofluid temperature distribution. It is observed that the temperature profile and the thermal boundary layer thickness are enhanced with an increase in the radiation parameter. Physically, higher value of the radiation parameter, implies that, more heat is transferred to the nanofluid since the mean absorption coefficient κ^* reduces with an increase in the radiation parameter. This temperature profile is similar to result of HAYAT et al [23]. The influence of the heat generation or

absorption parameter Q on the temperature profile is shown in Figure 14. As observed from the figure, the temperature distribution of the nanofluid is seen to be enhanced with an increase in the heat generation parameter ($Q > 0$) whereas a reverse trend is noticed with the heat absorption parameter ($Q < 0$). Figure 15 displays the effect of the thermal slip parameter A_2 on the temperature profile. From the plot, an increase in the thermal slip parameter is seen to decay the temperature and thermal boundary layer thickness. Physically, for higher values of the

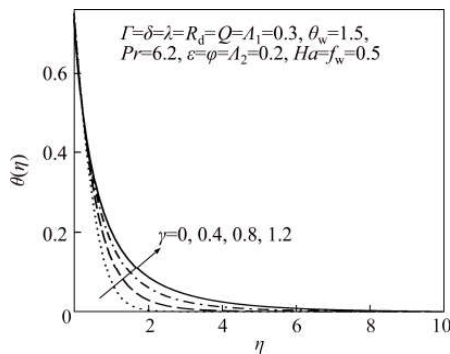


Figure 10 Effect of γ on $\theta(\eta)$

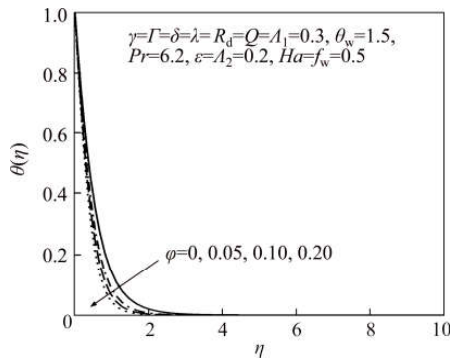


Figure 11 Effect of ϕ on $\theta(\eta)$

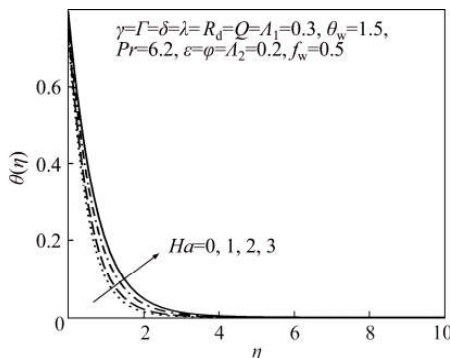


Figure 12 Effect of Ha on $\theta(\eta)$

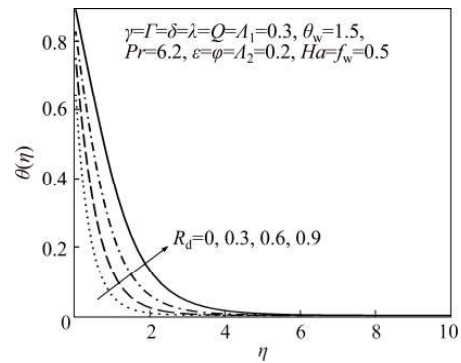


Figure 13 Effect of R_d on $\theta(\eta)$

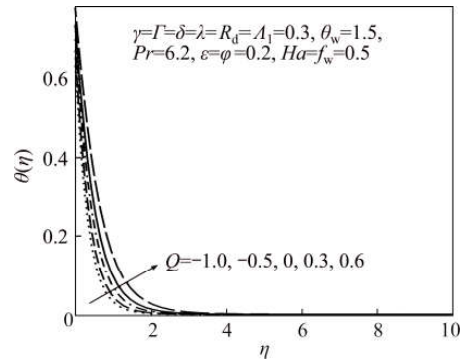


Figure 14 Effect of Q on $\theta(\eta)$

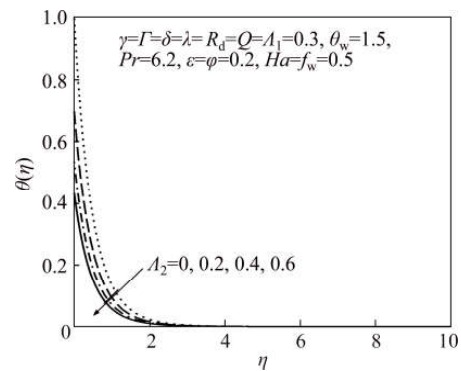


Figure 15 Effect of A_2 on $\theta(\eta)$

thermal slip parameter A_2 , the rate of heat transfer is reduced from the cylinder to the nanofluid, hence, damping the temperature profile.

The effect of distinct parameters on the skin friction coefficient is shown in Table 4. From the table, it is observed that, an increase in the parameters γ , ϕ , Γ , Ha and f_w reduces the skin friction coefficient. However, the skin friction coefficient increases with an increase in the parameters δ , λ , ε and A_1 . Table 5 shows the impact

Table 4 Skin friction coefficient for distinct values of φ , Γ , δ , Ha , λ , ε , f_w and A_1 when $\theta_w=1.5$, $Pr=6.2$, $R_d=Q=0.3$ and $A_2=0.2$

γ	φ	Γ	δ	Ha	λ	ε	f_w	A_1	$C_f Re_z^{-\frac{1}{2}}$
0	0.2	0.3	0.3	0.5	0.3	0.2	0.5	0.3	-1.72457165
0.4									-1.82643031
0.8									-1.91926419
0.3	0								-1.40208097
	0.1								-2.11987405
	0.2								-2.91604830
	0.2	0							-2.73968851
		0.3							-2.91604830
		0.7							-3.14385589
		0.3	0						-1.84910136
			0.3						-1.55497285
			0.6						-1.29603215
			0.3	0					-1.45050911
				1					-1.74698577
				2					-2.22417731
			0.5	0					-1.84910136
				2					-1.55497285
				4					-1.29603215
				0.3	0.8				-0.51484505
					0.9				-0.24927450
					1				0.02698366
					1.1				0.31283749
					0.2	0			-1.52513636
						0.3			-1.69013439
						0.5			-1.80186107
						0.5	0		-2.94442341
							0.3		-1.80186107
								0.5	-1.44583760

of the parameters γ , φ , ε , R_d , Q and A_2 on the rate of heat transfer. Higher values of the parameters γ , ε and R_d lead to an increase in the Nusselt number. The opposite trend is seen for an increase in the parameters φ , Q and A_2 .

5 Conclusions

We studied the mixed convective stagnation-point flow of magnetohydrodynamic Eyring-Powell copper-water nanofluid flow over a stretching vertical cylinder with slip effects. The conservation equations have been solved numerically using

Table 5 Nusselt number for distinct values of φ , ε , R_d , Q and A_2 when $\theta_w=1.5$, $Pr=6.2$, $\Gamma=\delta=\lambda=A_1=0.3$ and $Ha=f_w=0.5$

γ	φ	ε	R_d	Q	A_2	$Nu_z (Re_z)^{-\frac{1}{2}}$
0	0.2	0.2	0.3	0.3	0.2	2.45123397
0.4						2.51054333
0.8						2.57598052
0.3	0					5.33929482
	0.1					4.63850497
	0.2					4.02650363
	0.2	0.8				2.93121600
		0.9				2.98709520
		1				3.03987149
		1.1				3.08989857
		0.2	0			1.69297797
			0.3			2.49512955
			0.6			2.76986222
			0.3	-1		3.32718345
				-0.5		3.11749204
				0		2.83026971
				0.3		2.58649631
				0.6		2.21875985
				0.3	0	5.11095082
					0.2	2.95688385
					0.4	2.07243562

an iterative spectral quasi-linearization method. The major findings are summarised below:

- 1) An increase in the curvature parameter and nanoparticle volume fraction significantly increases the nanofluid velocity profiles.
- 2) Higher values of the mixed convection parameter and velocity slip parameter retard the skin friction coefficient.
- 3) The thermal radiation parameter and heat generation parameters ($Q>0$) increase the rate of heat transfer, while the nanoparticle volume fraction, heat absorption parameter ($Q<0$) and thermal slip parameter decay the heat transfer rate.
- 4) Increasing the fluid parameter Γ reduces the skin friction coefficient while an increase in the velocity slip parameter increases the skin friction coefficient.

Nomenclature

- a Radius
- u, v Axial and radial velocity, respectively

ν	Kinematic viscosity
ρ	Density
σ	Electrical conductivity
B_0	Uniform magnetic field
g	Gravitational acceleration
β	Thermal expansion coefficient
T	Fluid temperature
T_∞	Reference temperature
κ	Thermal conductivity
C_p	Specific heat capacity
q_r	Radiative heat flux
σ^*	Stefan-Boltzman constant
κ^*	Coefficient of mean absorption
u_e	Free stream velocity
v_w	Suction/injection
ϕ	Solid volume fraction of the nanoparticle
Q_0	Uniform volumetric heat generation/ absorption coefficient
e_1	Velocity slip coefficient
e_2	Thermal slip coefficient
γ	Curvature parameter
Γ, δ	Fluid parameters
Ha	Hartman number
ε	Velocity ratio
λ	Mixed convection parameter
R_d	Thermal radiation parameter
θ_w	Temperature ratio parameter
Pr	Prandtl number
Q	Heat generation/heat absorption parameter
f_w	Suction/injection parameter
A_1	Velocity slip parameter
A_2	Thermal slip parameter
C_f	Skin friction coefficient
Nu	Local Nusselt number

References

- [1] CHOI S U S. Enhancing thermal conductivity of fluid with nanoparticles, developments and applications of non-Newtonian flow [J]. ASME FED, 1995, 231: 95–105.
- [2] SAIDA Z, SAIDUR R, RAHIMB N A, ALIMA M A. Analyses of exergy efficiency and pumping power for a conventional flat plate solar collector using SWCNTs based nanofluid [J]. Energy and Buildings, 2014, 97: 1–9.
- [3] JAIN S, HIRST D G, O'NEILLIVAN J M. Gold nanoparticles as novel agents for cancer therapy [J]. The British Journal of Radiology, 2012, 85: 101–113.
- [4] BUONGIORNO J J. Convective transport in nanofluids [J]. ASME, 2005, 128: 240–250.
- [5] DAS S, JANA R N. Natural convective magneto-nanofluid flow and radiative heat transfer past a moving vertical plate [J]. Alexandria Engineering Journal, 2015, 54(1): 55–64.
- [6] BACHOK N, ISHAK A, POPI I. Stagnation-point flow over a stretching/shrinking sheet in a nanofluid [J]. Nanoscale Research Letters, 2011, 6(1): 623.
- [7] RAMZAN M, FAROOQ M, HAYAT T, ALSAEDI A, CAO J. MHD stagnation point flow by a permeable stretching cylinder with Soret-Dufour effects [J]. Journal of Central South University, 2015, 22(2): 707–716.
- [8] HAYAT T, FAROOQ M, ALSAEDI A. Stagnation point flow of carbon nanotubes over stretching cylinder with slip conditions [J]. Open Physics, 2015, 13(1): 188–197.
- [9] ISHAK A, NAXARI R, POP I. Post-stagnation-point boundary layer flow mixed convection heat transfer over a vertical linearly stretching sheet [J]. Archive of Mechanics, 2008, 60(4): 303–322.
- [10] PAL D, MAL G, VAJRAVALU K. Mixed convection stagnation-point flow of nanofluids over a stretching/shrinking sheet in a porous medium with internal heat generation/absorption [J]. Communications in Numerical Analysis, 2015, 2015(1): 30–50.
- [11] ABBAS Z, MASOOD T, OLANREWAJU P O. Dual solutions of MHD stagnation point flow heat transfer over a stretching/shrinking sheet with generalized slip condition [J]. Journal of Central South University, 2015, 22(6): 2376–2384.
- [12] MUKHOPADHYAY S. MHD boundary layer slip flow along a stretching cylinder [J]. Ain Shams Engineering Journal, 2013, 4(2): 317–324.
- [13] MUKHOPADHYAY S. Effects of thermal radiation variable fluid viscosity on stagnation point flow past a porous stretching sheet [J]. Meccanica, 2013, 48(1): 1717–1730.
- [14] SARI M R, KEZZAR M, ADJABI R. Heat transfer of copper/water nanofluid flow through converging-diverging channel [J]. Journal of Central South University, 2016, 23(2): 484–496.
- [15] MAJID S, MOHAMMAD J. Optimal selection of annulus radius ratio to enhance heat transfer with minimum entropy generation in developing laminar forced convection of water- Al_2O_3 nanofluid flow [J]. Journal of Central South University, 2017, 24(8): 1850–1865.
- [16] MAHMOODI M, KELOUSI S. Kerosene–alumina nanofluid flow heat transfer for cooling application [J]. Journal of Central South University, 2016, 23(4): 983–990.
- [17] WUSIMAN K, CHUNG H, MD J N, HANDRY A, EOM Y, KIM J, JEONG H. Heat transfer characteristics of nanofluid through circular tube [J]. Journal of Central South University, 2013, 20(1): 142–148.
- [18] POWELL R E, EYRING H. Mechanisms for the relaxation theory of viscosity [J]. Nature, 1944, 154(1): 427–428.
- [19] JAVED T, ALI N, ABBAS Z, SAJID M. Flow of an Eyring-Powell non-Newtonian fluid over a stretching sheet [J]. Chemical Engineering Communications, 2013, 200(3): 327–336.
- [20] HAYAT T, IQBAL Z, QASIM M, OBAIDAT S. Steady flow of an Eyring-Powell fluid over a moving surface with convective boundary conditions [J]. International Journal of

- Heat Mass Transfer, 2012, 55(7): 1817–1822.
- [21] AKBAR N S, EBAID A, KHAN Z H. Numerical analysis of magnetic field effects on Eyring-Powell fluid flow towards a stretching sheet [J]. Journal of Magnetism Magnetic Materials, 2015, 382: 355–358.
- [22] BABU J M, SEEP N, RAJU C S K. Heat and mass transfer in MHD Eyring-Powell nanofluid flow due to cone in porous medium [J]. International Journal of Engineering Research in Africa, 2015, 19: 57–74.
- [23] HAYAT T, KHAN M I, WAQAS M, ALSAEDI A. Effectiveness of magnetic nanoparticles in radiative flow of Eyring-Powell fluid [J]. Journal of Molecular Liquids, 2017, 231: 126–133.
- [24] RAMZAN M, BILAL M, KANWAL S, CHUNG J D. Effects of variable thermal conductivity non-linear thermal radiation past an Eyring-Powell nanofluid flow with chemical reaction [J]. Communications in Theoretical Physics, 2017, 67(6): 723–731.
- [25] MALIK M Y, KHAN I, HUSSAIN A, SALAHUDDIN T. Mixed convection flow of MHD Eyring-Powell nanofluid over a stretching sheet: A numerical study [J]. AIP Advances, 2015, 5(11): 117118.
- [26] KHAN I, KHAN M, MALIK M Y, SALAHUDDIN T. Mixed convection flow of Eyring-Powell nanofluid over a cone plate with chemical reactive species [J]. Results in Physics, 2017, 7: 3716–3722.
- [27] MOTSA S S. A new spectral local linearization method for nonlinear boundary layer flow problems [J]. Journal of Applied Mathematics, 2013. Article 423628. DOI: 1155/2013/423628..
- [28] ROSSELAND S. Astrophysik und atom-theoretische grundlagen [M]. Springer-Verlag, 1931.
- [29] BELLMAN R E, KALABA R E. Quasilinearization nonlinear boundary-value problems [M]. R Corporation, 1965.
- [30] MOTSA S S, DLAMINI P G, KHUMALO M. Spectral relaxation method spectral quasilinearization method for solving unsteady boundary layer flow problems [J]. Advances in Mathematical Physics, 2014, Article ID 341964. DOI: 10.1155/2014/341964.
- [31] CANUTO C, HUSSAINI M Y, QUARTERONI A, THOMAS JR A. Spectral methods in fluid dynamics [M]. Springer Science & Business Media, 2012.
- [32] TREFETHEN L N. Spectral methods in MATLAB [M]. SIAM, 2000.
- [33] MAHAPATRA T R, GUPTA A S. Heat transfer in stagnation-point flow towards a stretching sheet [J]. Heat Mass Transfer, 2002, 38: 517–521.
- [34] ZAIMI K, ISHAK A. Stagnation-point flow towards a stretching vertical sheet with slip effects [J]. Mathematics, 2016, 4(2): 27. DOI: 10.3390/math4020027.

(Edited by YANG Hua)

中文导读

Eyring-Powell 磁纳米流体在伸缩圆柱上的热滑移混合对流

摘要： 供热冷却系统的优化设计必须考虑非线性过程的热辐射。本文研究了铜-水纳米流体在伸缩圆筒上的 Eyring-Powell 磁热辐射的混合对流动力学。考虑到非线性热辐射和热滑移条件，建立了能量守恒模型，分析了所涉及的流动参数以及表面摩擦系数和换热速率的影响。与许多已有的研究不同，最近的谱准线性化方法被用来解决耦合非线性边界值问题。计算结果表明，增大纳米粒子的体积分数、热辐射参数和热源参数可增强温度分布。速度滑移参数和流体材料参数增大了表面摩擦力。将数值结果与文献结果就某些极限情况进行比较，结果表现出很好的一致性。

关键词： Eyring-Powell 模型；伸缩圆筒；纳米流体；热辐射；滑移效应；谱准线性化方法

Chapter 3

Dynamical analysis of hydromagnetic Brownian and thermophoresis effects of squeezing Eyring–Powell nanofluid flow with variable thermal conductivity and chemical reactions

The analysis of the flow and heat transfer in a non-Fourier reactive Eyring-Powell nanofluid flow between two parallel plates using the spectral local linearization method is discussed in this chapter. We modified the Eyring-Powell nanofluid model studied in Chapter 2 by changing the geometry of the flow to be parallel channel flow. The revised model accounted for the impact of Brownian motion, thermophoresis, and chemical reaction effects. Furthermore, the heat flux is modeled using the non-Fourier heat flux with variable thermal conductivity. The justification for using the non-Fourier heat flux is to study the impact of the relaxation time the flow system.

Dynamical analysis of hydromagnetic Brownian and thermophoresis effects of squeezing Eyring–Powell nanofluid flow with variable thermal conductivity and chemical reaction

Dynamical analysis of hydromagnetic Brownian

Received 8 January 2019
Revised 17 March 2019
18 April 2019
Accepted 5 June 2019

Hammed Abiodun Ogunseye

*School of Mathematics, Statistics and Computer Science,
University of KwaZulu-Natal – Pietermaritzburg Campus,
Pietermaritzburg, South Africa*

Sulyman Olakunle Salawu

Department of Mathematics, Landmark University, Omu Aran, Nigeria

Yusuf Olatunji Tijani

*Department of Mathematics and Applied Mathematics,
Nelson Mandela University, Port Elizabeth, South Africa*

Mustapha Riliwan

Department of Mathematics, Lagos State University, Lagos, Nigeria, and

Precious Sibanda

*School of Mathematics, Statistics and Computer Science,
University of KwaZulu-Natal – Pietermaritzburg Campus,
Pietermaritzburg, South Africa*

Abstract

Purpose – The purpose of this paper is to investigate the dynamical behavior of heat and mass transfer of non-Newtonian nanofluid flow through parallel horizontal sheet with heat-dependent thermal conductivity and magnetic field. The effects of thermophoresis and Brownian motion on the Eyring–Powell nanofluid heat and concentration are also considered. The flow fluid is propelled by squeezing force and constant pressure gradient. The hydromagnetic fluid is induced by periodic time variations.

Design/methodology/approach – The dimensionless momentum, energy and species balance equations are solved by the spectral local linearization method that is employed to numerically integrate the coupled non-linear differential equations.

Findings – The response of the fluid flow, temperature and concentration to variational increase in the values of the parameters is graphically presented and discussed accordingly.

Originality/value – The validity of the method used was checked by comparing it with previous related article.

Keywords Nanofluid, Squeezing flow, Brownian motion, Non-Newtonian, Chemical reactive, Thermal conductivity

Paper type Research paper

1. Introduction

The fluid flow through parallel walls leads to squeezing flow, and this has fascinated the scientific researchers as a result of its existence in many engineering operations and applications such as polymer and food industries, injection and compression shaping, liquid-metal lubrication, etc. (Hayat *et al.*, 2016). The interaction of electromagnetic fields and



conducting liquids is the most famous aspect of magnetohydrodynamic (MHD) fluid; such fluids have applications in liquid-metal lubrication bearings (Siddiqui *et al.*, 2008; Salawu, 2018). For example, the uses of MHD liquid as lubricant are important to avoid the unpredicted changes that occur in lubricant viscosity in certain extreme conditions due to changes in temperature. The experimental and theoretical solution of MHD lubrication under forced thrust bearing was examined by Maki *et al.* (1966). Several researchers have studied the influence of magnetic field on lubrication in the past, such as the works of Hughes and Elco (1962) and Kuzma *et al.* (1988). Sheikholeslami *et al.* (2016) examined the effects of Brownian motion and thermophoresis on a nanofluid between parallel plates. Domairry and Hatami (2014) investigated the squeezing unsteady Cu–water nanofluid flow through horizontal plates by applying a differential transform method. Sheikholeslami *et al.* (2013) studied squeezing flow under different hydrodynamic nanofluid using the Adomian decomposition method. Ferromagnetic fluid heat transfer phenomenon past a stretching plate in the presence of thermal stratification and magnetic dipole impact on a thermally stratified ferrofluid were reported by Muhammad *et al.* (2017) and Muhammad *et al.* (2018b), respectively. Nadeem *et al.* (2018) explained the mathematical understanding of a bio-convective micropolar fluid.

The squeezing flow of non-Newtonian fluids in the presence of the heat and chemical reaction is gaining attention due to its mileage in chemical engineering and biological processes. There are diverse non-Newtonian fluids, such as Eyring–Powell fluid, which was derived from the kinetic liquids theory, and at high or low shear rates, it can reduce to Newtonian fluid. These characteristics make Eyring–Powell fluid more valuable than other non-Newtonian liquids. The rheological properties of such fluids cannot be formulated by one constitutive model in the shear rate and stress relation. The common Eyring–Powell fluid is the human blood. The necessity of heat transfer of Eyring–Powell fluid in the presence of chemical reaction cannot be over emphasized due to its importance and applications in the chemical industry such as polymer production, paints, suspension granular, shampoos solutions and so on. Malik *et al.* (2015) studied Eyring–Powell MHD convective nanofluid past an elongated sheet. The study showed that the fluid flow rate increases by enhancing Eyring–Powell and convective parameters. Hayat *et al.* (2014) examined the influences of radiation and non-uniform heat absorption/generation on the Eyring–Powell flow fluid through stretching inclined plates. It was reported that the flow rate and the heat distributions reduce with a rise in the unsteadiness term, whereas radiation parameter encourages heat flux, which, in turn, increases the fluid flow rate and heat content within the system. Jalil *et al.* (2013) obtained similarity solutions for the Eyring–Powell heat and species transport over a motioning sheet with a variable surface temperature. Nadeem and Saleem (2015) investigated the unsteady flow of Eyring–Powell nanofluid by adopting a series solution. In the study, it was observed that the fraction of the nanoparticle declined with the Lewis number and Brownian particle motion.

Recently, the study of the nanofluid thermophysical properties is gaining interest among the scientific scholars due to their great prospective usage in biomedical applications and fluid heat transfer. A nanofluid contains nanoparticles, which are made up of carbon nanotubes or carbides, oxide, and metals. The common base fluids are oil, ethylene glycol and water (Witharana *et al.*, 2011; Muhammada and Nadeem, 2017). Nanofluids possess unique characteristics that make them suitable and applicable in several heat transfer processes such as domestic refrigerator, fuel cells, heat exchanger, microelectronics, chiller, powered hybrid engines and many more (Kuznetsov and Nield, 2009). Nanofluids encourage convective heat and thermal conductivity coefficient, and their rheological behavior is found to be essential in determining their aptness for heat convective applications. Salehi *et al.* (2011) and Salimi-Yasar, Saeed, Mehdi, Ahmad and Ali (2017) carried out experimental study on nanofluid flow with the consideration of some effects of thermophysical properties on the fluid flow. Choi (1995) initiated the concept of nanofluid; the author established that thermal conductivity increases when a

small nanoparticle quantity is added to fluid heat transfer. Buongiorno (2006) introduced two nanofluid components of the non-homogenous equation. In the study, seven mechanisms slip between base fluid and nanoparticles were introduced, and the thermophoresis and a Brownian particle motion were taken into consideration. Shooting method of solutions of nanofluids heat transfer of magnetohydrodynamic viscous dissipation flow, prompted by a stretching permeable power-law surface, was examined by Dhanai *et al.* (2015). Various flow parameters' dual solutions were obtained, and it was noticed that viscous dissipation had a significant influence on the heat transfer, whereas the Brownian motion impact was not encouraging. Haroun, Sibanda, Mondal and Motsa (2015) adopted spectral relaxation method for the transient convective MHD nanaofluid over a shrinking sheet. The obtained results revealed that the skin-friction effect rose as the stretching rate and nanoparticle parameters increased, but the species transfer rate reduced as the nanoparticle increased. Extensive research has been carried out on nanofluid and nanoparticles, such as the works of Saeed *et al.* (2013), Rashidi *et al.* (2015), Saeed *et al.* (2015), Muhammad *et al.* (2018a) and Salehi *et al.* (2013). Another recent analysis on nanofluid was carried out by Abolbashari *et al.* (2015), Dalir *et al.* (2015), Haroun, Mondal and Sibanda (2015), Mehmood *et al.* (2016), Sher Akbar and Khan (2016), Sher Akbar *et al.* (2016), Salimi-Yasar, Saeed and Mehd (2017) and Mohammad *et al.* (2017).

Following the above studies, little work has been done on the analysis of hydromagnetic squeezing Eyring–Powell nanofluid. The present study focuses on the investigation of the hydromagnetic viscous squeezing non-Newtonian fluid flow with variable thermal conductivity in the presence of nanoparticle and chemical reaction. The flow is through impermeable stretching plates with time-dependent velocity. The thermophoresis and the Brownian motion effects are also considered. The dimensionless formulated equations are solved using an iterative technique called spectral local linearization method (SLLM). Computations are carried out and analyzed for the momentum and energy equations as well as the physical quantities for various non-Newtonian fluid parameters.

2. Mathematical formulation

We examine the magnetohydrodynamic squeezing flow of an incompressible chemically reactive Eyring–Powell nanofluid between two infinite parallel plates. The plates are $h(t) = \sqrt{((\nu_f(1-ct))/a)}$ distance apart, where $a > 0$ denotes the stretching rate of the lower plate, ν_f is the base nanofluid kinematic viscosity and c is the characteristic parameter with a dimension of inverse of time. The squeezing motion of the upper plate toward and away from the lower plate at a distance $h(t)$ is characterized by the velocity $V_h(t) = (dh/dt)$. The stretching velocity of the lower plate is given by $U_w(x, t) = ax/(1-ct)$, for $ct < 1$. (T_w, C_w) are the temperature and nanoparticles concentration at the lower plate, respectively, whereas the upper plate temperature and concentration at the upper plate are represented by (T_h, C_h) . A constant magnetic intensity $B = B_0(1-ct)^{-1/2}$ is applied in the y -direction, with negligible induced magnetic field, due to negligible magnetic Reynolds number. Also, the influence of Hall current, viscous dissipation and Joule heating is ignored. The effect of Brownian motion and thermophoresis is considered in the flow analysis. Furthermore, the Cattaneo–Christov heat flux with a variable thermal conductivity model is used to analyze the heat transfer process. With the above assumptions, the equation for conservation of mass, momentum balance, energy balance and concentration for the Eyring–Powell nanofluid is given as the following (Mahanthesh *et al.* 2017; Ahmed *et al.*, 2014; Hayat *et al.*, 2016):

$$\text{div } \mathbf{V} = 0, \quad (1)$$

$$\rho_f \frac{d\mathbf{V}}{dt} = \text{div } \boldsymbol{\tau} + \mathbf{J} \times \mathbf{B}, \quad (2)$$

MMMS

$$(\rho c_p)_f \left(\frac{dT}{dt} + \mathbf{V} \cdot \nabla T \right) = -\nabla \cdot \mathbf{q} + (\rho c)_p \left[D_B \nabla C \cdot \nabla T + \frac{D_T}{T_m} \nabla T \cdot \nabla T \right], \quad (3)$$

$$\frac{dC}{dt} + \mathbf{V} \cdot \nabla C = D_B \nabla^2 C + \frac{D_T}{T_m} \nabla^2 T, \quad (4)$$

$$\mathbf{J} \times \mathbf{B} = \frac{\sigma_f B_0^2}{1 - ct} \boldsymbol{\mu}, \quad (5)$$

where \mathbf{V} is the velocity vector, ρ_f is the base fluid density, d/dt is the material time differentiation, t is the time, $\boldsymbol{\tau}$ is the Cauchy tensor stress, \mathbf{J} is the electric current density, $(\rho c_p)_f$ is the heat capacity of the base fluid, T is the base fluid temperature, ∇ is the gradient operator, \mathbf{q} is the heat flux vector, $(\rho c)_p$ denotes the heat capacity of the nanoparticles, D_B is the Brownian diffusion coefficient, C is the nanoparticles' concentration, D_T is the thermophoretic diffusion coefficient, T_m is the mean fluid temperature and σ_f is the electrical conductivity of the nanofluid.

The heat flux vector, \mathbf{q} , which satisfied the following relationship, is utilized according to the Cattaneo–Christov model represented by Christov (2009) and Nadeem *et al.* (2017):

$$\mathbf{q} + \lambda_T \left(\frac{\partial \mathbf{q}}{\partial t} + \mathbf{V} \cdot \nabla \mathbf{q} - \mathbf{q} \cdot \nabla \mathbf{V} + (\nabla \cdot \mathbf{V}) \mathbf{q} \right) = -K(T) \nabla T, \quad (6)$$

where λ_T stands for the relaxation time of heat flux, $K(T)$ is the temperature-dependent thermal conductivity of the base fluid. It can be noted that when $\lambda_T = 0$, Equation (6) reduces to classical Fourier's law. Applying the incompressible condition, that is $\nabla \cdot \mathbf{V} = \text{div } \mathbf{V} = 0$, Equation (6) reduces to the following:

$$\mathbf{q} + \lambda_T \left(\frac{\partial \mathbf{q}}{\partial t} + \mathbf{V} \cdot \nabla \mathbf{q} - \mathbf{q} \cdot \nabla \mathbf{V} \right) = -K(T) \nabla T. \quad (7)$$

For an incompressible homogeneous Eyring–Powell fluid, the constitutive equation can be expressed as follows (see Javed *et al.*, 2013):

$$\boldsymbol{\tau} = -p\mathbf{I} + \mu A_1 + \left[\frac{1}{\beta |A_1|} \sinh^{-1} \left(\frac{1}{\gamma} |A_1| \right) \right] A_1, \quad (8)$$

where p denotes the fluid pressure, \mathbf{I} represents the identity tensor, μ is the dynamic viscosity, β and γ are characteristics of Eyring–Powell fluid, A_1 represents the Rivlin–Ericksen tensor, which is given by the following:

$$A_1 = (\nabla \mathbf{V}) + (\nabla \mathbf{V})^{\text{tr}}, \quad (9)$$

and:

$$|A_1| = \sqrt{\frac{1}{2} \text{trace}(A_1^2)}, \quad (10)$$

where superscript tr is the transpose. The hyperbolic function \sinh^{-1} can be approximated by taking the second-order Taylor expansion and neglecting higher order term as follows:

$$\sinh^{-1} \left(\frac{1}{\gamma} |A_1| \right) \cong \frac{|A_1|}{\gamma} - \frac{|A_1|^3}{6\gamma^3}, \quad \left| \frac{|A_1|}{\gamma} \right| \ll 1. \quad (11)$$

An unsteady two-dimensional squeezing flow under the Cartesian coordinates (x, y, z, t) is considered in this study. We seek velocity, temperature and concentration field in the

following form:

$$\mathbf{V} = [u(x, y, t), v(x, y, t), 0], \quad T = T(x, y, t) \text{ and } C = C(x, y, t). \quad (12)$$

With Equations (7)–(12), Equations (1)–(4) can be written in component form as follows:

$$\frac{\partial u}{\partial x} + \frac{\partial v}{\partial y} = 0, \quad (13)$$

$$\begin{aligned} \frac{\partial u}{\partial t} + u \frac{\partial u}{\partial x} + v \frac{\partial u}{\partial y} = & -\frac{1}{\rho_f} \frac{\partial p}{\partial x} + \left(v_f + \frac{1}{\rho_f \beta \gamma} \right) \left(\frac{\partial^2 u}{\partial x^2} + \frac{\partial^2 u}{\partial y^2} \right) - \frac{1}{3\rho_f \beta \gamma^3} \frac{\partial}{\partial x} \left[\left(4 \left(\frac{\partial u}{\partial x} \right)^2 + \left(\frac{\partial u}{\partial y} + \frac{\partial v}{\partial x} \right)^2 \right) \frac{\partial u}{\partial x} \right] \\ & - \frac{1}{6\rho_f \beta \gamma^3} \frac{\partial}{\partial y} \left[\left(4 \left(\frac{\partial u}{\partial x} \right)^2 + \left(\frac{\partial u}{\partial y} + \frac{\partial v}{\partial x} \right)^2 \right) \left(\frac{\partial u}{\partial y} + \frac{\partial v}{\partial x} \right) \right] - \frac{\sigma_f B_0^2 u}{\rho_f (1-ct)}, \end{aligned} \quad (14)$$

$$\begin{aligned} \frac{\partial v}{\partial t} + u \frac{\partial v}{\partial x} + v \frac{\partial v}{\partial y} = & -\frac{1}{\rho_f} \frac{\partial p}{\partial y} + \left(v_f + \frac{1}{\rho_f \beta \gamma} \right) \left(\frac{\partial^2 v}{\partial x^2} + \frac{\partial^2 v}{\partial y^2} \right) - \frac{1}{3\rho_f \beta \gamma^3} \frac{\partial}{\partial y} \left[\left(4 \left(\frac{\partial u}{\partial x} \right)^2 + \left(\frac{\partial u}{\partial y} + \frac{\partial v}{\partial x} \right)^2 \right) \frac{\partial v}{\partial y} \right] \\ & - \frac{1}{6\rho_f \beta \gamma^3} \frac{\partial}{\partial x} \left[\left(4 \left(\frac{\partial u}{\partial x} \right)^2 + \left(\frac{\partial u}{\partial y} + \frac{\partial v}{\partial x} \right)^2 \right) \left(\frac{\partial u}{\partial y} + \frac{\partial v}{\partial x} \right) \right], \end{aligned} \quad (15)$$

$$\begin{aligned} \frac{\partial T}{\partial t} + u \frac{\partial T}{\partial x} + v \frac{\partial T}{\partial y} + \lambda_E \Omega_E = & \frac{1}{(\rho c_p)_f} \frac{\partial}{\partial x} \left(K(T) \frac{\partial T}{\partial x} \right) + \frac{1}{(\rho c_p)_f} \frac{\partial}{\partial y} \left(K(T) \frac{\partial T}{\partial y} \right) \\ & + \frac{(\rho c)_p D_B}{(\rho c)_f} \left(\frac{\partial C}{\partial x} \frac{\partial T}{\partial x} + \frac{\partial C}{\partial y} \frac{\partial T}{\partial y} \right) + \frac{(\rho c)_p D_T}{(\rho c)_f T_m} \left(\left(\frac{\partial T}{\partial x} \right)^2 + \left(\frac{\partial T}{\partial y} \right)^2 \right), \end{aligned} \quad (16)$$

$$\frac{\partial C}{\partial t} + u \frac{\partial C}{\partial x} + v \frac{\partial C}{\partial y} = D_B \left(\frac{\partial^2 C}{\partial x^2} + \frac{\partial^2 C}{\partial y^2} \right) + \frac{D_T}{T_m} \left(\frac{\partial^2 T}{\partial x^2} + \frac{\partial^2 T}{\partial y^2} \right), \quad (17)$$

where:

$$\begin{aligned} \Omega_E = & \frac{\partial T^2}{\partial t^2} + u^2 \frac{\partial T^2}{\partial x^2} + \left(u \frac{\partial u}{\partial x} + v \frac{\partial u}{\partial y} + \frac{\partial u}{\partial t} \right) \frac{\partial T}{\partial x} + 2u \frac{\partial^2 T}{\partial x \partial t} + v^2 \frac{\partial T^2}{\partial y^2} \\ & + \left(v \frac{\partial v}{\partial y} + u \frac{\partial v}{\partial x} + \frac{\partial v}{\partial t} \right) \frac{\partial T}{\partial y} + 2v \frac{\partial^2 T}{\partial y \partial t} + 2uv \frac{\partial^2 T}{\partial x \partial y}, \end{aligned} \quad (18)$$

with the relevant boundary conditions given as the following:

$$u = U_w = \frac{ax}{1-ct}, \quad v = -\frac{V_0}{(1-ct)}, \quad T = T_w, \quad C = C_w \text{ at } y = 0, \quad (19)$$

$$u = 0, \quad v = V_h(t) = \frac{dh}{dt} = -\frac{c}{2} \sqrt{\frac{v_f}{a(1-ct)}}, \quad T = T_w + \frac{T_w}{1-ct}, \quad C = C_w + \frac{C_w}{1-ct} \text{ at } y = h(t), \quad (20)$$

where $V_0 > 0$ signifies the suction and $V_0 < 0$ indicates the injection velocity. Equations (13)–(20) are presented in the non-dimensional form, further reducing to a system of

Dynamical
analysis of
hydromagnetic
Brownian

MMMS

ordinary differential equation by introducing the following non-dimensional variables and similarity variable:

$$\eta = \sqrt{\frac{a}{v_f(1-ct)}}y, \quad u = \frac{ax}{(1-ct)}f'(\eta), \quad v = -\sqrt{\frac{av_f}{(1-ct)}}f(\eta),$$

$$T = T_w + \frac{T_w}{(1-ct)}\theta(\eta), \quad C = C_w + \frac{C_w}{(1-ct)}\phi(\eta). \quad (21)$$

Furthermore, the temperature-dependent thermal conductivity $K(T)$ is expressed as follows (Mishra *et al.*, 2010):

$$K(T) = K_0(1 + \alpha\theta), \quad (22)$$

where K_0 is the fluid thermal conductivity at ambient temperature, α is the thermal conductivity parameter and θ is the dimensionless nanofluid temperature. With Equation (21), Equation(13) is automatically fulfilled and Equations (14) and (15) after eliminating the generalized pressure gradient yields:

$$(1 + \varepsilon)f'''' + ff'''' - f'f'' - \frac{S}{2}(3f'' + \eta f''') - \varepsilon\delta(2f''f'''' + f''^2f''''') - M^2f'' = 0. \quad (23)$$

In addition, Equations (16)–(20) are reduced to the following form:

$$\theta'' + \alpha(\theta\theta'' + \theta'^2) + \text{Pr}\left(f\theta' - \frac{S}{2}(2\theta + \eta\theta')\right) + \text{Pr}(Nb\theta'\phi' + Nt\theta'^2)$$

$$+ \text{Pr}\Gamma\left(\frac{S}{2}\eta f'\theta' + \eta S f\theta'' + \frac{7S}{2}f\theta' - \frac{S^2}{4}(7\eta\theta' + 8\theta + \eta^2\theta'') - f^2\theta'' - ff'\theta''\right) = 0, \quad (24)$$

$$\phi'' + Scf\phi' - \frac{ScS}{2}(2\phi + \eta\phi') + \frac{Nt}{Nb}\theta'' = 0, \quad (25)$$

$$f = f_w, \quad f' = 1, \quad \theta = 0, \quad \phi = 0, \quad \text{at } \eta = 0, \quad (26)$$

$$f = \frac{S}{2}, \quad f' = 0, \quad \theta = 1, \quad \phi = 1, \quad \text{at } \eta = 1, \quad (27)$$

where ε and δ denote fluid parameters, S is the squeezing parameter, M represents the magnetic field parameter, Pr is the Prandtl number, Nb stands for the Brownian motion parameter, Nt stands for thermophoresis parameter, Γ is thermal relaxation parameter, Sc denotes the Schmidt number and f_w represents the suction ($f_w > 0$) or injection ($f_w < 0$) parameter. These dimensionless parameters are defined as follows:

$$\varepsilon = \frac{1}{\mu_f\beta\gamma}, \quad S = \frac{c}{a}, \quad \delta = \left(\frac{a}{1-ct}\right)\frac{x^2}{v_f\gamma^2}, \quad M = B_0\sqrt{\frac{\sigma_f}{\rho_f a}}, \quad \text{Pr} = \frac{(\mu c_p)_f}{K_0}, \quad \Gamma = \frac{a\lambda_E}{1-ct}$$

$$\text{Nb} = \frac{C_w D_B (\rho c_p)_p}{v_f(1-ct)(\rho c_p)}, \quad \text{Nt} = \frac{T_w D_T (\rho c_p)_p}{v_f(1-ct)T_m(\rho c_p)_f}, \quad f_w = \sqrt{\frac{V_0}{av_f(1-ct)}}, \quad \text{Sc} = \frac{v_f}{D_B}. \quad (28)$$

Another physical property of interest is the skin-friction coefficient C_f , which is expressed as follows:

$$C_f = \frac{\tau_w}{\rho V_h^2}; \quad \tau_w = \left(\mu + \frac{1}{\beta\gamma} \right) \frac{\partial u}{\partial y} - \frac{1}{6\beta\gamma^3} \left(\frac{\partial u}{\partial y} \right)^3 \Big|_{y=h(t)}, \quad (29)$$

$$\text{Sh} = - \frac{x}{C_h - C_w} \frac{\partial C}{\partial y} \Big|_{y=h(t)}. \quad (30)$$

Dynamical
analysis of
hydromagnetic
Brownian

Equations (29)–(30) in dimensionless form are expressed as follows:

$$\frac{c^2}{4a^2} C_f \text{Re}_x^{-(1/2)} = (1 + \varepsilon) f''(1) - \frac{\varepsilon \delta}{3} f'''(1), \quad \text{Re}_x^{-(1/2)} \text{Sh} = -\phi'(1), \quad (31)$$

where $\text{Re}_x = (ax^2/(\nu(1-ct)))$ represents the local Reynolds number.

3. Method of solution

In this section, an efficient iterative method called the SLLM, which was proposed by Motsa (2013), is employed to numerically integrate the coupled non-linear differential Equations (23)–(25) with the boundary conditions (Equations (26) and (27)). To apply this technique, we consider the following non-linear differential operators:

$$\Omega_f = (1 + \varepsilon) f_n'''' + f_n f_n'' - f_n' f_n'' - \frac{S}{2} (3f_n'' + \eta f_n''') - \varepsilon \delta (2f_n'' f_n'' + f_n'' f_n''') - M^2 f_n'', \quad (32)$$

$$\begin{aligned} \Omega_\theta = & \theta_n'' + \alpha (\theta_n \theta_n'' + \theta_n'^2) + \text{Pr} \left(f_n \theta_n' - \frac{S}{2} (2\theta_n + \eta \theta_n') \right) + \text{Pr} (Nb \theta_n' \phi_n' + Nt \theta_n'^2) \\ & + \text{Pr} \Gamma \left(\frac{S}{2} \eta f_n' \theta_n' + \eta S f_n \theta_n'' + \frac{7S}{2} f_n \theta_n' - \frac{S^2}{4} (7\eta \theta_n' + 8\theta_n + \eta^2 \theta_n'') - f_n^2 \theta_n'' - f_n f_n' \theta_n' \right), \quad (33) \end{aligned}$$

$$\Omega_\phi = \phi_n'' + Sc f_n \phi_n' - \frac{ScS}{2} (2\phi_n + \eta \phi_n') + \frac{Nt}{Nb} \theta_n'', \quad (34)$$

Equations (32)–(34) can be decoupled according to the following algorithm:

- (1) From Ω_f , solve for f_n .
- (2) Next, solve for θ_n from Ω_θ using the updated solution of f_n , that is, f_{n+1} and assuming the solution of ϕ_n is known from the previous iteration.
- (3) Finally, solve for ϕ_n from Ω_ϕ using the solutions of f_n and θ_n .

In the framework of the SLLM, the following iterative scheme is obtained:

$$a_{1,n} f_{n+1}'''' + a_{2,n} f_{n+1}'' + a_{3,n} f_{n+1}' + a_{4,n} f_{n+1}' + a_{5,n} f_{n+1} = R^f, \quad (35)$$

$$a_{6,n} \theta_{n+1}'' + a_{7,n} \theta_{n+1}' + a_{8,n} \theta_{n+1} = R^\theta, \quad (36)$$

$$a_{9,n} \phi_{n+1}'' + a_{10,n} \phi_{n+1}' + a_{11,n} \phi_{n+1} = R^\phi, \quad (37)$$

$$\begin{aligned} f_{n+1}(0) = f_w, \quad f_{n+1}'(0) = 1, \quad f_{n+1}(1) = 1, \quad f_{n+1}'(1) = 0, \quad \theta_{n+1}(0) = 0, \\ \theta_{n+1}(1) = 1, \quad \phi_{n+1}(0) = 0, \quad \phi_{n+1}(1) = 1. \quad (38) \end{aligned}$$

MMMS

The coefficients in Equations (35)–(37) along with their right-hand side are defined as follows:

$$\begin{aligned}
a_{1,n} &= \frac{\partial \Omega_f}{\partial f_n''''}, & a_{2,n} &= \frac{\partial \Omega_f}{\partial f_n'''}, & a_{3,n} &= \frac{\partial \Omega_f}{\partial f_n''}, & a_{4,n} &= \frac{\partial \Omega_f}{\partial f_n'}, & a_{5,n} &= \frac{\partial \Omega_f}{\partial f_n}, & a_{6,n} &= \frac{\partial \Omega_\theta}{\partial \theta_n''}, & a_{7,n} &= \frac{\partial \Omega_\theta}{\partial \theta_n'}, \\
a_{8,n} &= \frac{\partial \Omega_\theta}{\partial \theta_n}, & a_{9,n} &= \frac{\partial \Omega_\phi}{\partial \phi_n''}, & a_{10,n} &= \frac{\partial \Omega_\phi}{\partial \phi_n'}, & a_{11,n} &= \frac{\partial \Omega_\phi}{\partial \phi_n}, \\
R^f &= a_{1,n} f_n'''' + a_{2,n} f_n'''' + a_{3,n} f_n'' + a_{4,n} f_n' + a_{5,n} f_n - \Omega_f, \\
R^\theta &= a_{6,n} \theta_n'' + a_{7,n} \theta_n' + a_{8,n} \theta_n - \Omega_\theta, & R^\phi &= a_{9,n} \phi_n'' + a_{10,n} \phi_n' + a_{11,n} \phi_n - \Omega_\phi.
\end{aligned} \tag{39}$$

Equations (36)–(38) are integrated numerically using the Chebyshev pseudo-spectral technique (see Canuto *et al.*, 2012; Motsa *et al.*, 2011; Maleki *et al.*, 2012). In order to apply this technique, the interval $[0, 1]$ is mapped into the interval $[-1, 1]$ using the transformation $\eta = (1/2)(\xi + 1)$, on which the Chebyshev pseudo-spectral technique can be used. The unknown functions $f(\eta)$, $\theta(\eta)$ and $\phi(\eta)$ are then discretized using the Chebyshev–Gauss–Lobatto collocation points:

$$\zeta_k = \cos\left(\frac{\pi k}{\bar{N}}\right), \quad k = 0, 1, \dots, \bar{N}; \quad -1 \leq \xi \leq 1. \tag{40}$$

The derivatives of $f(\eta)$, $\theta(\eta)$ and $\phi(\eta)$ are computed using the Chebyshev differentiation matrix D (see Trefethen, 2000) at the collocation points as a matrix vector product:

$$\begin{aligned}
\frac{df}{d\eta} &= \sum_{i=0}^{\bar{N}} D_{ij} f(\zeta_i) = \mathbf{D}F, \quad j = 0, 1, 2, \dots, \bar{N}, \\
\frac{d\theta}{d\eta} &= \sum_{i=0}^{\bar{N}} D_{ij} \theta(\zeta_i) = \mathbf{D}\Theta, \quad j = 0, 1, 2, \dots, \bar{N}, \\
\frac{d\phi}{d\eta} &= \sum_{i=0}^{\bar{N}} D_{ij} \phi(\zeta_i) = \mathbf{D}\Phi, \quad j = 0, 1, 2, \dots, \bar{N},
\end{aligned} \tag{41}$$

where $\bar{N} + 1$ is the number of collocation points, $\mathbf{D} = 2D$, $F = [f(\zeta_0), f(\zeta_1), \dots, f(\zeta_{\bar{N}})]^T$, $\Theta = [\theta(\zeta_0), \theta(\zeta_1), \dots, \theta(\zeta_{\bar{N}})]^T$ and $\Phi = [\phi(\zeta_0), \phi(\zeta_1), \dots, \phi(\zeta_{\bar{N}})]^T$ are vector functions at the collocation points. The higher order derivatives of f , θ and ϕ are evaluated as powers of \mathbf{D} :

$$f^s(\eta) = \mathbf{D}^s F, \quad \theta^s(\eta) = \mathbf{D}^s \Theta, \quad \phi^s(\eta) = \mathbf{D}^s \Phi. \tag{42}$$

Substituting Equations (41)–(43) into Equations (36)–(38) yields the following decoupled matrices:

$$\begin{bmatrix} 1 & & & & & \dots & 0 \\ \mathbf{D}_{1,1} & & & & & \dots & \mathbf{D}_{1,\bar{N}+1} \\ \text{diag}[a_{1,n}] \mathbf{D}^4 + \text{diag}[a_{2,n}] \mathbf{D}^3 + \text{diag}[a_{3,n}] \mathbf{D}^2 + \text{diag}[a_{4,n}] \mathbf{D} + \text{diag}[a_{5,n}] \mathbf{I} & & & & & \dots & \\ \mathbf{D}_{\bar{N},1} & & & & & \dots & \mathbf{D}_{\bar{N},\bar{N}+1} \\ 0 & & & & & \dots & 1 \end{bmatrix} \begin{bmatrix} f_{n+1}(\zeta_0) \\ f_{n+1}(\zeta_1) \\ \vdots \\ \vdots \\ f_{n+1}(\zeta_{\bar{N}-1}) \\ f_{n+1}(\zeta_{\bar{N}-1}) \end{bmatrix}$$

$$= \begin{bmatrix} \frac{S}{2} \\ R_{n+1}^f(\xi_1) \\ \vdots \\ \vdots \\ 1 \\ F_w \end{bmatrix}, \quad (43)$$

$$\begin{bmatrix} 1 & & & \dots & 0 \\ \text{diag}[a_{5,n}]\mathbf{D}^2 + \text{diag}[a_{6,n}]\mathbf{D} + \text{diag}[a_{7,n}]\mathbf{I} & & & & \\ 0 & & & \dots & 1 \end{bmatrix} \begin{bmatrix} \theta_{n+1}(\xi_0) \\ \vdots \\ \theta_{n+1}(\xi_{\bar{N}}) \end{bmatrix} = \begin{bmatrix} 1 \\ R_{n+1}^\theta(\xi_1) \\ \vdots \\ 0 \end{bmatrix}, \quad (44)$$

$$\begin{bmatrix} 1 & & & \dots & 0 \\ \text{diag}[a_{5,n}]\mathbf{D}^2 + \text{diag}[a_{6,n}]\mathbf{D} + \text{diag}[a_{7,n}]\mathbf{I} & & & & \\ 0 & & & \dots & 1 \end{bmatrix} \begin{bmatrix} \phi_{n+1}(\xi_0) \\ \vdots \\ \phi_{n+1}(\xi_{\bar{N}}) \end{bmatrix} \\ = \begin{bmatrix} 1 \\ R_{n+1}^\phi(\xi_1) \\ \vdots \\ 0 \end{bmatrix}, \quad (45)$$

here, \mathbf{I} is an $(\bar{N}+1) \times (\bar{N}+1)$ identity matrix and $\text{diag}[\]$ denotes a diagonal matrix. The following initial approximation is used to initialize the SLLM schemes:

$$f_0(\eta) = 2\eta^2 + \eta^3 + fw(2\eta^3 - 3\eta^2 + 1) + S\eta^2 \left(\frac{3}{2} - \eta \right), \quad \theta_0(\eta) = \eta, \quad \phi_0(\eta) = \eta. \quad (46)$$

4. Numerical validation

The case $\varepsilon = \alpha = 0$ and $\Gamma = 0$ corresponds to a Newtonian fluid with classical Fourier law with constant thermal conductivity, which has been studied by Hayat *et al.* (2016) using the homotopy analysis method. To validate the correctness of the numerical results obtained from the iterative scheme given by Equations (36)–(39), the local Sherwood number, $-\phi(1)$, at the fourth iteration, with $N = 20$, is compared with Hayat *et al.* (2016) in Table I. It is apparent from this table that there is a good agreement between the two results.

Nt	Nb	Hayat <i>et al.</i> (2016)	$f''(0)$ SLLM	Relative error
	0.5	1.21380	1.21380229	0
0.2		1.24143	1.24142703	0
0.5		1.37544	1.37544311	0
0.0		1.79329	1.79328569	0
0.2	1	1.25874	1.258739599	0
	1.5	1.26016	1.26016234	0

Table I.
Comparison of the SLLM results for $-\phi(1)$ with Hayat *et al.* (2016) for distinct values of Nt and Nb when $\varepsilon = \alpha = \Gamma = 0$, $M = 0.5$, and $S = \text{Pr} = \text{Sc} = 1$

5. Results and discussion

Figures 1 and 2 demonstrate the reaction of the fluid velocity to ascending changes in the fluid parameters values ε and δ . An increase in the term ε , as shown in Figure 1, discourages the fluid bonding forces by causing fast collision in the fluid particles, enhancing the fluid to move fast and thereby increasing the velocity distribution. In Figure 2, a rise in the values of the term δ leads to a decline in the flow rate. The term encourages the fluid viscosity by increasing the non-Newtonian viscoelasticity, which results in decreasing the velocity field as depicted in the plot.

The impact of the squeezing parameter S and the magnetic field parameter M on the flow momentum equation is presented in Figures 3 and 4. From Figure 3, a noteworthy increase in the profile is observed as the parameter values rise. This is because the parameter stimulated the heat source term in the equations that causes more heat to be generated within the non-Newtonian nanofluid system and leads to break down in the viscoelastic bonding force. Therefore, the flow is prompted and the velocity profile is increased. Figure 4 shows a decrease in the flow rate toward the center of the system due to the influence of the Lorentz force that drags and strengthens the nanofluid viscosity but rises gradually as it moves toward the free stream due to the impact of the squeezing force that relaxes the fluid dragging force.

Figure 5 illustrates the effect of the suction term f_w on the Eyring–Powell boundary layer fluid flow through parallel plates. The flow rate reduces monotonically with the increase in parameter f_w . This is an indication that the boundary layer growth is stabilized and hence prevents separation in the boundary layers. Thus, sucking the decelerated fluid particles reduces the growth of the fluid boundary layers. The effect of the squeezing term S on the heat profile is exhibited in Figure 6. The fluid temperature diminishes as the values of the term S rise due to thinning in the thermal boundary layer, which implies an increase in

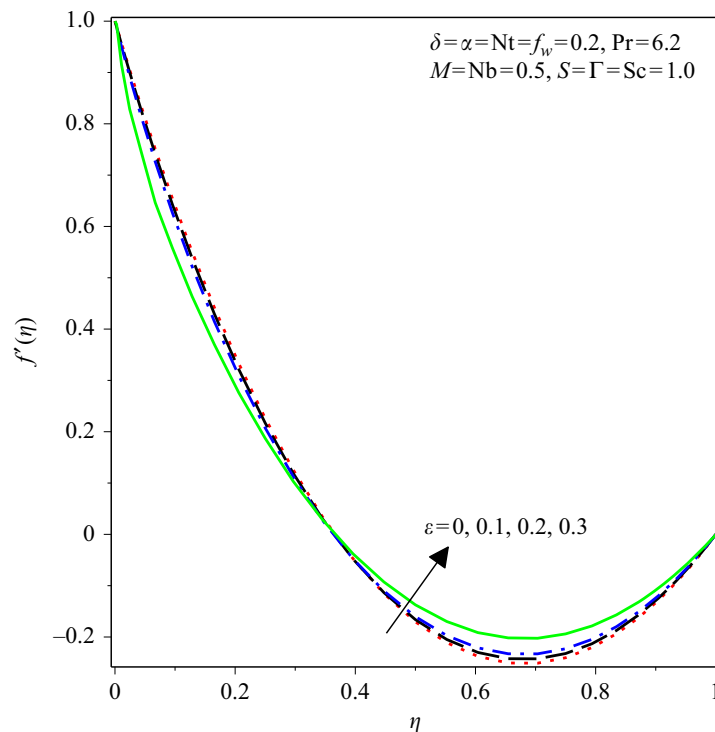


Figure 1.
Velocity profiles for
different values of the
fluid parameter ε

Dynamical
analysis of
hydromagnetic
Brownian

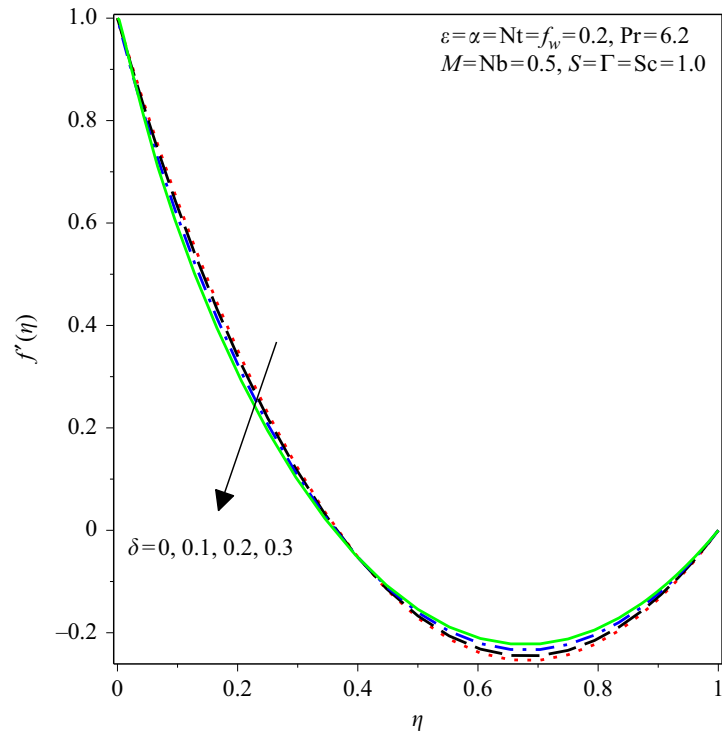


Figure 2.
Velocity profiles for
different values of the
fluid parameter δ

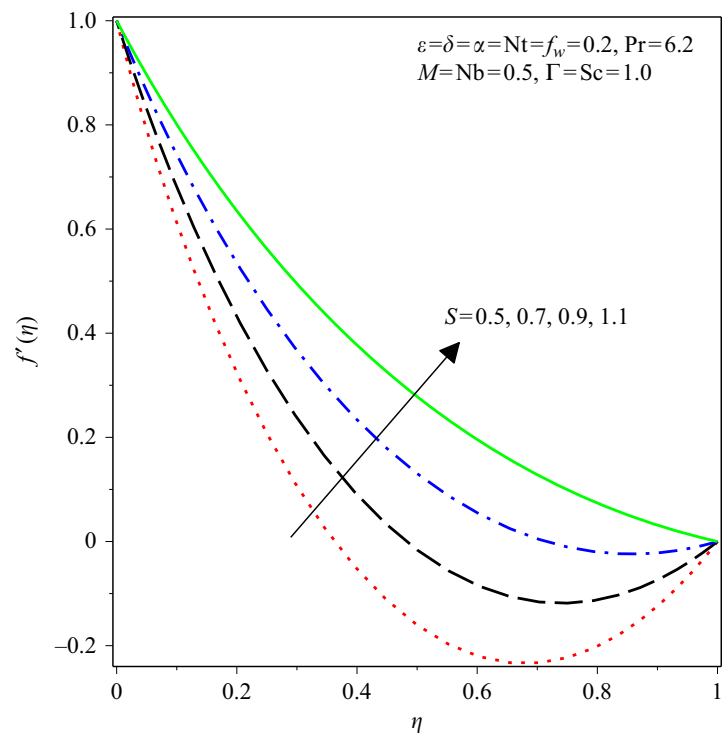


Figure 3.
Velocity profiles for
different values of the
squeezing parameter S

MMMS

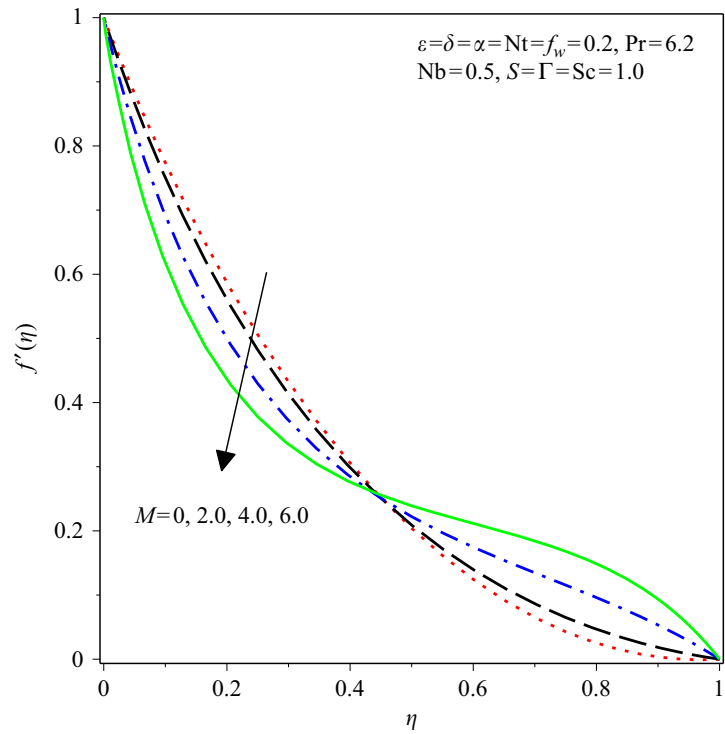


Figure 4.
Velocity profiles for different values of the magnetic parameter M

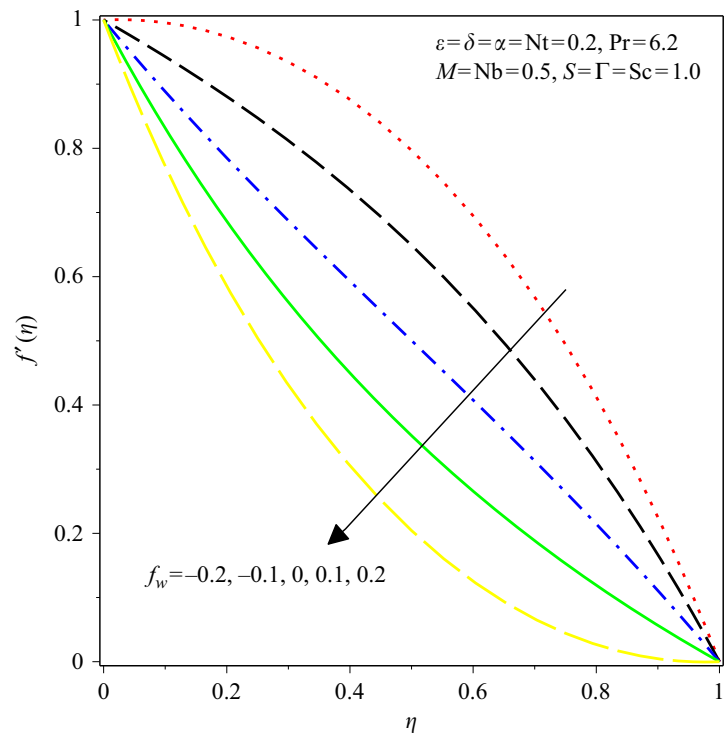


Figure 5.
Velocity profiles for different values of the suction/injection parameter f_w

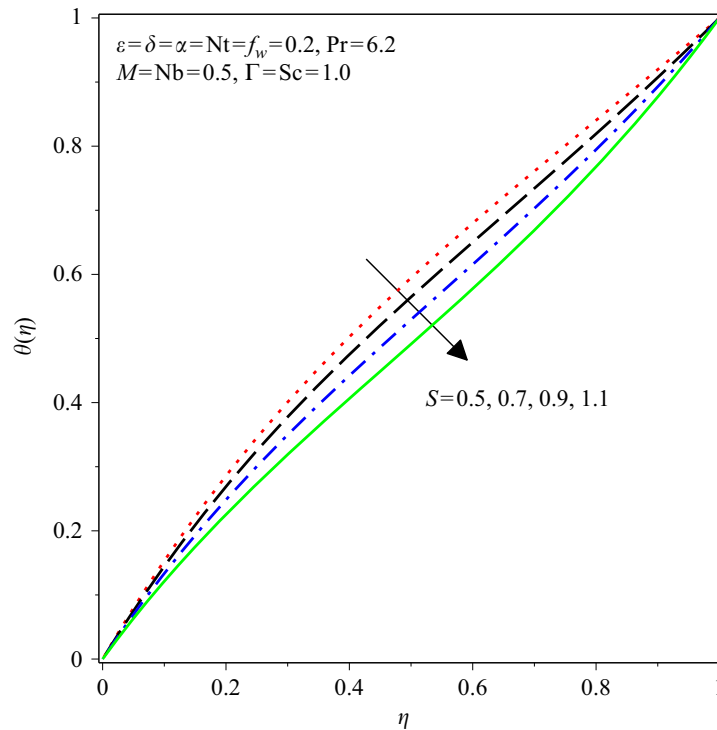


Figure 6.
Temperature profiles
for different values of
the squeezing
parameter S

the surface shear stress. Therefore, loss of heat to the surroundings is noticed, which, in turn, decreases the energy distribution within the system.

In Figures 7 and 8, the response of the nanofluid temperature to changes in the thermal conductivity and relaxation parameters α and Γ is, respectively, represented. An increase in the heat field is seen as the term α increases; this is expected, as it was previously reported by Choi (1995). The thermal conductivity term α is temperature dependent, and a change in the heat within the system is observed to increase the temperature. Hence, the heat distribution rises as the term increases. The presence of nanoparticles induces heat source term and fluid thermal conductivity, which significantly enhances temperature distribution. But enhancing the values of the term Γ reduces the heat transfer rate within the system, for the term relaxes the viscous heat source term by causing the temperature profile to decrease, as shown in Figure 8.

Figures 9 and 10 show the reaction of the Eyring–Powell nanofluid temperature to variational rise in the suction/injection f_w and thermophoresis Nt parameters. Both parameters enhance the viscous heat source term that leads to the increase in the internal heat production within the system and the thickness of the thermal boundary layer that reduces the quantity of heat that leaves the system. This thereby encourages a significant rise in the temperature distribution. Suction parameter f_w causes the flow of fluid and heat into a partially filled space, whereas thermophoresis (soret) is an occurrence where different nanoparticle types respond to heat gradient force differently. Therefore, the parameters boost the temperature field.

Figure 11 depicts the influence of the Brownian motion parameter Nb on the squeezing nanofluid flow temperature. Brownian motion term Nb causes fast random movement as a result of collision of the particles. The nanoparticles kinetic energies, vibrations and molecular rotations encourage the fluid's caloric component, which, in turn, leads to a high internal energy generation as the parameter Nb is enhanced. This stimulated the system

MMMS

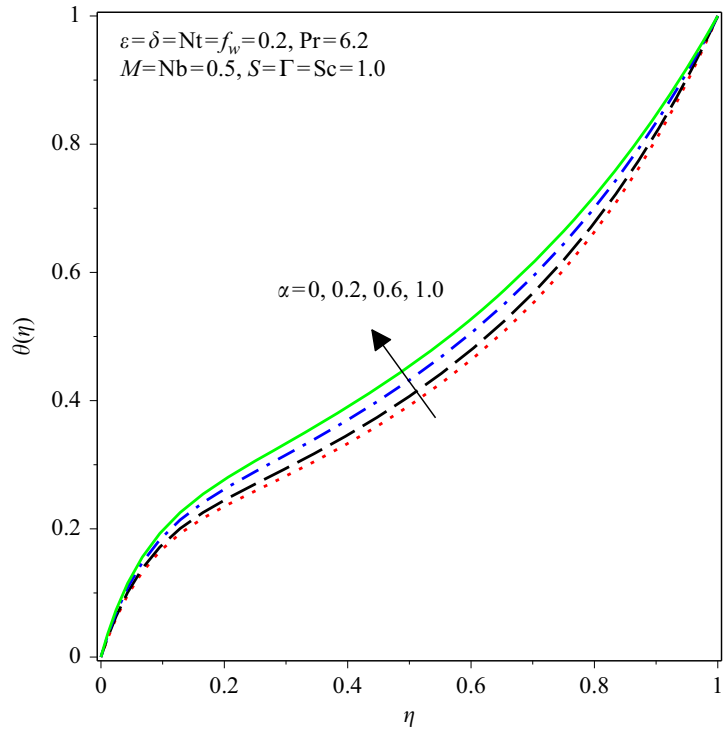


Figure 7.
Temperature profiles
for different values of
the thermal
conductivity
parameter α

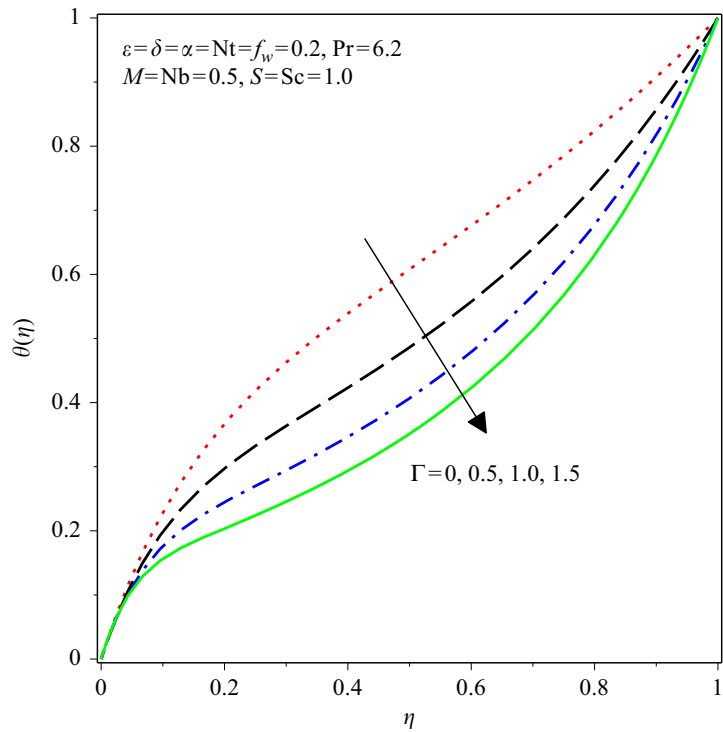


Figure 8.
Temperature profiles
for different values of
the thermal relaxation
parameter Γ

Dynamical
analysis of
hydromagnetic
Brownian

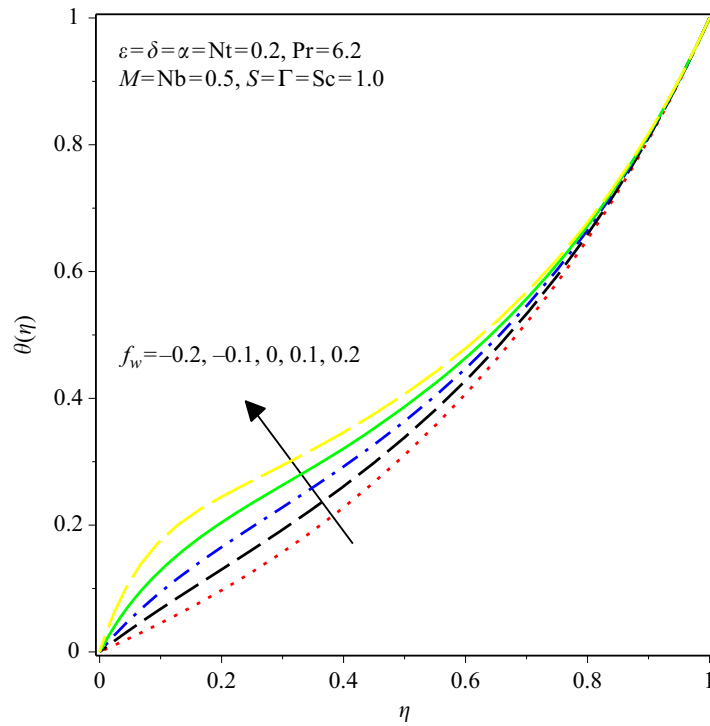


Figure 9.
Temperature profiles
for different values of
the suction/injection
parameter f_w

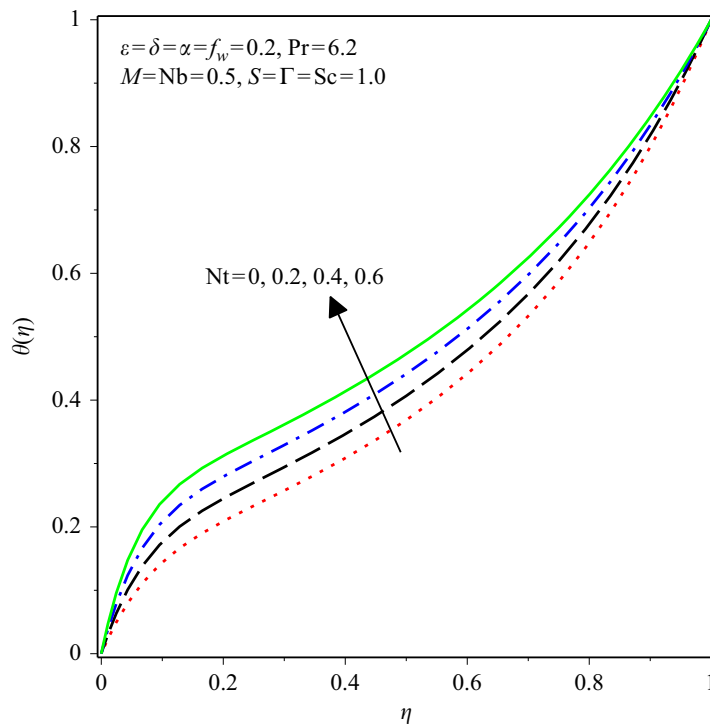


Figure 10.
Temperature profiles
for different values of
the thermophoresis
parameter Nt

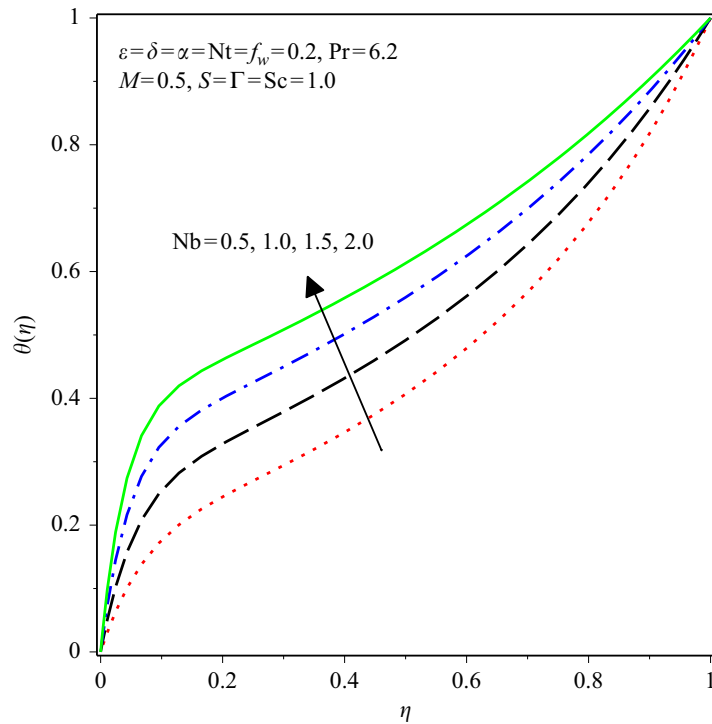


Figure 11.
Temperature profiles for different values of the Brownian motion parameter Nb

heat content, which, in turn, produced an increasing temperature profile. Figure 12 demonstrates the concentration distribution for different ascending values of Schmidt number Sc . Schmidt number Sc is the ratio of viscosity and mass diffusivities; it relates the species boundary layer and hydrodynamic layer. An increase in parameter Sc diminishes the nanofluid species transfer profile. This is because the species reaction rate term decreases with the increase in the parameter values, thereby slowing down the chemical reaction rate profile.

The impact of thermophoresis term Nt and Brownian motion term Nb is, respectively, presented in Figures 13 and 14. The squeezing flow effect is seen in Figure 13, as parameter Nt initially decreases the Eyring–Powell nanaofluid concentration field near the plate surface but rises as it moves farther distance from the plate. In Figure 14, the Brownian motion influence on the concentration is displayed. The results show that an increase in the term Nb discourages the mass transfer within the system, resulting in the reduction of the profile.

6. Conclusion

By using graphical illustration plotted on Maple computing platform, the study revealed that hydromagnetic Brownian parameter reduces the mass transfer, which then leads to a reduction in the concentration profile. Meanwhile, a different trend is noticed in the temperature profile, as increase in the hydromagnetic Brownian parameter enhances the temperature profile. Thermophoresis parameter has similar behavior with hydromagnetic Brownian parameter, except in the concentration profile in which the parameter at first retards the profile but at a later time, far away from the plate, increases the profile.

Dynamical analysis of hydromagnetic Brownian

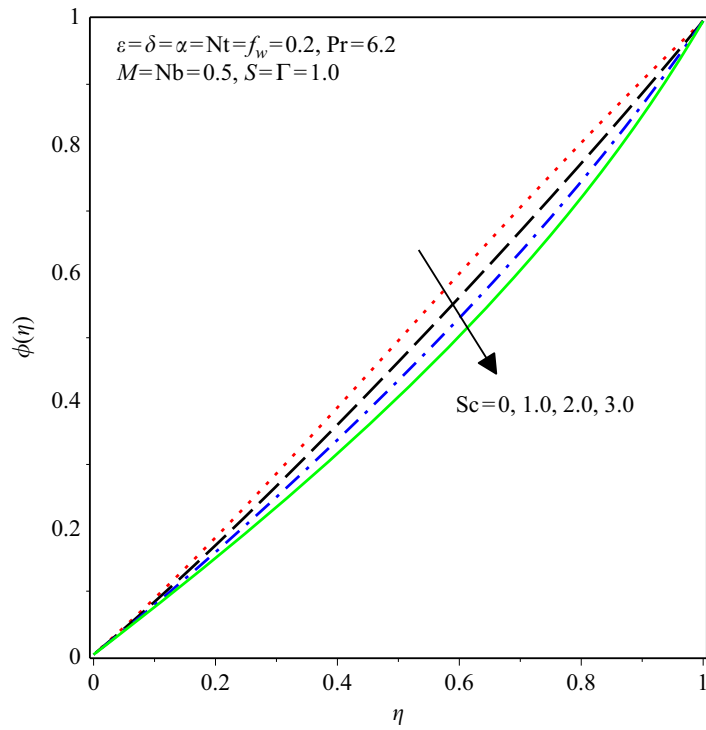


Figure 12. Concentration profiles for different values of the Schmidt number Sc

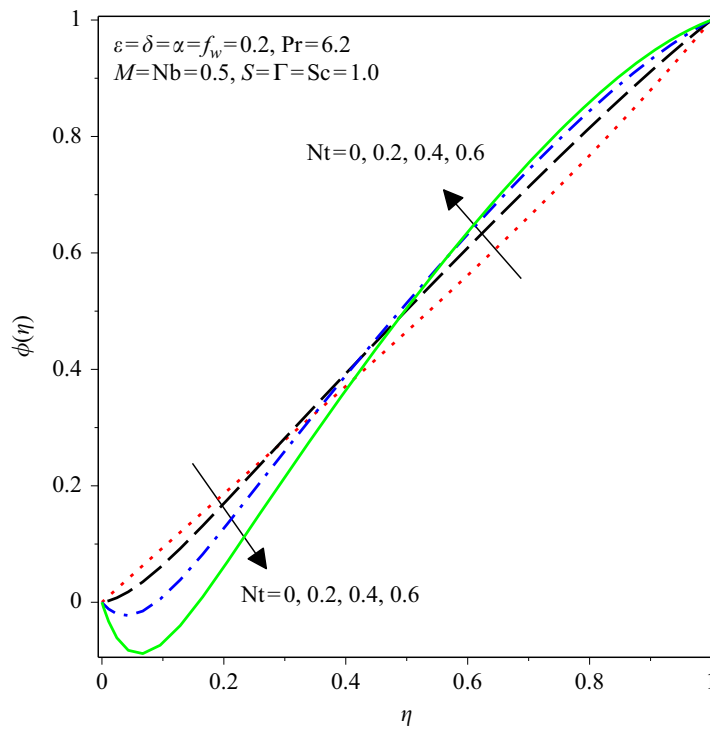


Figure 13. Concentration profiles for different values of the thermophoresis parameter Nt

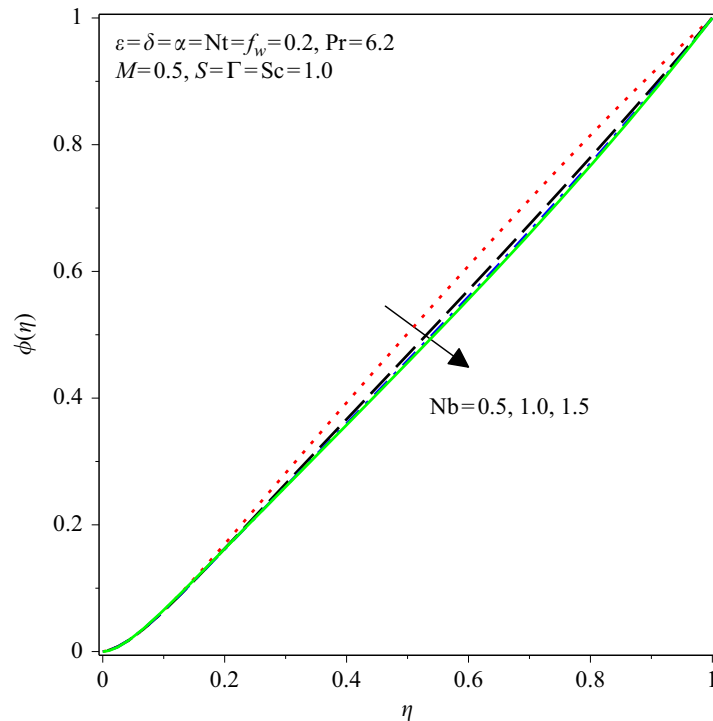


Figure 14.
Concentration profiles
for different values of
the Brownian motion
parameter Nb

References

- Abolbashari, M.H., Freidoonimehr, N., Nazari, F. and Rashidi, M.M. (2015), "Analytical modeling of entropy generation for Casson nano-fluid flow induced by a stretching surface", *Advanced Powder Technology*, Vol. 26 No. 2, pp. 542-552.
- Ahmed, S., Anwar, B. and Ghosh, S.K. (2014), "Couple stress fluid modeling on free convection oscillatory hydromagnetic flow in an inclined rotating channel", *Ain Shams Engineering Journal*, Vol. 5 No. 4, pp. 1249-1265.
- Buongiorno (2006), "Convective transport in nanofluids", *Journal of Heat Transfer*, Vol. 128 No. 3, pp. 240-250.
- Canuto, C., Hussaini, M.Y., Quarteroni, A., Thomas, A. Jr and Zang, T.A. (2012), *Spectral Method in Fluid Dynamic*, Springer Science & Business Media, Berlin.
- Choi, S.U.S. (1995), "Enhancing thermal conductivity of fluids with nanoparticles", *ASME International Mechanical Engineering Congress & Exposition*, Vol. 231 No. 1, pp. 99-106.
- Christov, C.I. (2009), "On frame indifferent formulation of the Maxwell–Cattaneo model of finite-speed heat conduction", *Mechanics Research Communications*, Vol. 36 No. 4, pp. 481-486.
- Dalir, N., Dehsara, M. and Salman, S.S. (2015), "Entropy analysis for magnetohydrodynamic flow and heat transfer of a Jeffrey nanofluid over a stretching sheet", *Energy*, Vol. 79, pp. 351-362, available at: <https://doi.org/10.1080/01430750.2019.1614984>
- Dhanai, R., Rana, P. and Kumar, L. (2015), "Multiple solutions of MHD boundary layer flow and heat transfer behavior of nanofluids induced by a power-law stretching/shrinking permeable sheet with viscous dissipation", *Powder Technology*, Vol. 273 No. 2, pp. 62-70.
- Domairry, G. and Hatami, H. (2014), "Squeezing cu-water nanofluid flow analysis between parallel plates by DTM-Pade method", *Journal of Molecular Liquids*, Vol. 193 No. 1, pp. 37-44.

- Haroun, N.A., Sibanda, P., Mondal, S. and Motsa, M.M. (2015), "On unsteady MHD mixed convection in a nanofluid due to a stretching/shrinking surface with suction/injection using the spectral-relaxation method", *Boundary Value Problems*, Vol. 1 No. 3, pp. 1-17.
- Haroun, N.A.H., Mondal, S. and Sibanda, P. (2015), "Unsteady natural convective boundary-layer flow of MHD nanofluid over a stretching surfaces with chemical reaction using the spectral relaxation method: a revised model", *Procedia Engineering*, Vol. 127 No. 1, pp. 18-24.
- Hayat, T., Asad, S., Mustafa, M. and Alsaedi, A. (2014), "Radiation effects on the flow of Powell-Eyring fluid past an unsteady inclined stretching sheet with non-uniform heat source/sink", *Plos One*, Vol. 9 No. 7, pp. 1-14.
- Hayat, T., Muhammad, T., Qayyum, A., Alsaedi, A. and Mustafa, M. (2016), "On squeezing flow of nanofluid in the presence of magnetic field effects", *Journal of Molecular Liquids*, Vol. 213 No. 1, pp. 179-185.
- Hughes, W.F. and Elco, R.A. (1962), "Magneto-hydrodynamic lubrication flow between parallel rotating disks", *Journal of Fluid Mechanics*, Vol. 13 No. 1, pp. 21-32.
- Jalil, M., Asghar, S. and Imran, S.M. (2013), "Self similar solutions for the flow and heat transfer of Powell-Eyring fluid over a moving surface in a parallel free stream", *International Journal of Heat and Mass Transfer*, Vol. 65 No. 1, pp. 73-79.
- Javed, T., Ali, N., Abbas, Z. and Sajid, M. (2013), "Flow of an Eyring-Powell non-Newtonian fluid over a stretching sheet", *Chemical Engineering Communications*, Vol. 200 No. 3, pp. 327-336.
- Kuzma, D.C., Maki, E.R. and Donnelly, R.L. (1988), "The magneto-hydrodynamic squeeze film", *Journal of Tribology*, Vol. 110 No. 2, pp. 375-377.
- Kuznetsov, A.V. and Nield, D.A. (2009), "Natural convective boundary-layer flow of a nanofluid past a vertical plate", *International Journal of Thermal Sciences*, Vol. 49 No. 2, pp. 243-247.
- Mahanthesh, B., Giresha, J. and Reddy Gorla, R.S. (2017), "Eyring-Powell fluid past a convectively heated stretching sheet in the presence of thermal radiation, viscous dissipation and joule heating", *Journal of the Association of Arab Universities for Basic and Applied Sciences*, Vol. 23 No. 2, pp. 75-82.
- Maki, E.R., Kuzma, D.C., Donnelly, R.L. and Kim, B. (1966), "Magneto-hydrodynamic lubrication flow between parallel plates", *Journal of Fluid Mechanics*, Vol. 26 No. 3, pp. 537-543.
- Maleki, M., Hashim, I. and Abbasbandy, S. (2012), "Analysis of IVPs and BVPs on semi-infinite domains via collocation methods", *Journal of Applied Mathematics*, Vol. 12 No. 2, pp. 1-21.
- Malik, M.Y., Khan, I., Hussain, A. and Salahuddin, T. (2015), "Mixed convection flow of MHD Eyring-Powell nanofluid over a stretching sheet: a numerical study", *AIP Advances*, Vol. 5 No. 11, pp. 117-118.
- Mehmood, R., Nadeem, S. and Sher Akbar, N. (2016), "Non aligned ethylene-glycol 30 percent based stagnation point fluid over a stretching surface with hematite nano particles", *Journal of Applied Fluid Mechanics*, Vol. 9 No. 3, pp. 1359-1366.
- Mishra, M.K., Ahmad, N. and Siddiqui, Z.U. (2010), "Boundary layer flow and thermal transfer past a stretching plate with variable thermal conductivity", *International Journal of Non-Linear Mechanics*, Vol. 45 No. 3, pp. 306-309.
- Mohammad, N., Sohail, N. and Tahir, M. (2017), "Squeezed flow of a nanofluid with Cattaneo-Christov heat and mass fluxes", *Results in Physics*, Vol. 7 No. 3, pp. 862-869.
- Motsa, S.S. (2013), "A new spectral local linearization method for nonlinear boundary layer flow problems", *Journal of Applied Mathematics*, p. 15.
- Motsa, S.S., Sibanda, P. and Shateyi, S. (2011), "On a new quasi-linearization method for systems of nonlinear boundary value problems", *Mathematical Methods in the Applied Sciences*, Vol. 34 No. 11, pp. 1406-1413.
- Muhammad, N., Nadeem, S. and Ulhaq, R. (2017), "Heat transport phenomenon in the ferromagnetic fluid over a stretching sheet with thermal stratification", *Results in Physics*, Vol. 7 No. 3, pp. 854-861.

-
- Muhammad, N., Nadeem, S. and Mustafa, M.T. (2018a), "Analysis of ferrite nanoparticles in the flow of ferromagnetic nanofluid", *PloS One*, Vol. 13 No. 1, pp. 1-23.
- Muhammad, S., Nadeem, S. and Mustafa, M.T. (2018b), "Impact of magnetic dipole on a thermally stratified ferrofluid past a stretchable surface", *Proceedings of the Institution of Mechanical Engineers, Part E: Journal of Process Mechanical Engineering*.
- Muhammada and Nadeem, S. (2017), "Ferrite nanoparticles Ni-ZnFe₂O₄, Mn-ZnFe₂O₄ and Fe₂O₄ in the flow of ferromagnetic nanofluid", *The European Physical Journal Plus*, Vol. 132 No. 9, p. 377.
- Nadeem, S. and Saleem, S. (2015), "Series solution of unsteady Eyring Powell nanofluid flow on a rotating cone", *American Journal of Computational Mathematics*, Vol. 52 No. 11, pp. 725-737.
- Nadeem, S., Ahmad, S. and Muhammad, N. (2017), "Cattaneo-Christov flux in the flow of a viscoelastic fluid in the presence of Newtonian heating", *Journal of Molecular Liquids*, Vol. 237 No. 3, pp. 180-184.
- Nadeem, S., Khan, M.N., Muhammad, N. and Ahmad, S. (2018), "Mathematical analysis of bio-convective micropolar nanofluid", *Journal of Computational Design and Engineering*, available at: <https://doi.org/10.1016/j.jcde.2018.07.004>
- Rashidi, S., Farzin, F., Amiri, A., Shanbedi, M., Rahimipناه, M., Savari, M., Taghizadeh Tabari, Z. and Saeed, Z.H. (2015), "Heat transfer coefficient prediction of metal oxides based water nanofluids under laminar flow regime using adaptive neuro-fuzzy inference system", *Journal of Dispersion Science and Technology*, doi: 10.1080/01932691.2015.1090318.
- Saeed, Z.H., Ahmadi, F. and Mahian, O. (2013), "Pressure drop and performance characteristics of water-based Al₂O₃ and CuO nanofluids in a triangular duct", *Journal of Dispersion Science and Technology*, Vol. 34 No. 10, pp. 1368-1375.
- Saeed, Z.H., Farzin, F. and Sardarabadi, H. (2015), "Experimental comparison among thermal characteristics of three metal oxide nanoparticles/turbine oil-based nanofluids under laminar flow regime", *International Journal of Thermophysics*, Vol. 36 No. 4, pp. 760-782.
- Salawu, S.O. (2018), "Analysis of third-grade heat absorption hydromagnetic exothermic chemical reactive flow in a Darcy-Forchheimer porous medium with convective Cooling", *WSEAS Transaction on Mathematics*, Vol. 17 No. 4, pp. 280-289.
- Salehi, H., Saeed, Z.H. and Seyyed, H.N. (2011), "Experimental study of a two-phase closed thermosyphon with nanofluid and magnetic field effect", *Journal of Enhanced Heat Transfer*, Vol. 18 No. 3, pp. 261-269.
- Salehi, H., Saeed, Z.H., Esfandyari, M. and Koolivand, M. (2013), "Nero-fuzzy modeling of the convection heat transfer coefficient for the nanofluid", *Heat Mass Transfer*, Vol. 49 No. 4, pp. 575-583.
- Salimi-Yasar, H., Saeed, Z.H. and Mehd, S. (2017), "Influence of soluble oil-based TiO₂ nanofluid on heat transfer performance of cutting fluid", *Tribology International*, Vol. 112 No. 3, pp. 147-154.
- Salimi-Yasar, H., Saeed, Z.H., Mehdi, S., Ahmad, A. and Ali, K. (2017), "Experimental investigation of thermal properties of cutting fluid using soluble oil-based TiO₂ nanofluid", *Powder Technology*, Vol. 310 No. 2, pp. 213-220.
- Sheikholeslami, M., Ganji, D.D. and Ashorynejad, H.R. (2013), "Investigation of squeezing unsteady nanofluid flow using ADM", *Powder Technol.*, Vol. 239 No. 2, pp. 259-265.
- Sheikholeslami, M., Rashidi, M.M., Dhafer Al Saad, M., Firouzi, F., Houman, B.R. and Domairry, G. (2016), "Steady nanofluid flow between parallel plates considering thermophoresis and Brownian effects", *Journal of King Saud University – Science*, Vol. 28 No. 4, pp. 380-389.
- Sher Akbar, N. and Khan, Z.H. (2016), "Effect of variable thermal conductivity and thermal radiation on the flow of CNTS over a stretching sheet with convective slip boundary conditions", *Journal of Molecular Liquids*, Vol. 222 No. 1, pp. 279-286.
- Sher Akbar, N., Khan, Z., Nadeem, S. and Khan, W. (2016), "Double-diffusive natural convective boundary-layer flow of a nanofluid over a stretching sheet with magnetic field", *International Journal of Numerical Methods for Heat & Fluid Flow*, Vol. 26 No. 1, pp. 108-121.

-
- Siddiqui, A.M., Irum, S. and Ansari, A.R. (2008), "Unsteady squeezing flow of a viscous MHD fluid between parallel plates, a solution using the homotopy perturbation method", *Mathematical Modelling and Analysis*, Vol. 13 No. 4, pp. 565-576.
- Trefethen, L.N. (2000), *Spectral Methods in MATLAB*, Vol. 10, Siam, Oxford University, Oxford.
- Witharana, S., Chen, H. and Ding, Y. (2011), "Stability of nanofluids in quiescent and shear flow fields", *Nanoscale Research Letters*, Vol. 6 No. 1, pp. 231-239.

Dynamical
analysis of
hydromagnetic
Brownian

Corresponding author

Hammed Abiodun Ogunseye can be contacted at: ogunseyehammed@gmail.com

For instructions on how to order reprints of this article, please visit our website:
www.emeraldgroupublishing.com/licensing/reprints.htm
Or contact us for further details: permissions@emeraldinsight.com

Chapter 4

Lie group analysis of a Powell–Eyring nanofluid flow over a stretching surface with variable properties

This chapter presents a study of the boundary layer flow and heat transfer in a Powell-Eyring nanofluid past a stretching surface. We modify the problem formulated in Chapter 2 to consider a two-dimensional flow past a stretching surface. The nanofluid model is temperature and nanoparticle size-dependent, and is based on experimental studies in the literature. Lastly, we introduce the Lie group analysis to obtain self-similar equations that are then solved using the spectral local linearization method. Among other results, we observe that, the Nusselt number increases with an increase in both the temperature ratio parameter and thermal radiation.



Research Article

Lie group analysis of a Powell–Eyring nanofluid flow over a stretching surface with variable properties



Hammed Abiodun Ogunseye¹ · Hiranmoy Mondal² · Precious Sibanda¹ · Hermane Mambili-Mamboundou¹

Received: 29 August 2019 / Accepted: 5 December 2019
© Springer Nature Switzerland AG 2019

Abstract

New applications of nanofluids that have enhanced thermo-physical properties have spurred new studies into the flow and heat transfer in nanofluids in the last decade. Most reported studies have considered the case where the fluid viscosity and thermal conductivity depend only on the size of nanoparticles. However, experimental data show that these properties may depend on the size of nanoparticles and the temperature. In this study, we investigate the flow and heat transfer in a Powell–Eyring nanofluid flow past a stretching surface using the nanofluid viscosity and thermal conductivity models derived from experimental data. Using Lie group analysis, the equations describing the flow and energy balance are reduced to a system of coupled differential equations. These equations are then solved using an efficient iterative spectral local linearization method. The computational results show that increasing the nanoparticle volume fraction and thermal radiation parameter enhances the temperature profiles, while an increase in the fluid parameter increased the velocity profiles. In addition, among other results, the Nusselt number increases with an increase in the temperature ratio parameter and thermal radiation. The results from this study may be useful to engineers in designing cooling devices for the enhancement of thermal systems.

Keywords Powell–Eyring model · Nanofluid · Thermal radiation · Variable viscosity and thermal conductivity · Spectral local linearization method

1 Introduction

Efforts to improve the efficiency and performance of industrial and engineering processes have led to the replacement of traditional heat transfer fluids (e.g water, oil or ethylene glycol) with nanofluids. A nanofluid is a colloidal suspension containing metals or oxides, for example, copper oxide, alumina, zinc oxide or iron oxide having a diameter less than 100 nm. The applications of these fluids can be found in solar technology, where nanofluids are used to enhance the productivity and efficiency of a solar thermal system when used as a collector. In biomedical sciences, nanofluids find applications in cancer

therapeutics and cryosurgery. A comprehensive review of other applications of nanofluids is given by Wong and De Leon [1], Robert et al. [2], Devendiran and Amirtham [3] and Munyalo and Zhang [4].

The superiority of nanofluids over traditional heat transfer fluids can be attributed to their stability and higher thermo-physical properties. Due to these remarkable characteristics and new applications of nanofluids, many studies have been carried out on the flow and heat transfer of nanofluids. Khan and Pop [5] studied the thermal boundary layer flow of a nanofluid past a stretching plate. In their study, emphasis was placed on the Brownian motion and thermophoresis effect. The implicit finite

✉ Hiranmoy Mondal, hiranmoymondal@yahoo.co.in | ¹School of Mathematics, Statistics and Computer Science, University of KwaZulu-Natal, Private Bag X01, Scottsville, Pietermaritzburg 3209, South Africa. ²Department of Mathematics, Durgapur Institute of Advanced Technology and Management, Maulana Abul Kalam Azad University of Technology, Kolkata, West Bengal 713212, India.



SN Applied Sciences

(2020) 2:115

| <https://doi.org/10.1007/s42452-019-1852-y>

Published online: 19 December 2019

difference method was used to solve the flow equations. The exact solution to the thermal transport problem of different types of nanofluids was given by Turkyilmazoglu [6]. Sandeep and Gnanaswara [7] scrutinized the effects of nonlinear thermal radiation on the flow of a Cu–water nanofluid. The Runge–Kutta Newton–Raphson algorithm was used to solve the flow equations. Dhlamini et al. [8] discussed the second-grade nanofluid flow over a nonlinearly stretching sheet. Das et al. [9] solved the equations for the Casson nanofluid flow and heat transfer in a porous medium using a spectral quasi-linearization approximation. El-Aziz [10] studied the effect of variable viscosity on the flow and heat transfer of a power-law nanofluid. Recently, Das et al. [11] examined the influence of variable fluid properties on nanofluid flow over a wedge with surface slip.

The studies above considered the viscosity and thermal conductivity of the nanofluid to be a function of nanoparticle size. However, these properties may also change with temperature (Ogunseye et al. [12]). To accurately predict the heat transfer properties of nanofluids, it is important to consider a viscosity and thermal conductivity model that depends on the nanoparticle size and temperature. In recent years, scientists have proposed numerous viscosity and thermal conductivity models that are nanoparticle size and temperature dependent, and among these, the studies by Masoud et al. [13] and Hassani et al. [14] are worth mentioning.

Lie group symmetry analysis is a powerful technique for finding similarity solutions to a given set of partial differential equations. Using Lie group analysis, we can find similarity transformations that reduces m independent variables of a partial differential equation into $m - 1$ independent variables. Many authors have applied Lie group symmetry analysis to fluid flow models. Akgül and Pakdemirli [15] studied the transient flow of a power-law fluid using the Lie group symmetry analysis. Jalil and Asghar [16] analysed the boundary layer flow of a Powell–Eyring fluid using the Lie group symmetry analysis. The scaling group of transformations, a special form of the Lie group symmetry, was used by Rehman et al. [17] in studying the heat and mass transfer in a Powell–Eyring fluid flow past a stretching plate. Afify and El-Aziz [10] discussed the scaling group for the flow and heat transfer behaviour in a power-law nanofluid. Other studies using the Lie group analysis are reported in [18–21].

The main focus of this study is the flow and heat transfer analysis in a non-Newtonian nanofluid with variable viscosity and thermal conductivity using the Lie group symmetry analysis. The Powell–Eyring model [22] is adopted due to its diverse advantages over other non-Newtonian fluid models. The model is derived from the molecular theory of fluids and not on empirical relations. Further, under

low and high shear rates the Powell–Eyring fluid is reduced to a Newtonian fluid. A considerable number of studies on the Powell–Eyring fluid flow with constant viscosity have been reported by several authors such as Javed et al. [23], Jalil and Asghar [16], Hayat et al. [24], Mahanthesh et al. [25], Agbaje et al. [26] and Ramzan et al. [27]. However, the Powell–Eyring nanofluid flow with variable properties is yet to be considered. The second-order partial differential equation that models the thermal transportation problem is transformed into an ordinary differential equation using the classical Lie group symmetry approach. The equations are solved using an efficient iterative spectral local linearization method. The viscosity and thermal conductivity adopted here are derived from experimental data. The findings in this study may be useful for engineers in the design of heat exchangers and thermal solar collectors.

2 Formulation of the problem

A steady, two-dimensional, laminar flow of an incompressible Powell–Eyring nanofluid past a stretching surface is considered. The flow is restricted to the region $\bar{y} > 0$, and the stretching velocity is assumed to be $u_w(\bar{x})$. The nanofluid is aluminium oxide Al_2O_3 –water system. Further, the physical properties of the fluid are assumed to vary with the nanoparticle size and temperature.

Following the work of Javed et al. [23] and under the usual boundary layer approximation, the continuity, equations of momentum and energy balance for the Powell–Eyring nanofluid are as follows,

$$\frac{\partial \bar{u}}{\partial \bar{x}} + \frac{\partial \bar{v}}{\partial \bar{y}} = 0, \quad (1)$$

$$\rho_{nf} \left(\bar{u} \frac{\partial \bar{u}}{\partial \bar{x}} + \bar{v} \frac{\partial \bar{u}}{\partial \bar{y}} \right) = \frac{\partial}{\partial \bar{y}} \left(\mu_{nf} \frac{\partial \bar{u}}{\partial \bar{y}} \right) + \frac{1}{\beta \gamma} \frac{\partial^2 \bar{u}}{\partial \bar{y}^2} - \frac{1}{2\beta \gamma^3} \left(\frac{\partial \bar{u}}{\partial \bar{y}} \right)^2 \frac{\partial^2 \bar{u}}{\partial \bar{y}^2}, \quad (2)$$

$$\rho_{nf} C_{nf} \left(\bar{u} \frac{\partial \bar{T}}{\partial \bar{x}} + \bar{v} \frac{\partial \bar{T}}{\partial \bar{y}} \right) = \frac{\partial}{\partial \bar{y}} \left(k_{nf} \frac{\partial \bar{T}}{\partial \bar{y}} \right) + \frac{16\sigma_s}{3k_m} \frac{\partial}{\partial \bar{y}} \left(\bar{T}^3 \frac{\partial \bar{T}}{\partial \bar{y}} \right). \quad (3)$$

The relevant boundary conditions to Eqs. (1)–(3) are

$$\begin{aligned} \bar{y} = 0 : \quad & \bar{u} = U_0 u_w \left(\frac{\bar{x}}{L} \right), \quad \bar{v} = V_0 v_w \left(\frac{\bar{x}}{L} \right), \quad \bar{T} = T_w, \\ \bar{y} \rightarrow \infty : \quad & \bar{u} \rightarrow 0, \quad \bar{T} \rightarrow T_\infty, \end{aligned} \quad (4)$$

where (\bar{u}, \bar{v}) are the velocity components in the (\bar{x}, \bar{y}) directions, β and γ are Powell–Eyring fluid material constants, \bar{T} is the nanofluid temperature, σ_s is the Stefan–Boltzmann constant, k_m is the mean absorption coefficient, U_0 and V_0 are the reference velocities, L is the characteristic length, T_w is the wall temperature and T_∞ is the nanofluid temperature far away from the wall.

The density (ρ_{nb}) and specific heat capacity (C_{nb}) of the nanofluid are given by the expressions (see Khanafer and Vafai [28]),

$$\begin{aligned} \rho_{nf} &= (1 - \phi)\rho_{bf} + \phi\rho_p, \\ C_{nf} &= (1 - \phi)\rho_{bf}C_{bf} + \phi\rho_pC_p, \end{aligned} \tag{5}$$

where the subscripts *bf* and *p* represent the base fluid and nanoparticle, respectively, and ϕ is the volume fraction of the nanoparticle.

Following Masoud et al. [13], the nanofluid viscosity is defined by

$$\begin{aligned} \frac{\mu_{nf}}{\mu_{bf}} &= \exp \left[m + \alpha \left(\frac{\bar{T}}{T_\infty} \right) \right. \\ &\quad \left. + \beta_1 \phi \left(1 + \frac{2r}{d_p} \right)^3 + \gamma_1 \left(\frac{d_p}{1+r} \right) \right]. \end{aligned} \tag{6}$$

The thermal conductivity is determined by the new empirical correlations proposed by Hassani et al. [14], which is expressed as,

$$\begin{aligned} \frac{k_{nf}}{k_{bf}} &= \frac{k_p + 2k_{bf} - 2(k_{bf} - k_p)\phi}{k_p + 2k_{bf} + (k_{bf} - k_p)\phi} + 5 \\ &\quad \times 10^4 \frac{\beta_2 \phi \rho_{bf} C_{bf}}{k_{bf}} \sqrt{\frac{\kappa \bar{T}}{\rho_p d_p}} f(\bar{T}, \phi), \end{aligned} \tag{7}$$

where

$$\begin{aligned} f(\bar{T}, \phi) &= (2.8217 \times 10^{-2} \phi + 3.917 \times 10^{-3}) \left(\frac{\bar{T}}{T_\infty} \right) \\ &\quad - (3.0669 \times 10^{-2} \phi + 3.91123 \times 10^{-3}), \end{aligned}$$

where μ is the viscosity, k is the thermal conductivity, m is a factor that depends on the nanoparticles, the base fluid and their interaction, α , β_1 , β_2 and γ_1 are empirical parameters determined from experimental data, d_p is the diameter of the nanoparticle, r is the capping layer thickness and κ is the Boltzmann constant. The values of these empirical parameters are given in Table 1, and the thermo-physical properties of water and aluminium oxide Al_2O_3 are presented in Table 2.

Table 1 Empirical parameters for aluminium oxide Al_2O_3 –water nanofluid [13, 14]

m	α	β_1	γ_1	β_2	Volume fraction
0.72	-0.485	14.94	0.0105	$8.4407(100\phi)^{-1.07304}$	$1\% \leq \phi \leq 10\%$

Table 2 Thermo-physical properties of water and aluminium oxide Al_2O_3

	ρ	c_p (J kg ⁻¹ K)	k (Wm ⁻¹ K)
Water fluid	997.1	4179	0.613
Al_2O_3	3970	765	40

Equations (1)–(4) are nondimensionalized by introducing the following dimensionless variables:

$$x = \frac{\bar{x}}{L}, \quad y = \frac{\bar{y}}{L} \left(\frac{U_0 \rho_{bf} L}{\mu_{bf}} \right)^{\frac{1}{2}}, \quad u = \frac{\bar{u}}{U_0}, \tag{8}$$

$$v = \frac{\bar{v}}{U_0} \left(\frac{U_0 \rho_{bf} L}{\mu_{bf}} \right)^{\frac{1}{2}}, \quad T = \frac{\bar{T} - T_\infty}{T_w - T_\infty}.$$

We define the stream function ψ as

$$u = \frac{\partial \psi}{\partial y}, \quad v = -\frac{\partial \psi}{\partial x}. \tag{9}$$

Substituting Eqs. (8) and (9) into Eqs. (2)–(4) yields:

$$\begin{aligned} \frac{\partial}{\partial y} \left(\exp(A_1 + \alpha[1 + \Delta T]) \frac{\partial^2 \psi}{\partial y^2} \right) + \lambda \frac{\partial^3 \psi}{\partial y^3} - \lambda \delta \left(\frac{\partial^2 \psi}{\partial y^2} \right)^2 \frac{\partial^3 \psi}{\partial y^3} \\ - A_2 \left(\frac{\partial \psi}{\partial y} \frac{\partial^2 \psi}{\partial x \partial y} - \frac{\partial \psi}{\partial x} \frac{\partial^2 \psi}{\partial y^2} \right) = 0, \end{aligned} \tag{10}$$

$$\begin{aligned} \frac{\partial}{\partial y} \left([A_3 + A_4[1 + \Delta T]^{\frac{3}{2}} - A_5[1 + \Delta T]^{\frac{1}{2}}] \frac{\partial T}{\partial y} \right) \\ + Nr \frac{\partial}{\partial y} \left([1 + \Delta T]^3 \frac{\partial T}{\partial y} \right) - Pr A_6 \left(\frac{\partial \psi}{\partial y} \frac{\partial T}{\partial x} - \frac{\partial \psi}{\partial x} \frac{\partial T}{\partial y} \right) = 0 \end{aligned} \tag{11}$$

$$\begin{aligned} y = 0 : \quad \frac{\partial \psi}{\partial y} = u_w(x), \quad \frac{\partial \psi}{\partial x} = F_w v_w(x), \quad T = 1, \\ y \rightarrow \infty : \quad \frac{\partial \psi}{\partial y} \rightarrow 0, \quad T \rightarrow 0. \end{aligned} \tag{12}$$

where λ and δ are fluid parameters, Pr is the Prandtl number, Nr is the thermal radiation parameter, Δ is the temperature difference, F_w is the suction or injection parameter and A_i , ($i = 1, \dots, 5$) are constants. These parameters and constants are defined as

$$\begin{aligned}
 A_1 &= m + \beta_1 \phi \left(1 + \frac{2r}{d_p} \right)^3 + \gamma_1 \left(\frac{d_p}{1+r} \right), \\
 A_2 &= \left((1-\phi) + \frac{\rho_p}{\rho_{bf}} \phi \right), \quad A_3 = \frac{k_p + 2k_{bf} - 2(k_{bf} - k_p)\phi}{k_p + 2k_{bf} + (k_{bf} - k_p)\phi}, \\
 F_w &= -V_0 \left(\frac{L\rho_f}{U_0\mu_\infty} \right) \\
 A_4 &= (1.4109 \times 10^3 \phi^2 + 1.9585 \times 10^2 \phi) \frac{\beta_2 \rho_{bf} C_{bf}}{k_{bf}} \sqrt{\frac{\kappa T_\infty}{\rho_p d_p}}, \\
 A_5 &= (1.5334 \times 10^3 \phi^2 + 1.9556 \times 10^2 \phi) \frac{\beta_2 \rho_{bf} C_{bf}}{k_{bf}} \sqrt{\frac{\kappa T_\infty}{\rho_p d_p}}, \\
 A_6 &= (1-\phi) + \frac{\rho_p C_p}{\rho_{bf} C_{bf}} \phi, \quad \lambda = \frac{1}{\mu_{bf} \beta \gamma}, \quad \delta = \frac{U_0^3 \rho_{bf}}{2LC^2 \mu_{bf}}, \\
 Pr &= \frac{C_{bf} \mu_{bf}}{k_{bf}}, \quad Nr = \frac{16\sigma_s T_\infty^3}{3k_m k_{bf}}, \quad \Delta = \theta_w - 1, \quad \theta_w = \frac{T_w}{T_\infty}.
 \end{aligned} \tag{13}$$

3 Lie symmetry analysis

In this section, we seek the similarity solution to Eqs. (10)–(12) using the Lie symmetry group approach. Finding symmetry group is equivalent to finding the infinitesimal generator that renders Eqs. (10)–(12) invariant. We consider a one-parameter group Lie group of infinitesimal transformations with Lie group parameter ϖ defined as:

$$\begin{aligned}
 x^* &= x + \varpi \xi_1(s, y, \psi, T) + \mathcal{O}(\varpi^2), \\
 y^* &= y + \varpi \xi_2(s, y, \psi, T) + \mathcal{O}(\varpi^2), \\
 \psi^* &= \psi + \varpi \varphi_1(s, y, \psi, T) + \mathcal{O}(\varpi^2), \\
 T^* &= T + \varpi \varphi_2(s, y, \psi, T) + \mathcal{O}(\varpi^2),
 \end{aligned} \tag{14}$$

the infinitesimal generator is prolonged to first, second and third derivatives, and it is defined by:

$$\begin{aligned}
 X &= \xi_1 \frac{\partial}{\partial x} + \xi_2 \frac{\partial}{\partial y} + \varphi_1 \frac{\partial}{\partial \psi} + \varphi_2 \frac{\partial}{\partial T} + \varphi_{1x} \frac{\partial}{\partial \psi_x} + \varphi_{1y} \frac{\partial}{\partial \psi_y} \\
 &+ \varphi_{1xy} \frac{\partial}{\partial \psi_{xy}} + \varphi_{1yy} \frac{\partial}{\partial \psi_{yy}} + \varphi_{1yyy} \frac{\partial}{\partial \psi_{yyy}} \\
 &+ \varphi_{2x} \frac{\partial}{\partial T_x} + \varphi_{2y} \frac{\partial}{\partial T_y} + \varphi_{2yy} \frac{\partial}{\partial T_{yy}},
 \end{aligned} \tag{15}$$

where

$$\begin{aligned}
 \varphi_{1R} &= D_R \varphi_1 - \psi_x D_R \xi_1 - \psi_y D_R \xi_2, \\
 \varphi_{2R} &= D_R \varphi_2 - \varphi_{2x} D_R \xi_1 - \varphi_{2y} D_R \xi_2, \\
 \varphi_{1SR} &= D_R \varphi_{1S} - \psi_{Sx} D_R \xi_1 - \psi_{Sy} D_R \xi_2, \\
 \varphi_{2SR} &= D_R \varphi_{2S} - \psi_{Sx} D_R \xi_1 - \psi_{Sy} D_R \xi_2, \\
 D_x &= \frac{\partial}{\partial x} + \psi_x \frac{\partial}{\partial \psi} + T_x \frac{\partial}{\partial x} + \psi_{xx} \frac{\partial}{\partial \psi_x} \\
 &+ T_{xx} \frac{\partial}{\partial T_x} + \psi_{xy} \frac{\partial}{\partial \psi_y} + \dots, \\
 D_y &= \frac{\partial}{\partial y} + \psi_y \frac{\partial}{\partial \psi} + T_y \frac{\partial}{\partial y} + \psi_{yy} \frac{\partial}{\partial \psi_y} \\
 &+ T_{yy} \frac{\partial}{\partial T_y} + \psi_{xy} \frac{\partial}{\partial \psi_x} + \dots,
 \end{aligned} \tag{16}$$

R, S represent either x or y depending on the component.

Using X on Eqs. (10) and (11), we obtain the following infinitesimals after some algebraic simplification:

$$\xi_1 = c_1 x + c_2, \quad \xi_2 = \frac{1}{3} c_1 y + g(x), \quad \varphi_1 = \frac{2}{3} c_1 \psi + c_3, \quad \varphi_2 = 0. \tag{17}$$

where $c_j (j = 1, \dots, 3)$ are arbitrary constants. Thus, we obtain a three-dimensional space of operator. By setting $g(x) = 0$ and any of two the constants to zero, the following infinitesimal generators can be obtained:

$$X_1 = x \frac{\partial}{\partial x} + \frac{y}{3} \frac{\partial}{\partial y} + \frac{2}{3} \frac{\partial}{\partial \psi}, \quad X_2 = \frac{\partial}{\partial x}, \quad X_3 = \frac{\partial}{\partial \psi}. \tag{18}$$

The implication of Eq. (18) is that Eqs. (10) and (11) admit three one-parameter transformation groups. X_1 corresponds to scaling group of transformation, while X_2 and X_3 are translation groups of transformation.

Applying X to the boundary conditions, Eq. (12) yields:

$$\begin{aligned}
 \frac{du_w}{dx} &= \frac{c_1}{3(c_1 x + c_2)} u_w, \\
 \frac{dv_w}{dx} &= -\frac{c_2}{3(c_1 x + c_2)} v_w,
 \end{aligned} \tag{19}$$

which implies that:

$$\begin{aligned}
 u_w(x) &= k_1 (c_1 x + c_2)^{\frac{1}{3}}, \\
 v_w(x) &= k_2 (c_1 x + c_2)^{-\frac{1}{3}},
 \end{aligned} \tag{20}$$

where k_1 and k_2 are constants of integration.

Obviously, X_2 and X_3 do not have an invariant solution; hence, we consider only X_3 . Under X_3 , Eq. (20) is transformed into:

$$u_x(x) = x^{\frac{1}{3}} \text{ and } v_w(x) = x^{-\frac{1}{3}}. \tag{21}$$

The characteristic equation to X_1 is:

$$\frac{dx}{x} = \frac{3dy}{y} = \frac{3d\psi}{2\psi} = \frac{dT}{0}, \tag{22}$$

on solving Eq. (22), we obtain the following similarity variables and function:

$$\eta = yx^{-\frac{1}{3}}, \quad \psi = x^{\frac{2}{3}}f(\eta), \quad T = \theta(\eta). \tag{23}$$

Finally, substituting Eqs. (21) and (22) into Eqs. (10) and (12) yields:

$$\begin{aligned} &(\exp(A_1 + \alpha(1 + \Delta\theta)) + \lambda)f'''' + \alpha\Delta \exp(A_1 + \alpha(1 + \Delta\theta))\theta'f'' \\ &- \lambda\delta(f'')^2f''' + A_2\left(\frac{2}{3}ff'' - \frac{1}{3}f'^2\right) = 0, \end{aligned} \tag{24}$$

$$\begin{aligned} &(A_3 + A_4(1 + \Delta\theta)^{\frac{3}{2}} - A_5(1 + \Delta\theta)^{\frac{1}{2}} + Nr(1 + \Delta\theta)^3)\theta'' \\ &+ \Delta\left(\frac{3A_4}{2}(1 + \Delta\theta)^{\frac{1}{2}} - \frac{A_5}{2}(1 + \Delta\theta)^{-\frac{1}{2}} + 3Nr(1 + \Delta\theta)^2\right)\theta'^2 \\ &+ \frac{2}{3}PrA_6f\theta' = 0 \end{aligned} \tag{25}$$

$$\begin{aligned} \eta = 0 : \quad &f' = 1, \quad f = F_w, \quad \theta = 1, \\ \eta \rightarrow \infty : \quad &f' \rightarrow 0, \quad \theta \rightarrow 0. \end{aligned} \tag{26}$$

Pantokratoras [29] pointed out that assuming a uniform Prandtl number when thermo-physical properties are temperature dependent may lead to unrealistic results. Hence, to take care of this paradox, the Prandtl number of the nanofluid is defined as

$$\begin{aligned} Pr_v &= \frac{\mu_{nf}C_{nf}}{k_{nf}} = \frac{A_6 \exp(A_1 + \alpha(1 + \Delta\theta))}{A_3 + A_4(1 + \Delta\theta)^{\frac{3}{2}} - A_5(1 + \Delta\theta)^{\frac{1}{2}}} \\ &\frac{C_{bf}\mu_{bf}}{k_{bf}} \\ &= \frac{\mu_{nf}C_{nf}}{k_{nf}} = \frac{A_6 \exp(A_1 + \alpha(1 + \Delta\theta))}{A_3 + A_4(1 + \Delta\theta)^{\frac{3}{2}} - A_5(1 + \Delta\theta)^{\frac{1}{2}}} Pr. \end{aligned} \tag{27}$$

Using Eq. (27) in Eq. (25) gives a modified thermal boundary layer equation with a variable Prandtl number, that is,

$$\begin{aligned} &(A_3 + A_4(1 + \Delta\theta)^{\frac{3}{2}} - A_5(1 + \Delta\theta)^{\frac{1}{2}} + Nr(1 + \Delta\theta)^3)\theta'' \\ &+ \Delta\left(\frac{3A_4}{2}(1 + \Delta\theta)^{\frac{1}{2}} - \frac{A_5}{2}(1 + \Delta\theta)^{-\frac{1}{2}} + 3Nr(1 + \Delta\theta)^2\right)\theta'^2 \\ &+ \frac{2}{3}Pr_v f\theta' \left(\frac{A_3 + A_4(1 + \Delta\theta)^{\frac{3}{2}} - A_5(1 + \Delta\theta)^{\frac{1}{2}}}{\exp(A_1 + \alpha(1 + \Delta\theta))}\right) = 0 \end{aligned} \tag{28}$$

The skin friction coefficient C_f and the Nusselt number Nu_x which are of interest in thermal engineering design are defined as follows:

$$C_f = \frac{\tau_w}{\rho_f U_0^2} \text{ and } Nu_x = \frac{\left(\frac{x}{L}\right)q_w}{k_{nf}(\bar{T})(T_w - T_\infty)} \tag{29}$$

and the wall shear stress τ_w and the wall flux q_w are expressed as:

$$\begin{aligned} \tau_w &= \left(\mu_{nf} + \frac{1}{\beta\gamma}\right)\left(\frac{\partial \bar{u}}{\partial \bar{y}}\right) - \frac{1}{6\beta\gamma^3}\left(\frac{\partial \bar{u}}{\partial \bar{y}}\right)^3 \Big|_{\bar{y}=0} \\ \text{and } q_w &= -\left(k_{nf} + \frac{16\sigma_s \bar{T}^3}{3k_m}\right)\left(\frac{\partial \bar{T}}{\partial \bar{y}}\right) \Big|_{\bar{y}=0}. \end{aligned} \tag{30}$$

Equation (29) can be written as:

$$C_f(Re)^{\frac{1}{2}} = (\exp(A_1 + 2\alpha) + \lambda)f''(0) - \frac{\lambda\delta}{3}(f''(0))^3, \tag{31}$$

$$Nu_x\left(\frac{x}{L}\right)(Re)^{-\frac{1}{2}} = -\left(1 + \frac{Nr\theta_w^3}{A_7}\right)\theta'(0). \tag{32}$$

where $Re = \frac{U_0 L}{\nu_\infty}$ represents the local Reynolds number and $A_7 = A_3 + A_4\theta_w^{\frac{3}{2}} - A_5\theta_w^{\frac{1}{2}}$.

4 Method of solution

Spectral methods are a class of numerical methods used to solve differential equations arising in applied mathematics, science and engineering. The name spectral methods is derived from the fact that the solution is expressed as a

series of orthogonal eigenfunctions of some linear operator. Although the SQLM has a very high convergence, it is limited to cases where there is only one independent variable. In this section, an efficient iterative spectral local linearization method (SLLM) which was proposed by Motsa [30] is used to numerically integrate the coupled nonlinear differential Eqs. (24) and (28) with the boundary condition Eqs. (26). To apply this technique, we consider the following nonlinear differential operators

$$\Omega_f = (\exp(A_1 + \alpha(1 + \Delta\theta_n)) + \lambda)f_n'''' + \alpha\Delta \exp(A_1 + \alpha(1 + \Delta\theta_n))\theta_n' f_n'' - \lambda\delta(f_n'')^2 f_n'''' + A_2\left(\frac{2}{3}f_n f_n'' - \frac{1}{3}f_n'^2\right) \quad (33)$$

$$\Omega_\theta = \left(A_3 + A_4(1 + \Delta\theta_n)^{\frac{3}{2}} - A_5(1 + \Delta\theta_n)^{\frac{1}{2}} + \text{Nr}(1 + \Delta\theta_n)^3\right)\theta_n'' + \Delta\left(\frac{3A_4}{2}(1 + \Delta\theta_n)^{\frac{1}{2}} - \frac{A_5}{2}(1 + \Delta\theta_n)^{-\frac{1}{2}} + 3\text{Nr}(1 + \Delta\theta_n)^2\right)\theta_n'^2 + \frac{2}{3}\text{Pr}_v f_n \theta_n' \left(A_3 + A_4(1 + \Delta\theta_n)^{\frac{3}{2}} - A_5(1 + \Delta\theta_n)^{\frac{1}{2}}\right) \exp(-A_1 - \alpha(1 + \Delta\theta_n)) = 0; \quad (34)$$

Eqs. (33) and (34) can be decoupled according to the following algorithm:

1. From Eq. (33) Ω_f , solve f_{n+1} assuming that θ_n is known from a previous iteration.
2. Solve θ_{n+1} from Eq. (34) Ω_θ using the updated solution of f_n .
3. Subsequent iterative solutions are obtained by repeating steps 1 and 2.

In the framework of the SLLM, the following iterative scheme is obtained

$$a_{1,n} f_{n+1}'''' + a_{2,n} f_{n+1}'' + a_{3,n} f_{n+1}' + a_{4,n} f_{n+1} = R^f, \quad (35)$$

$$a_{5,n} \theta_{n+1}'' + a_{6,n} \theta_{n+1}' + a_{7,n} \theta_{n+1} = R^\theta, \quad (36)$$

$$f_{n+1}(0) = F_w, \quad f_{n+1}'(0) = 1, \quad f_{n+1}'(\infty) = 0, \quad (37)$$

$$\theta_{n+1}(0) = 1, \quad \theta_{n+1}(\infty) = 0.$$

The coefficients in Eqs. (35) and (36) along with their right-hand sides are defined as follows:

$$a_{1,n} = \frac{\partial \Omega_f}{\partial f_n''''} = A_1 \exp(A_1 + \alpha(1 + \Delta\theta_n)) + \lambda \left(1 - \delta f_n''^2\right), \quad a_{3,n} = \frac{\partial \Omega_f}{\partial f_n''} = -2/3 A_2 f_n'$$

$$a_{2,n} = \frac{\partial \Omega_f}{\partial f_n''} = \alpha \Delta \exp(A_1 + \alpha(1 + \Delta\theta_n)) \theta_n' - 2 \delta \lambda f_n'' f_n'''' + \frac{2}{3} A_2 f_n', \quad a_{4,n} = \frac{\partial \Omega_f}{\partial f_n} = \frac{2}{3} A_2 f_n''$$

$$a_{5,n} = \frac{\partial \Omega_\theta}{\partial \theta_n''} = A_3 + A_4 (\Delta \theta_n + 1)^{\frac{3}{2}} - A_5 (\Delta \theta_n + 1)^{\frac{1}{2}} + \text{Nr} (\Delta \theta_n + 1)^3$$

$$a_{6,n} = \frac{\partial \Omega_\theta}{\partial \theta_n'} = 2 \Delta \left(\frac{3}{2} A_4 (\Delta \theta_n + 1)^{\frac{1}{2}} - \frac{1}{2} A_5 (\Delta \theta_n + 1)^{-\frac{1}{2}} + 3 \text{Nr} (\Delta \theta_n + 1)^2\right) \theta_n' + \frac{2}{3} \text{Pr}_v f_n \left(A_3 + A_4 (\Delta \theta_n + 1)^{\frac{3}{2}} - A_5 (\Delta \theta_n + 1)^{\frac{1}{2}}\right) \exp(-A_1 - \alpha(1 + \Delta\theta_n))$$

$$a_{7,n} = \frac{\partial \Omega_\theta}{\partial \theta_n} = \Delta \left(\frac{3}{2} A_4 (1 + \Delta \theta_n)^{\frac{1}{2}} - \frac{1}{2} A_5 (\Delta \theta_n + 1)^{-\frac{1}{2}} + 3 \text{Nr} (\Delta \theta_n + 1)^2\right) \theta_n'' + \Delta^2 \left(\frac{3}{4} A_4 (1 + \Delta \theta_n)^{-\frac{1}{2}} + \frac{1}{4} A_5 (\Delta \theta_n + 1)^{-\frac{3}{2}} + 6 \text{Nr} (\Delta \theta_n + 1)\right) \theta_n'^2 + \frac{1}{3} \text{Pr}_v f_n \theta_n' \Delta \exp(-A_1 - \alpha(1 + \Delta\theta_n)) \left[3A_4 (\Delta \theta_n + 1)^{\frac{1}{2}} - A_5 (\Delta \theta_n + 1)^{-\frac{1}{2}} - 2\alpha \left(A_3 + A_4 (\Delta \theta_n + 1)^{\frac{3}{2}} - A_5 (\Delta \theta_n + 1)^{\frac{1}{2}}\right)\right],$$

$$R^f = a_{1,n} f_n'''' + a_{2,n} f_n'' + a_{3,n} f_n' + a_{4,n} f_n - \Omega_f,$$

$$R^\theta = a_{5,n} \theta_n'' + a_{6,n} \theta_n' + a_{7,n} \theta_n - \Omega_\theta. \quad (38)$$

Equations (35)–(37) are integrated numerically using the Chebyshev pseudo-spectral technique (see Mondal et al. [31], Motsa et al. [32] and Maleki et al. [33]). In order to apply this technique, the semi-infinite domain $\eta \in [0, \infty)$ is replaced with a truncated domain $\eta \in [0, \varpi_\infty]$, where $\varpi_\infty \in \mathbb{Z}^+$ is a mapping parameter. Using the transformation $\eta = \frac{1}{2}(\xi + 1)\varpi_\infty$, the interval $[0, \varpi_\infty]$ is mapped to $[-1, 1]$ which the Chebyshev pseudo-spectral technique can be used. The unknown functions $f(\eta)$ and $\theta(\eta)$ are

discretized using the Chebyshev–Gauss–Lobatto collocation points:

$$\xi_k = \cos\left(\frac{\pi k}{\bar{N}}\right), \quad k = 0, 1, \dots, \bar{N}; \quad -1 \leq \xi \leq 1. \quad (39)$$

The derivatives of $f(\eta)$ and $\theta(\eta)$ are computed using the Chebyshev differentiation matrix D , at the collocation points as a matrix vector product, that is:

$$\frac{df}{d\eta} = \sum_{i=0}^{\bar{N}} D_{ij} f(\xi_i) = \mathbf{D}F, \quad j = 0, 1, 2, \dots, \bar{N}, \quad (40)$$

where $\bar{N} + 1$ is the number of collocation points, $\mathbf{D} = 2D/\varpi_\infty$ and $F = [f(\xi_0), f(\xi_1), \dots, f(\xi_{\bar{N}})]^T$ is a vector function at the collocation point.

Let Θ be a similarity vector function representing θ . The higher-order derivatives of f and θ are evaluated as powers of \mathbf{D} , that is

$$f^s(\eta) = \mathbf{D}^s F, \quad \theta^s(\eta) = \mathbf{D}^s \Theta. \quad (41)$$

Substituting Eqs. (39)–(41) into Eqs. (35)–(37) yields the following decoupled matrices

$$\begin{bmatrix} \mathbf{D}_{1,1} & \dots & \mathbf{D}_{1,\bar{N}+1} \\ \text{diag}[a_{1,n}]\mathbf{D}^3 + \text{diag}[a_{2,n}]\mathbf{D}^2 + \text{diag}[a_{3,n}]\mathbf{D} + \text{diag}[a_{4,n}]\mathbf{I} & & \\ & \mathbf{D}_{\bar{N},1} & \dots & \mathbf{D}_{\bar{N},\bar{N}+1} \\ & 0 & \dots & 1 \end{bmatrix} \times \begin{bmatrix} f_{n+1}(\xi_0) \\ f_{n+1}(\xi_1) \\ \vdots \\ f_{n+1}(\xi_{\bar{N}-1}) \\ f_{n+1}(\xi_{\bar{N}}) \end{bmatrix} = \begin{bmatrix} 0 \\ R_{n+1}^f(\xi_1) \\ \vdots \\ 1 \\ F_w \end{bmatrix}, \quad (42)$$

$$\begin{bmatrix} 1 & 0 \dots & 0 \\ \text{diag}[a_{5,n}]\mathbf{D}^2 + \text{diag}[a_{6,n}]\mathbf{D} + \text{diag}[a_{7,n}]\mathbf{I} & & \\ & 0 & \dots & 1 \end{bmatrix} \begin{bmatrix} \theta_{n+1}(\xi_0) \\ \vdots \\ \theta_{n+1}(\xi_{\bar{N}}) \end{bmatrix} = \begin{bmatrix} 0 \\ R_{n+1}^\theta(\xi_1) \\ \vdots \\ 1 \end{bmatrix} \quad (43)$$

Here \mathbf{I} is an $(\bar{N} + 1) \times (\bar{N} + 1)$ identity matrix, and $\text{diag}[\]$ denotes a diagonal matrix. A suitable initial approximation for the SLLM scheme is

$$f_0(\eta) = F_w + 1 - \exp(-\eta), \quad \theta_0(\eta) = \exp(-\eta), \quad (44)$$

5 Numerical validation

The cases $\lambda = A_1 = A_4 = A_5 = 0$, $\theta_w = A_2 = 1$ and $A_3 = 1$ correspond to a Newtonian fluid with constant viscosity, thermal conductivity and linear thermal radiation which has been studied by Jalil and Asghar [16] using the Keller-box method. To validate the correctness of the numerical results obtained from the iterative scheme given by Eqs. (35–37), the skin friction coefficient $f''(0)$ at the seventh iterates with $N = 80$ is compared with Jalil and Asghar [16] in Table 3. It is apparent that there is a good agreement between the two results.

6 Results and discussion

In this section, we give the results of the numerical simulation and the effects of the nanoparticle volume fraction, ϕ , fluid parameter, λ , suction/injection parameter, F_w , thermal radiation parameter, Nr , and temperature ratio parameter, θ_w on the nanofluid velocity profile, $f'(\eta)$, temperature profile, $\theta(\eta)$, skin friction coefficient and Nusselt number are performed and discussed. The range of parameters is as follows: $1\% \leq \phi \leq 10\%$, $0 \leq \lambda \leq 5$, $0 \leq \delta \leq 3$, $1.2 \leq \theta_w \leq 2.1$ and $-1 \leq F_w \leq 1$. (See Jalil and Asghar [16] and Sandeep and Gnaneswara [7]). The default parameter values used in simulating the velocity and temperature profiles are $\lambda = \delta = Nr = F_w = 1$, $\phi = 0.1$, $\theta_w = 1.5$ and $Pr_v = 6.96$. Therefore, where these parameter values are not explicitly stated, it will be understood that such a parameter is assigned the default value.

The nanoparticle volume fraction quantifies the amount of the Al_2O_3 nanoparticles contained in the synthesized nanofluid. The nanofluid velocity and temperature profiles for different values of nanoparticle volume fraction are displayed in Fig. 1. We observed that both the velocity and temperature profiles are enhanced with an increase in the value of nanoparticle volume fraction. Also, the

Table 3 Comparison of the SLLM results for $-f''(0)$ with Jalil and Asghar [16] for distinct values of F_w when $\lambda = A_1 = A_4 = A_5 = 0$, $\theta_w = A_2 = 1$ and $A_3 = 1$

F_w	$f''(0)$		
	Jalil and Asghar [16]	SLLM	Relative error
0.75	0.984436	0.98443940	0
0.50	0.873640	0.87364290	0
0	0.677647	0.67764824	0
-0.50	0.518869	0.51887049	0
-0.75	0.453523	0.45352500	0

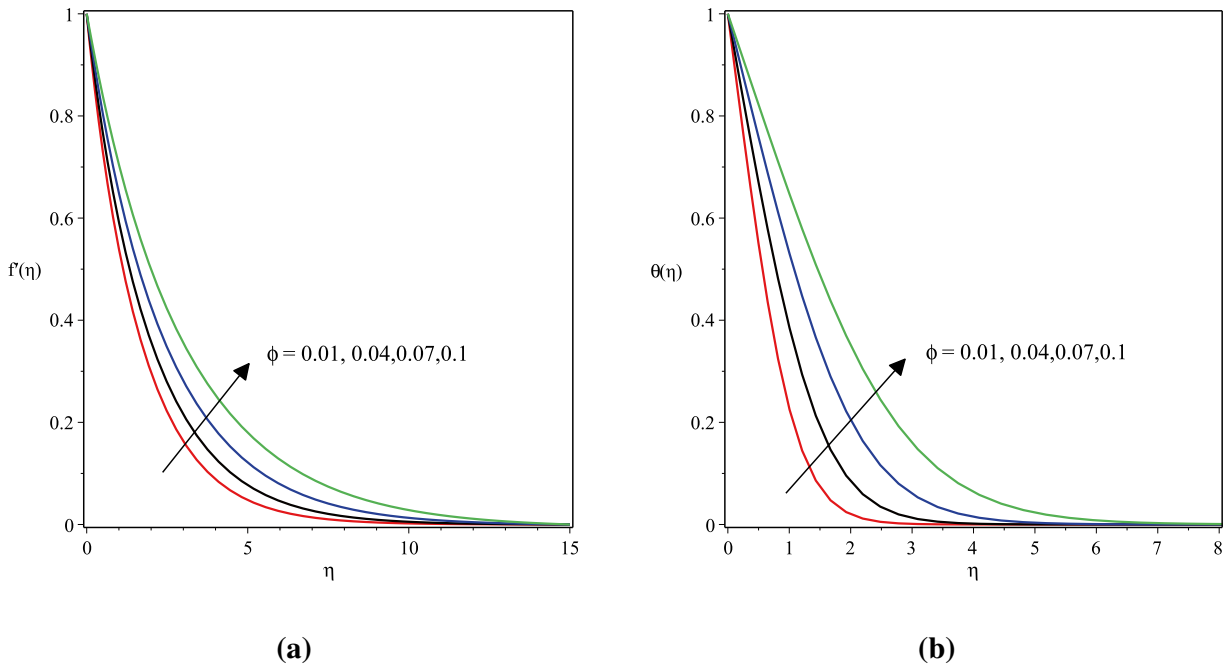


Fig. 1 Effect of the nanoparticle volume fraction on the velocity and temperature profiles

momentum and thermal boundary layers become thicker with an increase in the nanoparticle volume fraction. Figure 2 shows the effect of the fluid parameter on the nanofluid velocity profiles. It is seen that with an increase in the fluid parameter, the nanofluid velocity profiles and

the momentum boundary layer thickness are enhanced. Physically, this is correct since the fluid parameter has an inverse relation with the nanofluid dynamic viscosity; thus, the fluid becomes less viscous with large value of the fluid parameter. Hence, the velocity profiles are enhanced. This

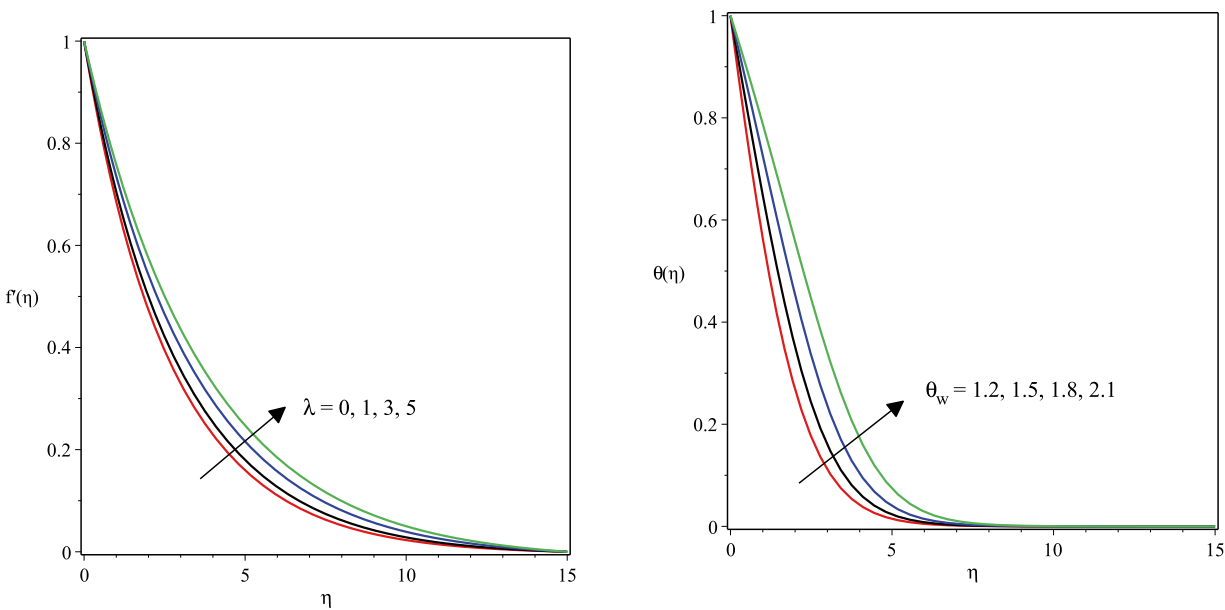


Fig. 2 Effect of the fluid parameter on the velocity profile

Fig. 3 Effect of the nanoparticle volume fraction on the temperature profile

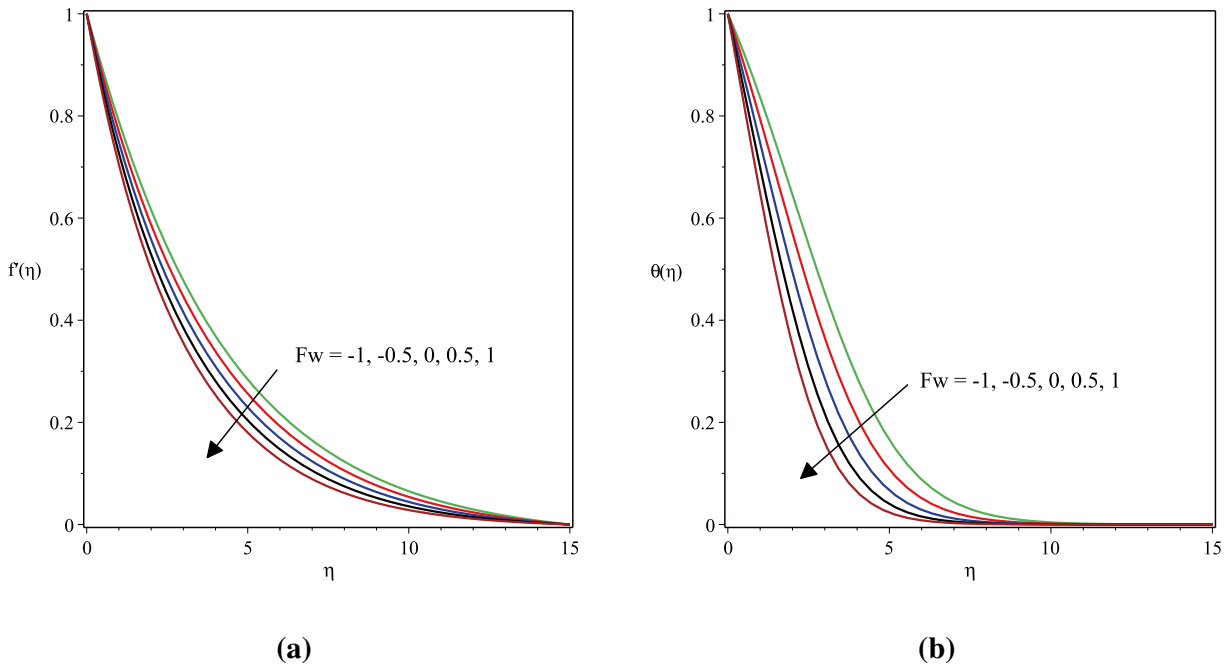


Fig. 4 Effect of the suction/injection parameter on the velocity and temperature profile

finding is consistent with Javed et al. [23] for the case of a pure fluid.

Figure 3 shows the effect of the temperature ratio parameter on the nanofluid temperature profiles. We observed that the temperature profiles, as well as the

thermal boundary layer thickness, are enhanced with an increase in the value of the temperature ratio parameter. This trend is in agreement with Sandeep and Ganeswara [7].

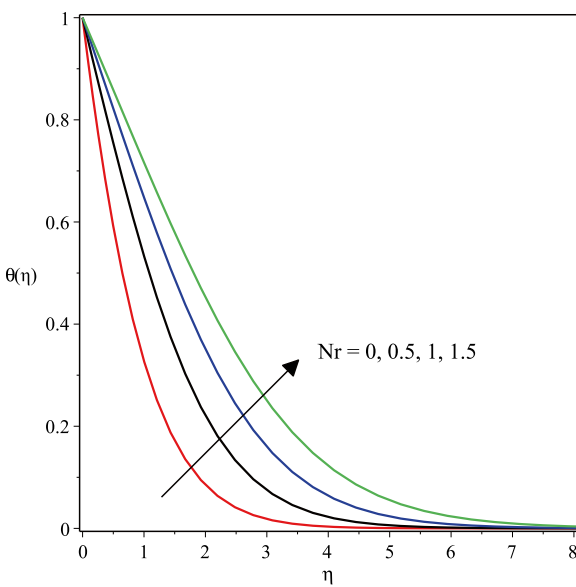


Fig. 5 Effect of the thermal radiation parameter on the temperature profile

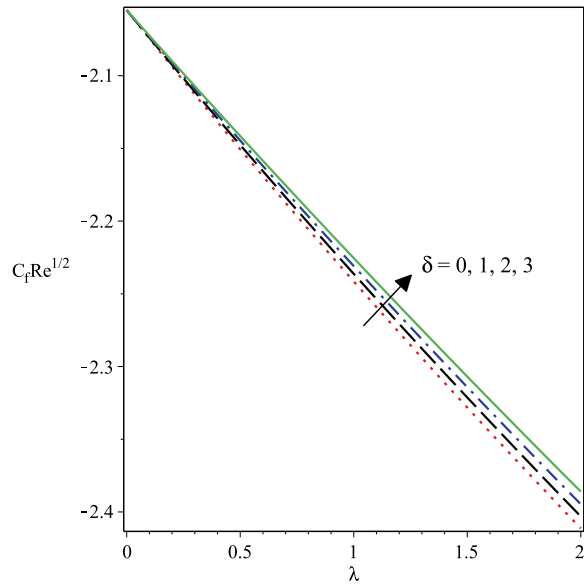


Fig. 6 Effect of the fluid parameter, λ , on the skin friction coefficient for different values of the fluid parameter, δ

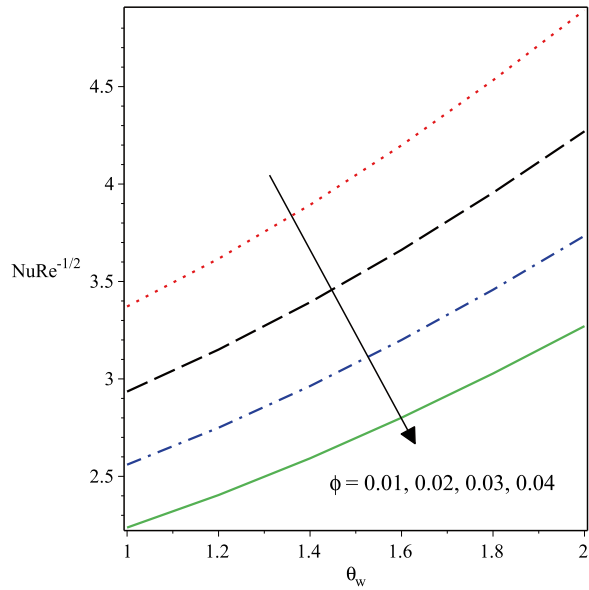


Fig. 7 Effect of the temperature ratio parameter on the Nusselt number for different values of nanoparticle volume fraction

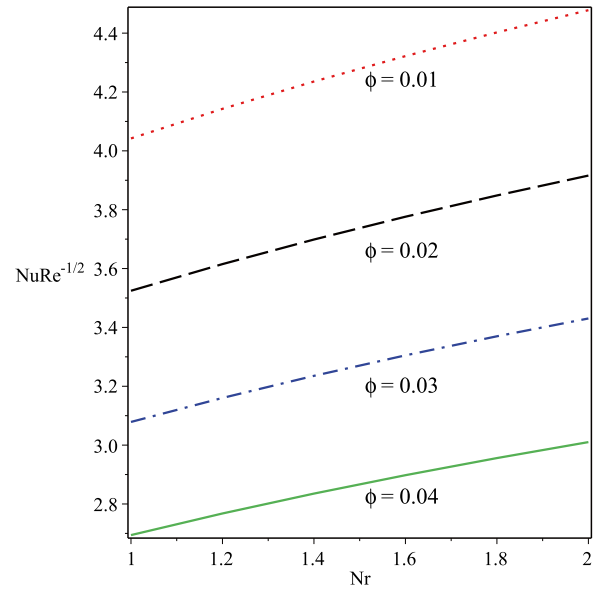


Fig. 8 Effect of the thermal radiation parameter on the Nusselt number for different values of nanoparticle volume fraction

Figure 4 shows the effect of the suction ($f_w > 0$) and injection ($f_w < 0$) parameter on the nanofluid velocity and temperature profiles. From Fig. 4a, it is seen that the

velocity profiles, as well as the thickness of the momentum boundary layer, decrease with an increase in the suction parameter. However, the velocity and momentum

Table 4 The computed results for skin friction coefficient, C_f , and Nusselt number, Nu, for Al_2O_3 /water nanofluid for varying the parameters: $\phi, \lambda, \delta, fw, \theta_w$ and Nr

ϕ	λ	δ	fw	θ_w	Nr	C_f	Nu
0.01	1	1	1	1.5	1	-1.31566819	4.04218773
0.04						-1.53640389	2.69425801
0.07						-1.83309969	1.82571968
0.1						-2.23626267	1.25732143
	0					-2.05499683	1.24567815
	1					-2.23626267	1.25732143
	3					-2.55833356	1.27519931
	5					-2.84185954	1.28832024
		1				-2.23626267	1.25732143
		1.5				-2.23360279	1.25715057
		2				-2.23091741	1.25697829
		2.5				-2.22820586	1.25680457
			-1			-1.47135446	0.51499994
			-0.5			-1.64056501	0.67145981
			0.5			-2.02355151	1.04510263
			1			-2.23626267	1.25732143
				1.2		-2.03895232	1.11810439
				1.5		-2.23626267	1.25732143
				1.8		-2.43248202	1.41661565
				2.1		-2.62786066	1.59104731
					0	-2.27747031	0.97952469
					0.5	-2.25163761	1.14019626
					1	-2.23626267	1.25732143
					1.5	-2.22583993	1.34955641

boundary layers are enhanced with an increase in the injection parameter. Similarly, the temperature profiles and the thermal boundary layer thickness reduce with an increase in the suction parameter, whereas an opposite trend is observed for the case of injection as shown in Fig. 4b. This result is in agreement with the findings of Jalil and Asghar [16].

The impact of the thermal radiation parameter on the nanofluid temperature profiles is presented in Fig. 5. From this plot, the nanofluid temperature profile is an increasing function of the thermal radiation parameter. The physical reason for this observed trend is that, for a higher value of the radiation parameter, more heat is transferred to the nanofluid since the mean absorption coefficient k_m reduces with an increase in the radiation parameter. This temperature profile is similar to Ramzan et al. [27] for the case of pure fluid.

Figure 6 displays the effect of the fluid parameter, λ , on the skin friction for distinct values of the fluid parameter, δ . Clearly, it is seen that the skin friction coefficient increases with an increase δ . The influence of the temperature ratio parameter and the thermal radiation parameter on the Nusselt number is displayed in Figs. 7 and 8. It is evident from these plots that the Nusselt number increases with an increase in the values of θ_w and Nr (Table 4).

7 Conclusions

The flow and heat transfer in a Powell–Eyring nanofluid flow past a stretching surface have been studied. The similarity solution to the model describing the nanofluid flow and energy balance was found using the Lie group analysis. An iterative spectral local linearization method was used to solve the conservation equations. The effects of nanoparticles, thermal radiation and suction/injection have been considered in the problem. The effects of these parameters on the nanofluid velocity and temperature profiles, as well as the skin friction coefficient and Nusselt number, are determined and discussed. A summary of the results of the study is as follows:

1. The velocity profiles are enhanced with an increase in the fluid parameter, λ and nanoparticle volume fraction.
2. The velocity and temperature profiles are decreasing functions of the suction parameter, while injection shows an opposite trend.
3. An increase in the nanoparticle volume fraction, thermal radiation parameter and temperature ratio parameter enhances the thermal boundary layer thickness as well as the temperature profiles.

4. The skin friction coefficient increases with an increase in the fluid parameter, δ .
5. Increasing the temperature ratio parameter and thermal radiation parameter increases the Nusselt number.

Funding The authors are grateful to the University of KwaZulu-Natal, South Africa, for financial support.

Compliance with ethical standards

Conflict of interest The authors declare that they have no conflict of interest.

References

1. Wong KV, De Leon O (2010) Applications of nanofluids: current and future. *Adv Mech Eng* 2:519659
2. Robert T, Sylvain C, Todd O, Patrick P, Andrey G, Wei L, Gary R, Ravi P, Himanshu T (2013) Small particles, big impacts: a review of the diverse applications of nanofluids. *J Appl Phys* 113(1):011301
3. Devendiran DK, Amirtham VA (2016) A review on preparation, characterization, properties and applications of nanofluids. *Renew Sustain Energy Rev* 60:21–40 ISSN 1364–0321
4. Munyalo JM, Zhang X (2018) Particle size effect on thermophysical properties of nanofluid and nanofluid based phase change materials: a review. *J Mol Liq* 265:77–87
5. Khan WA, Pop I (2010) Boundary-layer flow of a nanofluid past a stretching sheet. *Int J Heat Mass Transf* 53:2477–2483
6. Turkyilmazoglu M (2012) Exact analytical solutions for heat and mass transfer of MHD slip flow in nanofluids. *Chem Eng Sci* 84:182–187
7. Sandeep N, Gnanaswara RM (2017) Heat transfer of nonlinear radiative magnetohydrodynamic cu-water nanofluid flow over two different geometries. *J Mol Liq* 225:87–94
8. Dhlamini M, Mondal H, Sibanda P, Motsa S (2018) Spectral quasi-linearization methods for Powell–Eyring mhd flow over a nonlinear stretching surface. *J Nanofluids* 7(5):917–927
9. Das S, Mondal H, Kundu PK, Sibanda P (2019) Spectral quasi-linearization method for Casson fluid with homogeneous heterogeneous reaction in presence of nonlinear thermal radiation over an exponential stretching sheet. *Multidiscip Model Mater Struct* 15(2):398–417
10. Afify A A, El-Aziz M Abd (2017) Lie group analysis of flow and heat transfer of non-Newtonian nanofluid over a stretching surface with convective boundary condition. *Pramana* 88(2):31
11. Das K, Acharya N, Kundu PK (2018) Influence of variable fluid properties on nanofluid flow over a wedge with surface slip. *Arab J Sci Eng* 43(5):2119–2131. <https://doi.org/10.1007/s13336-9-017-2499-x>
12. Ogunseye HA, Sibanda P, Mondal H (2019) Mhd mixed convective stagnation-point flow of Eyring–Powell nanofluid over stretching cylinder with thermal slip conditions. *J Central South Univ* 26(5):1172–1183
13. Masoud HS, Moghadassi AR, Henneke DE (2010) A new dimensionless group model for determining the viscosity of nanofluids. *J Therm Anal Calorim* 100(3):873–877. <https://doi.org/10.1007/s10973-010-0721-0>

14. Hassani S, Saidur R, Mekhilef S, Hepbasli A (2015) A new correlation for predicting the thermal conductivity of nanofluids; using dimensional analysis. *Int J Heat Mass Transf* 90:121–130. <https://doi.org/10.1016/j.jheatmasstransfer.2015.06.040>
15. Akgül MB, Pakdemirli MM (2012) Lie group analysis of a non-newtonian fluid flow over a porous surface. *Sci Iran* 19(6):1534–1540
16. Jalil M, Asghar S (2013) Flow and heat transfer of Powell-Eyring fluid over a stretching surface: a lie group analysis. *J Fluids Eng* 135(12):121201–121206
17. Rehman K, Saba N, Malik MY, Malik AA (2017) Encountering heat and mass transfer mechanisms simultaneously in Powell-Eyring fluid through lie symmetry approach. *Case Stud Therm Eng* 10:541–549
18. Pakdemirli M, Yurusoy M (1998) Similarity transformations for partial differential equations. *SIAM Rev* 40(1):96–101
19. Hayat T, Herman Mambili-Mamboundou H, Momoniat E, Mahomed F M (2008) The Rayleigh problem for a third grade electrically conducting fluid in a magnetic field. *J Nonlinear Math Phys* 15(sup1):77–90
20. Abd-el Malek MB, Hassan HS (2010) Symmetry analysis for steady boundary-layer stagnation-point flow of Rivlin-Ericksen fluid of second grade subject to suction. *Nonlinear Anal: Modell Control* 15(4):379–396
21. Roşca NC, Roşca AV, Pop I (2016) Lie group symmetry method for mhd double-diffusive convection from a permeable vertical stretching/shrinking sheet. *Comput Math Appl* 71(8):1679–1693
22. Powell RE, Eyring H (1944) Mechanisms for the relaxation theory of viscosity. *Nature* 154(1):427–428
23. Javed T, Ali N, Abbas Z, Sajid M (2013) Flow of an Eyring–Powell non-Newtonian fluid over a stretching sheet. *Chem Eng Commun* 200(3):327–336
24. Hayat T, Iqbal Z, Qasim M, Obaidat S (2012) Steady flow of an Eyring-Powell fluid over a moving surface with convective boundary conditions. *Int J Heat Mass Transf* 55(7):1817–1822
25. Mahanthesh B, Gireesha BJ, Gorla RSR (2017) Unsteady three-dimensional MHD flow of a nano Eyring–Powell fluid past a convectively heated stretching sheet in the presence of thermal radiation, viscous dissipation and Joule heating. *J Assoc Arab Univ Basic Appl Sci* 23:75–84
26. Agbaje TM, Mondal S, Motsa SS, Sibanda P (2017) A numerical study of unsteady non-Newtonian Powell–Eyring nanofluid flow over a shrinking sheet with heat generation and thermal radiation. *Alex Eng J* 56(1):81–91
27. Ramzan M, Bilal M, Kanwal S, Chung JD (2017) Effects of variable thermal conductivity and non-linear thermal radiation past an Eyring-Powell nanofluid flow with chemical reaction. *Commun Theor Phys* 67(6):723
28. Khanafer K, Vafai K (2011) A critical synthesis of thermo-physical characteristics of nanofluids. *Int J Heat Mass Transf* 54(19):4410–4428
29. Pantokratoras A (2004) Further results on the variable viscosity on flow and heat transfer to a continuous moving flat plate. *Int J Eng Sci* 42(17):1891–1896
30. Motsa SS (2013) A new spectral local linearization method for nonlinear boundary layer flow problems. *J Appl Math Article ID* 423628, 15 pages
31. Mondal H, Almakki M, Sibanda P (2019) Dual solutions for three-dimensional magnetohydrodynamic nanofluid flow with entropy generation. *J Comput Des Eng* 6(4):657–665. <https://doi.org/10.1016/j.jcde.2019.01.003>
32. Motsa SS, Sibanda P, Shateyi S (2011) On a new quasi-linearization method for systems of nonlinear boundary value problems. *Math Methods Appl Sci* 34(11):1406–1413. <https://doi.org/10.1002/mma.1449>
33. Maleki M, Hashim I, Abbasbandy S (2012) Analysis of IVPS and BVPS on semi-infinite domains via collocation methods. *J Appl Math Article ID* 696574, 21 pages

Publisher's Note Springer Nature remains neutral with regard to jurisdictional claims in published maps and institutional affiliations.

Chapter 5

A mathematical model for entropy generation in a Powell-Eyring nanofluid flow in a porous channel

In this chapter we investigate the entropy generation rate in a mixed convective flow of a hydro-magnetic aluminum oxide-water Powell-Eyring nanofluid flow through a vertical channel. Using the nanofluid dynamic viscosity model based on experimental data, we analyze the combined effects of the magnetic field, viscous dissipation, suction/injection and convective cooling on the heat transfer and entropy generation rate. The spectral local linearization method is utilized in solving the conversation equations. This is the first model in this thesis in which we consider the entropy generation rate in the system. We found that the nanoparticle volume fraction and the Brinkman number are significant in minimizing the entropy generation rate in the channel flow. Hence, by increasing the nanoparticle volume fraction and reducing the Brinkman number the entropy generation rate in the channel can be optimized.



A mathematical model for entropy generation in a Powell-Eyring nanofluid flow in a porous channel



Hammed Abiodun Ogunseye*, Precious Sibanda

University of KwaZulu-Natal, School of Mathematics, Statistics and Computer Science, Private Bag X01, Scottsville, Pietermaritzburg 3209, South Africa

ARTICLE INFO

Keywords:

Applied mathematics
Computational mathematics
Thermodynamics

ABSTRACT

The continuous generation of entropy leads to exergy destruction which reduces the performance of a physical system. Hence, entropy minimization becomes necessary. New applications of nanofluids due to their enhanced thermo-physical properties has spurred new studies into the heat transfer and entropy generation rate in nanofluids in the last decade. In this study, we investigate the heat transfer performance and entropy generation rate in a mixed convective flow of a hydromagnetic Aluminum oxide-water Powell-Eyring nanofluid flow through a vertical channel. The nanofluid dynamic viscosity adopted is based on experimental data. The combined effects of the magnetic field, nonlinear thermal radiation, viscous dissipation, suction/injection and convective cooling on the heat transfer and entropy generation were considered. The dimensionless equations describing the flow and energy balance were solved using an efficient iterative spectral local linearization method. The computational analysis of the rate of entropy generation in the channel for various flow parameters is presented. The result shows that increasing the nanoparticle volume fraction and thermal radiation parameter enhanced the temperature profiles, entropy generation and the Bejan number. The results from this study may help engineers in the optimization of thermal systems.

1. Introduction

Nanofluids are stable and uniform colloids of nanometer-sized metals or metallic oxides called nanoparticles. These fluids have a higher thermal conductivity relative to the base fluid. Choi [1] reported that the thermal conductivity of the base fluid is significantly enhanced by adding a low volume fraction of nanoparticles. Nanofluids now find applications in the enhancement of chemical engineering operations, polymer processing and petrochemical applications. A comprehensive review of other applications of nanofluids is reported in the study by Wong and De Leon [2]. In recent years, considerable attention has been focused on the study of the transport phenomenon in nanofluid flow due to their wide applications. The study of the magnetohydrodynamics (MHD) nanofluid flow past a channel was investigated by Sheikholeslami et al. [3]. They obtained a series solution to the flow equations by using the Least Square and Galerkin methods. Raza et al. [4] extended the Sheikholeslami et al. [3] model to include heat transfer analysis. The heat equation was solved using the Runge-Kutta-Fehlberg shooting technique. Hayat et al. [5] studied the MHD nanofluid flow in a rotating porous disk. Malvandi and Ganji [6] examined the thermal transport in a nanofluid within a circular microchannel. Das et al.

[7] presented the radiative hydromagnetic buoyancy-induced flow and heat transfer in a nanofluid.

In these studies, emphasis was dominantly placed on the Newtonian constitutive model. However, in recent years, the focus of researchers has been centered on the study of non-Newtonian fluids due to their industrial, technological and medical applications. These fluids exhibit complex relations between stress and the rate of strain, hence, they deviate from the Newton's law of viscosity. A single constitutive relation cannot be used to understand the complex nature of non-Newtonian fluids. On account of this fact, several non-Newtonian constitutive models have been put forward by scientist, among which but not limited to, are the power-law fluid model, Casson fluid model, viscoelastic fluid model and Powell-Eyring fluid model. Researchers have focused attention on the Powell-Eyring model [8] due to its advantages over other non-Newtonian models. The Powell-Eyring model is derived from the kinetics theory of fluids and not on an empirical relation. Further, under certain shear rates, the model reduces to a Newtonian model. The flow and heat transport in a Powell-Eyring fluid has been studied by many researchers. Tanveer et al. [9] studied the mixed convection peristaltic flow of a Powell-Eyring nanofluid in a curved channel. Khan and Pop [10] investigated the heat and mass transfer in a nanofluid past a

* Corresponding author.

E-mail address: ogunseyehammed@gmail.com (H.A. Ogunseye).

<https://doi.org/10.1016/j.heliyon.2019.e01662>

Received 6 January 2019; Received in revised form 3 April 2019; Accepted 2 May 2019

2405-8440/© 2019 Published by Elsevier Ltd. This is an open access article under the CC BY-NC-ND license (<http://creativecommons.org/licenses/by-nc-nd/4.0/>).

stretching plate. Agbaje et al. [11] studied the transient developing flow of a Powell-Eyring nanofluid over a shrinking plane. The effects of slip conditions on the flow of a Powell-Eyring nanofluid was discussed by Hina [12]. Hayat et al. [13] reported the heat transport in a radiative Powell-Eyring nanofluid.

Exergy loss is a major challenge in many industrial processes. Recently, the interest of many researchers has shifted towards entropy generation analysis in a nanofluid flow. This is important in many thermal engineering processes, because the continuous generation of entropy eventually leads to exergy destruction in the system. Therefore, the optimization of the performance of industrial and engineering processes is necessary and could be achieved by minimizing entropy generation [14]. The second law of thermodynamics is an efficient and accurate tool for optimizing a given system as opposed to the first law of thermodynamics. Following Bejan [14] several studies on the entropy generation minimization based on second law thermodynamics analysis have appeared in the literature. Pakdemirli and Yilbas [15] analyzed the entropy generation in a third-grade fluid. Das et al. [16] studied the entropy generation in the hydrodynamics pseudo-plastic in a nanofluid flow through a porous channel. Ting et al. [17] discussed the effect of viscous dissipation on the entropy generation in a nanofluid flow in a channel. The exact solution to the study of entropy generation in the magnetohydrodynamic fluid flow was presented by Ibáñez [18]. López et al. [19] reported on the entropy generation in a magnetohydrodynamic flow of a nanofluid in a porous channel. They considered the effect of non-linear thermal radiation and convective-radiative boundary conditions. Makinde and Eegunjobi [20] studied numerically, the impact of convective heating on the entropy generation rate of a steady flow between two permeable walls. Recently, Nagaraju et al. [21] considered the effect of suction and magnetic field effects on the entropy generation in the fluid flow through a circular pipe. The homotopy perturbation method was used for the solution of the flow equations. Computational simulation on the role of magnetic forces on ferrofluid second law treatment was scrutinized by Sheikholeslami [22]. Jangili et al. [23] studied the entropy generation in a couple stress fluid flow. The homotopy analysis method was utilized for their analysis. Further studies on the minimization of entropy generation in the fluid flow using second law analysis under different geometry are reported in [24, 25, 26, 27, 28].

The aim of this study is to examine the entropy generation in the flow of a Powell-Eyring nanofluid in a porous channel. The mathematical formulation includes the effects of hydrodynamic slip, viscous dissipation, nonlinear thermal radiation and convective boundary conditions. The flow equations are solved numerically using an iterative spectral local linearization method. The findings may be useful in optimizing thermal engineering processes such as crude pyrolysis.

2. Model

2.1. Mathematical formulation and analysis

The mixed convective laminar, viscous flow of an incompressible Powell-Eyring nanofluid through a vertical channel separated by a distance h apart is considered. The schematic diagram for the flow geometry is shown in Fig. 1. It is assumed that an external transverse and uniform magnetic field of strength B_0 is applied parallel to the flow field. We assumed the magnetic Reynold number and induced electric field to be negligible.

With the above assumptions, the momentum and heat balance equations for the Powell-Eyring nanofluid flow are written as [11, 19]

$$\rho_{nf} V_0 \frac{d\bar{u}}{d\bar{y}} = -\frac{d\bar{P}}{d\bar{x}} + \left(\mu_{nf} + \frac{1}{bc}\right) \frac{d^2\bar{u}}{d\bar{y}^2} - \frac{1}{2bc^3} \left(\frac{d\bar{u}}{d\bar{y}}\right)^2 \frac{d^2\bar{u}}{d\bar{y}^2} - \sigma_{nf} B_0^2 \bar{u} + g(\rho\beta)_{nb} (T - T_0), \tag{1}$$

$$(\rho C_p)_{np} V_0 \frac{d\bar{T}}{d\bar{y}} = k_{nf} \frac{d^2\bar{T}}{d\bar{y}^2} + \frac{16\sigma_s}{3k_m} \frac{d}{d\bar{y}} \left(\bar{T}^3 \frac{d\bar{T}}{d\bar{y}}\right) + \left(\mu_{nf} + \frac{1}{bc}\right) \left(\frac{d\bar{u}}{d\bar{y}}\right)^2 - \frac{1}{6bc^3} \left(\frac{d\bar{u}}{d\bar{y}}\right)^4 + \sigma_{nf} B_0^2 \bar{u}^2, \tag{2}$$

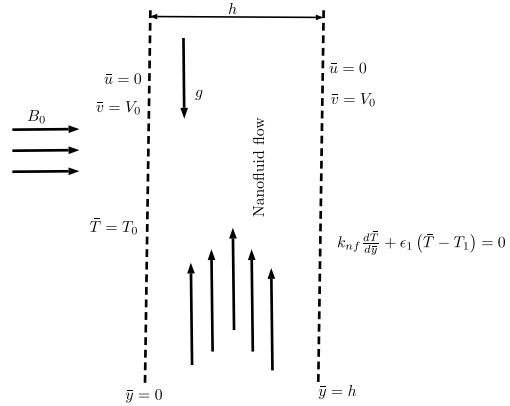


Fig. 1. Geometry of the flow.

where V_0 is the uniform suction/injection velocity at the channel plates, \bar{u} is the axial velocity, μ_{nf} is the dynamic viscosity of nanofluid, b and c are fluid constants, σ_{nf} is the nanofluid electrical conductivity, g is the gravitational acceleration, ρ_{nf} is the nanofluid density, β_{nb} is the thermal expansion coefficient of nanofluid, \bar{T} is the nanofluid temperature, T_0 is the ambient temperature, $(C_p)_{nb}$ is the heat capacitance of nanofluid, k_{nf} is nanofluid thermal conductivity, σ_s is the Stefan-Boltzman constant and k_m is the mean absorption coefficient.

The relevant boundary conditions for Eqs. (1) and (2) are:

$$\bar{u} = 0, \quad \bar{T} = T_0, \quad \text{at } \bar{y} = 0, \tag{3}$$

$$\bar{u} = 0, \quad k_{nf} \frac{d\bar{T}}{d\bar{y}} + \epsilon_1 (\bar{T} - T_1) = 0, \quad \text{at } \bar{y} = h \tag{4}$$

where ϵ_1 is the convective heat transfer coefficients.

Nguyen et al. [29] proposed a new model for the dynamic viscosity of Al_2O_3 -water nanofluid based on their experimental data. Adopting the Nguyen et al. [29] model, the nanofluid viscosity can be represented by the relation

$$\frac{\mu_{nf}}{\mu_{bf}} = 1 + 0.025\phi + 0.015\phi^2. \tag{5}$$

The density, thermal expansion coefficient, electrical conductivity, specific heat capacity and thermal conductivity of the nanofluid are determined by the expressions (see Khanafer and Vafai [30] and Das and Jana [31]),

$$\left. \begin{aligned} \frac{\rho_{nf}}{\rho_{bf}} &= 1 - \phi + \phi \frac{\rho_s}{\rho_{bf}}, \\ \frac{(\rho\beta)_{nf}}{(\rho\beta)_{bf}} &= 1 - \phi + \phi \frac{(\rho\beta)_s}{(\rho\beta)_{bf}}, \\ \frac{\sigma_{nf}}{\sigma_{bf}} &= \left[1 + \frac{3 \left(\frac{\sigma_s}{\sigma_{bf}} - 1\right) \phi}{\left(\frac{\sigma_s}{\sigma_{bf}} + 2\right) - \left(\frac{\sigma_s}{\sigma_{bf}} - 1\right) \phi} \right], \\ \frac{(\rho C_p)_{nf}}{(\rho C_p)_{bf}} &= 1 - \phi + \phi \frac{(\rho C_p)_s}{(\rho C_p)_{bf}}, \\ \frac{k_{nf}}{k_{bf}} &= \frac{k_s + 2k_{bf} - 2(k_{bf} - k_s) \phi}{k_s + 2k_{bf} + (k_{bf} - k_s) \phi}. \end{aligned} \right\} \tag{6}$$

In Eqs. (5) and (6), ϕ denotes the nanoparticle volume fraction, the subscripts bf and s represent the properties of the base fluid and nanoparticles respectively. The thermo-physical properties of the Al_2O_3 -water nanofluid are presented in Table 1.

Table 1

Thermo-physical properties of water and Al₂O₃ [16].

	ρ	C_p (J kg ⁻¹ K ⁻¹)	k (Wm ⁻¹ K ⁻¹)	$\beta \times 10^5$ (K ⁻¹)	σ (Sm ⁻¹)
Water	997.1	4179	0.613	21	5.5×10^{-6}
Al ₂ O ₃	3970	765	40	0.85	35×10^6

In order to express Eqs. (1), (2), (3) and (4) in a nondimensional form, it is necessary to define the dimensionless variables accordingly, and the following variables are chosen [19, 23, 26]:

$$y = \frac{\bar{y}}{h}, \quad x = \frac{\bar{x}}{h}, \quad u = \frac{\bar{u}h\rho_{bf}}{\mu_{bf}}, \quad P = \frac{\bar{P}h^2\rho_{bf}}{\mu_{bf}^2}, \quad \theta = \frac{\bar{T} - T_0}{T_1 - T_0}. \quad (7)$$

Using Eq. (7), Eqs. (1), (2), (3) and (4) yields the following dimensionless form;

$$(1 + 0.025\phi + 0.015\phi^2 + \lambda) \frac{d^2u}{dy^2} - \delta\lambda \left(\frac{du}{dy}\right)^2 \frac{d^2u}{dy^2} - \frac{\sigma_{nf}}{\sigma_{bf}} Ha^2 u + \frac{(\rho\beta)_{nf}}{(\rho\beta)_{bf}} Gr\theta - \frac{\rho_{nf}}{\rho_{bf}} Re \frac{du}{dy} + G = 0, \quad (8)$$

$$\left(\frac{k_{nf}}{k_{bf}} + Nr[(\theta_w - 1)\theta + 1]^3\right) \frac{d^2\theta}{dy^2} + 3Nr(\theta_w - 1)[(\theta_w - 1)\theta + 1]^2 \left(\frac{d\theta}{dy}\right)^2 - \frac{(C_p)_{nf}}{(C_p)_{bf}} RePr \frac{d\theta}{dy} + Br \left[(1 + 0.025\phi + 0.015\phi^2 + \lambda) \left(\frac{du}{dy}\right)^2 - \frac{\delta\lambda}{3} \left(\frac{du}{dy}\right)^4 + \frac{\sigma_{nf}}{\sigma_{bf}} Ha^2 u^2 \right] = 0, \quad (9)$$

$$u = 0, \quad \theta = 0, \quad \text{at } y = 0, \quad (10)$$

$$u = 0, \quad \frac{k_{nf}}{k_{bf}} \frac{d\theta}{dy} + \gamma(\theta - 1) = 0, \quad \text{at } y = 1, \quad (11)$$

where λ and δ are fluid constants, Ha is the Hartmann number, Gr is the Grashof number, Re is the suction/injection parameter, G is the axial pressure gradient parameter, Nr is the thermal radiation parameter, θ_w is the temperature ratio parameter, Pr is the Prandtl number, Br is the Brinkman number which is related to the Eckert number, γ is the Biot number. These parameters are defined as;

$$\lambda = \frac{1}{bc\mu_{bf}}, \quad \delta = \frac{\mu_{bf}^2}{2c^2\rho_{bf}^2h^4}, \quad Ha^2 = \frac{\sigma_{bf}B_0h^2}{\mu_{bf}},$$

$$Gr = \frac{g\beta_{bf}\rho_{bf}^2(T_1 - T_0)h^3}{\mu_{bf}^2}, \quad Re = \frac{\rho_{bf}V_0h}{\mu_{bf}}, \quad \gamma = \frac{hc_1}{k_{bf}}, \quad (12)$$

$$G = -\frac{dP}{dx}, \quad Nr = \frac{16\sigma_s T_0^3}{3k_m k_{bf}}, \quad \theta_w = \frac{T_1}{T_0}, \quad Pr = \frac{\mu_{bf}(C_p)_{bf}}{k_{bf}},$$

$$Br = \frac{\mu_{bf}^3}{\rho_{bf}k_{bf}(T_1 - T_0)h^2}, \quad \gamma_2 = \frac{hc_2}{k_{bf}}.$$

Other important physical properties are the skin-friction coefficient C_f and local Nusselt number Nu which are defined as follows:

$$C_f = \frac{\rho_{bf}h^2\tau_w}{\mu_{bf}}; \quad \tau_w = \left(\mu_{nf} + \frac{1}{bc}\right) \left(\frac{d\bar{u}}{d\bar{y}}\right) - \frac{1}{6bc^3} \left(\frac{d\bar{u}}{d\bar{y}}\right)^3 \Big|_{\bar{y}=0} = 0, \quad (13)$$

$$Nu = \frac{hq_w}{k_{bf}(T_1 - T_0)}; \quad q_w = -\left(k_{nf} + \frac{16\sigma_s\bar{T}^3}{3k_m}\right) \frac{d\bar{T}}{d\bar{y}} \Big|_{\bar{y}=0}. \quad (14)$$

In terms of Eq. (7), the dimensionless forms of Eqs. (13) and (14) are given by

$$C_f = (1 + 0.025\phi + 0.015\phi^2 + \lambda) \frac{du}{dy} \Big|_{y=0} - \frac{\delta\lambda}{3} \left(\frac{du}{dy} \Big|_{y=0}\right)^3, \quad (15)$$

$$Nu = -\left(\frac{k_{nf}}{k_{bf}} + Nr\right) \frac{d\theta}{dy} \Big|_{y=0}. \quad (16)$$

2.2. Entropy generation

In many thermodynamic processes, energy management is of great concern when a large amount of energy is dissipated as heat. Hence, it is important to investigate the entropy generation of the system. Conforming with Bejan [14], the entropy generation rate per volume in the nanofluid flow in the channel can be expressed as

$$S_G = \underbrace{\frac{1}{T_0^2} \left(k_{nf} + \frac{16\sigma_s\bar{T}^3}{3k_m}\right) \left(\frac{d\bar{T}}{d\bar{y}}\right)^2}_{\text{First term}} + \underbrace{\frac{1}{T_0} \left[\left(\mu_{nf} + \frac{1}{bc}\right) \left(\frac{d\bar{u}}{d\bar{y}}\right)^2 - \frac{1}{6bc^3} \left(\frac{d\bar{u}}{d\bar{y}}\right)^4\right]}_{\text{Second term}} + \underbrace{\frac{\sigma_{nf}B_0^2}{T_0} \bar{u}^2}_{\text{Third term}}. \quad (17)$$

In Eq. (17) the first term represents the heat entropy generation due to heat transfer and thermal radiation, the second term denotes the entropy production due to fluid frictional interaction and finally, the third term indicates the entropy generation due to magnetic field.

Using Eq. (7), we can rewrite Eq. (17) as

$$N_s = \frac{T_0h^2S_G}{k_{bf}(T_1 - T_0)^2} = \left(\frac{k_{nf}}{k_{bf}} + Nr[(\theta_w - 1)\theta + 1]^3\right) \left(\frac{d\theta}{dy}\right)^2 + \frac{Br}{\theta_w - 1} \left[(1 + 0.025\phi + 0.015\phi^2 + \lambda) \left(\frac{du}{dy}\right)^2 - \frac{\delta\lambda}{3} \left(\frac{du}{dy}\right)^4 + \frac{\sigma_{nf}}{\sigma_{bf}} Ha^2 u^2 \right] \quad (18)$$

Let us define the following variables

$$N_f = \frac{Br}{\theta_w - 1} \left[(1 + 0.025\phi + 0.015\phi^2 + \lambda) \left(\frac{du}{dy}\right)^2 - \frac{\delta\lambda}{3} \left(\frac{du}{dy}\right)^4 + \frac{\sigma_{nf}}{\sigma_{bf}} Ha^2 u^2 \right],$$

$$N_h = \left(\frac{k_{nf}}{k_{bf}} + Nr[(\theta_w - 1)\theta + 1]^3\right) \left(\frac{d\theta}{dy}\right)^2, \quad (19)$$

then N_f is the irreversibility due to combined effects of viscous dissipation and magnetic field and N_h is the heat transfer with thermal radiation irreversibility.

The Bejan number can be used to determine the relative effects of the heat transfer irreversibility and irreversibility due to combined effects of viscous dissipation and magnetic field in the entropy generation. Thus, we define the Bejan, number, Be , as (see Bejan [14])

$$Be = \frac{N_h}{N_h + N_f} = \frac{1}{1 + M}, \quad (20)$$

where $M = N_f/N_h$ is the irreversibility ratio.

3. Calculation

3.1. Numerical solution

In this section, an efficient iterative spectral local linearization method (SLLM) proposed by Motsa [32] is used to numerically integrate the coupled non-linear differential Eqs. (8) and (9) with the boundary conditions Eqs. (10) and (11). To apply this technique, we consider the following non-linear differential operators

$$\Omega_u = (1 + 0.025\phi + 0.015\phi^2 + \lambda) u_n'' - \delta\lambda (u' - n)^2 u_n'' - \frac{\sigma_{nf}}{\sigma_{bf}} Ha^2 u_n + \frac{(\rho\beta)_{nf}}{(\rho\beta)_{bf}} Gr\theta_n - \frac{\rho_{nf}}{\rho_{bf}} Re u_n' + G \quad (21)$$

$$\begin{aligned} \Omega_\theta &= \left(\frac{k_{nf}}{k_{bf}} + Nr [(\theta_w - 1)\theta_n + 1]^3 \right) \theta''_n \\ &+ 3Nr (\theta_w - 1) [(\theta_w - 1)\theta_n + 1]^2 (\theta'_n)^2 - \frac{(C_p)_{nf}}{(C_p)_{bf}} Re Pr \theta'_n \\ &+ Br \left[(1 + 0.025\phi + 0.015\phi^2 + \lambda) (u'_n)^2 - \frac{\delta\lambda}{3} (u'_n)^4 + \frac{\sigma_{nf}}{\sigma_{bf}} Ha^2 u_n^2 \right] \end{aligned} \quad (22)$$

where the prime denotes derivative with respect to y .

Eqs. (21) and (22) can be decoupled according to the following algorithm;

1. From Ω_u , find u_{n+1} assuming that θ_n is known from the previous iteration.
2. Solve for θ_{n+1} from Ω_θ using the updated solution of f_n .
3. Subsequent iterative solutions are obtained by repeating step 1 and 2.

In the framework of the SLLM, the following iterative scheme is obtained

$$a_{1,n} u''_{n+1} + a_{2,n} u'_{n+1} + a_{3,n} u_{n+1} = R^u, \quad (23)$$

$$a_{4,n} \theta''_{n+1} + a_{5,n} \theta'_{n+1} + a_{6,n} \theta_{n+1} = R^\theta, \quad (24)$$

$$u_{n+1}(0) = 0, \quad \theta_{n+1}(0) = 0, \quad (25)$$

$$u_{n+1}(1) = 0, \quad \frac{k_{nf}}{k_{bf}} \theta'_{n+1}(1) + \gamma (\theta_{n+1}(1) - 1) = 0. \quad (26)$$

The coefficients in Eqs. (23) and (24) along with their right hand sides are defined as follows

$$a_{1,n} = \frac{\partial \Omega_u}{\partial u''_n} = 1 + 0.025\phi + 0.015\phi^2 + \lambda - \delta \lambda u_n^2,$$

$$a_{2,n} = \frac{\partial \Omega_u}{\partial u'_n} = -2 \lambda \delta u_n u'_n - \frac{\rho_{nf}}{\rho_{bf}} Re$$

$$a_{3,n} = \frac{\partial \Omega_u}{\partial u_n} = -\frac{\sigma_{nf}}{\sigma_{bf}} Ha^2, \quad a_{4,n} = \frac{\partial \Omega_\theta}{\partial \theta''_n} = \left(\frac{k_{nf}}{k_{bf}} + Nr [(\theta_w - 1)\theta_n + 1]^3 \right)$$

$$a_{5,n} = \frac{\partial \Omega_\theta}{\partial \theta'_n} = 6Nr (\theta_w - 1) (1 + (\theta_w - 1)\theta_n)^2 \theta'_n - \frac{(C_p)_{nf}}{(C_p)_{bf}} Re Pr \quad (27)$$

$$a_{6,n} = \frac{\partial \Omega_\theta}{\partial \theta_n} = 3Nr (\theta_w - 1) [(\theta_w - 1)\theta_n + 1]^2 \theta''_n + 6Nr (\theta_w - 1)^2 [(\theta_w - 1)\theta_n + 1] (\theta'_n)^2$$

$$R^u = a_{1,n} u''_n + a_{2,n} u'_n + a_{3,n} u_n - \Omega_f, \quad R^\theta = a_{4,n} \theta''_n + a_{5,n} \theta'_n + a_{6,n} \theta_n - \Omega_\theta.$$

The Eqs. (23), (24), (25), (26) and (26), are solved numerically using the Chebyshev pseudo-spectral technique. To apply this method, we first map the interval $[0, 1]$ to $[-1, 1]$ using the transformation $y = (\xi + 1)/2$ for $\xi \in [-1, 1]$. Then, we discretize using Chebyshev-Gauss-Labatto collocation points

$$\xi_k = \cos\left(\frac{\pi k}{N}\right), \quad k = 0, 1, \dots, N; \quad -1 \leq \xi \leq 1. \quad (28)$$

The derivatives of $u(y)$ and $\theta(y)$ are computed using the Chebyshev differentiation matrix D (see [33]), at the collocation points as a matrix vector product, that is:

$$\frac{du}{dy} = \sum_{i=0}^{\bar{N}} D_{ij} f(\xi_i) = \mathbf{D}\mathbf{F}, \quad j = 0, 1, 2, \dots, \bar{N}, \quad (29)$$

$$\frac{d\theta}{dy} = \sum_{i=0}^{\bar{N}} D_{ij} \theta(\xi_i) = \mathbf{D}\Theta, \quad j = 0, 1, 2, \dots, \bar{N}, \quad (30)$$

where $\bar{N} + 1$ is the number of collocation points, $\mathbf{D} = 2D$, $\mathbf{F} = [u(\xi_0), u(\xi_1), \dots, u(\xi_{\bar{N}})]^T$ and $\Theta = [\theta(\xi_0), \theta(\xi_1), \dots, \theta(\xi_{\bar{N}})]^T$ are vector functions at the collocation points. The second order derivatives of

u and θ can be computed as the powers of \mathbf{D} , that is, $\theta''(y) = \mathbf{D}^2 \theta(y)$ and $u''(y) = \mathbf{D}^2 u(y)$.

Substituting Eqs. (28), (29) and (30) into Eqs. (23), (24), (25) and (26) and imposing the boundary conditions, gives the following decoupled matrices

$$\begin{aligned} &\begin{bmatrix} 1 & \dots & 0 \\ \text{diag}[a_{1,n}]\mathbf{D}^2 + \text{diag}[a_{2,n}]\mathbf{D} + \text{diag}[a_{3,n}]\mathbf{I} \\ 0 & \dots & 1 \end{bmatrix} \begin{bmatrix} u_{n+1}(\xi_0) \\ u_{n+1}(\xi_1) \\ \vdots \\ u_{n+1}(\xi_{\bar{N}-1}) \\ u_{n+1}(\xi_{\bar{N}}) \end{bmatrix} \\ &= \begin{bmatrix} 0 \\ R_{n+1}^f(\xi_1) \\ \vdots \\ R_{n+1}^f(\xi_{\bar{N}-1}) \\ 0 \end{bmatrix}, \end{aligned} \quad (31)$$

$$\begin{aligned} &\begin{bmatrix} 1 & \dots & 0 \\ \text{diag}[a_{4,n}]\mathbf{D}^2 + \text{diag}[a_{5,n}]\mathbf{D} + \text{diag}[a_{6,n}]\mathbf{I} \\ \frac{k_{nf}}{k_{bf}}\mathbf{D} + \gamma\mathbf{I} \end{bmatrix} \begin{bmatrix} \theta_{n+1}(\xi_0) \\ \theta_{n+1}(\xi_1) \\ \vdots \\ \theta_{n+1}(\xi_{\bar{N}-1}) \\ \theta_{n+1}(\xi_{\bar{N}}) \end{bmatrix} \\ &= \begin{bmatrix} 0 \\ R_{n+1}^\theta(\xi_1) \\ \vdots \\ R_{n+1}^\theta(\xi_{\bar{N}-1}) \\ \gamma \end{bmatrix}, \end{aligned} \quad (32)$$

where \mathbf{I} is an identity matrix of dimension $(\bar{N} + 1) \times (\bar{N} + 1)$ and $\text{diag}[\]$ denotes a diagonal matrix.

4. Results & discussion

The nanofluid velocity profiles, temperature profiles, entropy generation rate and Bejan number for distinct values of the fluid parameter λ , Hartmann number Ha , Grashof number Gr , suction/injection parameter Re , thermal radiation parameter Nr , temperature ratio parameter θ_w , Brinkman number Br and Biot number γ are presented in Figs. 2, 3, 4, 5, 6, 7, 8, 9 and 10 and discussed based on physical laws. In these profiles, unless otherwise stated, we have assigned the following default values to the parameters: $\lambda = Ha = Gr = G = Re = Nr = Br = \gamma = 1$, $\theta_w = 1.5$ and $Pr = 6.97$.

Fig. 2A–D represents the effects of various values of the nanoparticle fraction volume ranging from $0 \leq \phi \leq 0.3$ on the velocity profiles, temperature profiles, entropy generation rate and Bejan number. In general, a parabolic trajectory is obtained for the nanofluid velocity profiles with the maximum value attained near the centerline. Fig. 2A shows that as the nanoparticle volume fraction increases, there is a corresponding decrease in the nanofluid flow. This is physically correct since increasing volume fraction would have a direct impact on the internal viscous shear stresses which in-turn shortens the inter-molecular forces between the fluid particles. An increment in the volume fraction of the nanoparticle leads to a further increment in the temperature profiles close the left permeable wall in the region of $y \in [0, 0.6]$. Thereafter, the temperature profile decreases in the rest of the region towards the right permeable wall. Interestingly, we observed that entropy generation rate decreases with an increase in the nanoparticle volume fraction while the Bejan number is an increasing function of the nanoparticle volume fraction as illustrated in Fig. 2C and D respectively.

The effect of varying the fluid material parameter, λ in the range $0 \leq \lambda \leq 1.5$ on the nanofluid velocity profiles, temperature profiles, entropy generation rate and Bejan number is displayed in Fig. 3A to C. We observed that as the material fluid parameter increases, there is a decrease in the nanofluid dynamic viscosity, hence, the fluid flow in the channel is reduced as represented in Fig. 3A. It is worth mentioning that $\lambda = 0$ corresponds to the Newtonian case and the velocity profiles

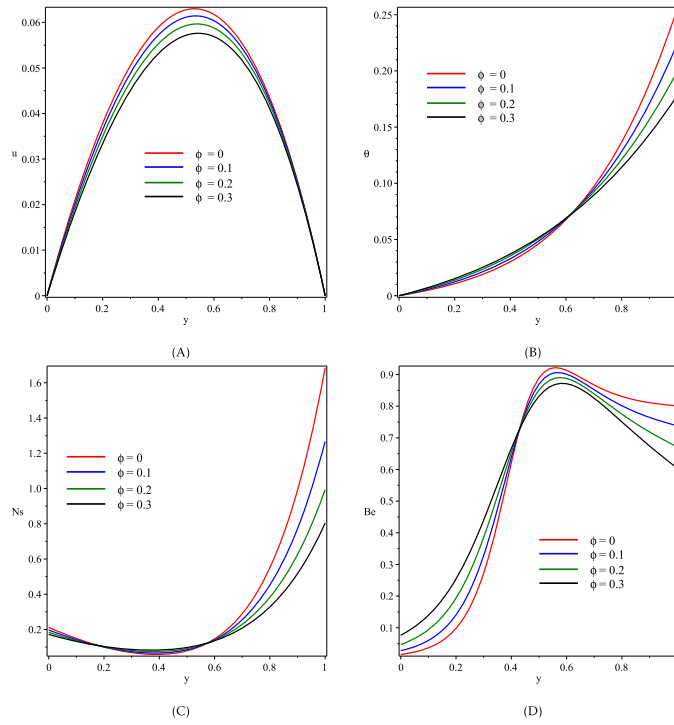


Fig. 2. Effect of varying the nanoparticle volume fraction on the nanofluid (A) velocity profiles, (B) temperature profiles, (C) entropy generation rate, (D) Bejan number.

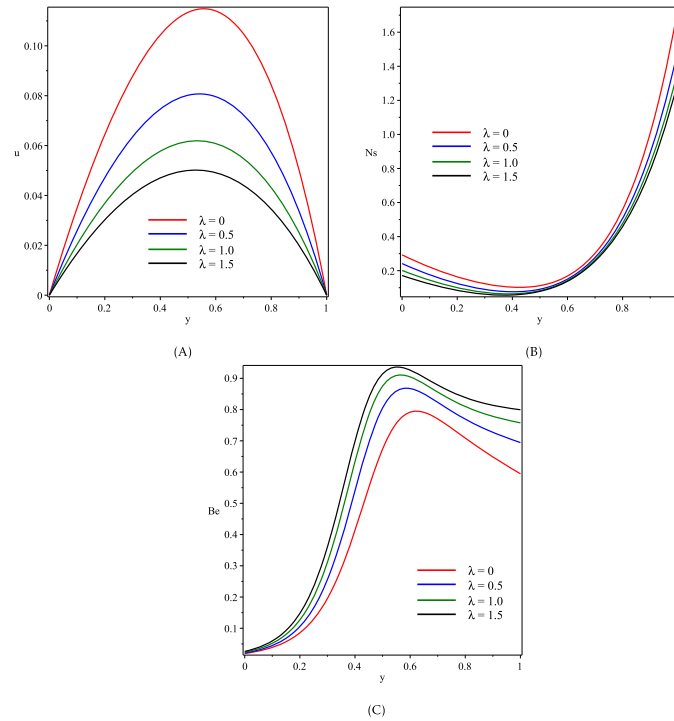


Fig. 3. Effect of varying the fluid material parameter on the nanofluid (A) velocity profiles, (B) entropy generation rate, (C) Bejan number.

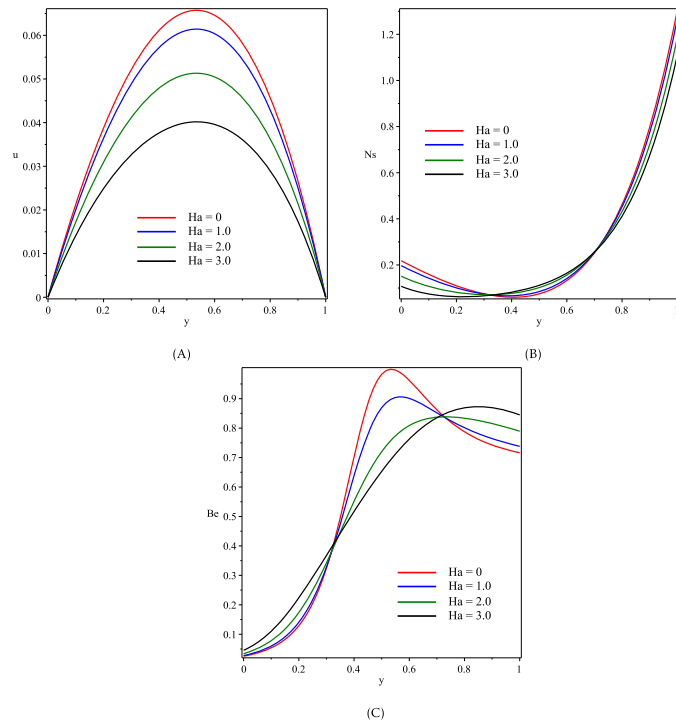


Fig. 4. Effect of increasing the Hartmann number on the nanofluid (A) velocity profiles, (B) entropy generation rate, (C) Bejan number.

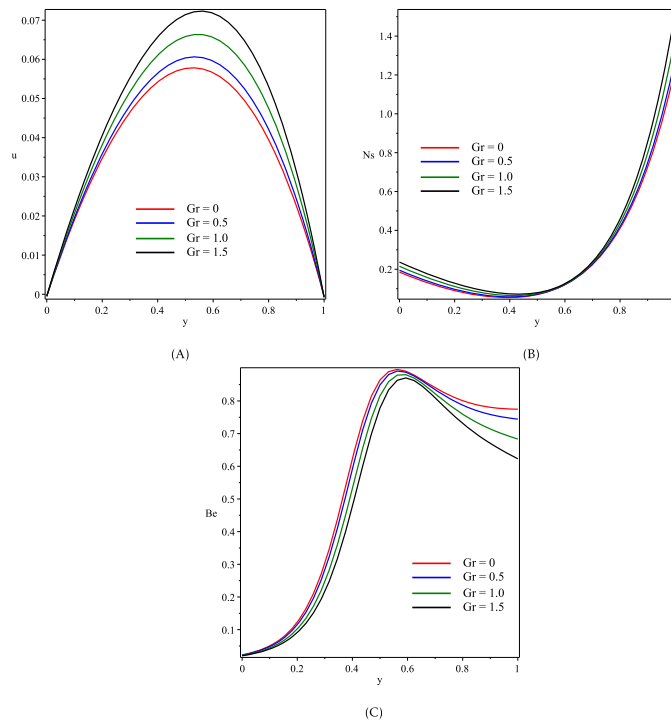


Fig. 5. Effect of increasing the Grashof number on the nanofluid (A) velocity profiles, (B) entropy generation rate, (C) Bejan number.

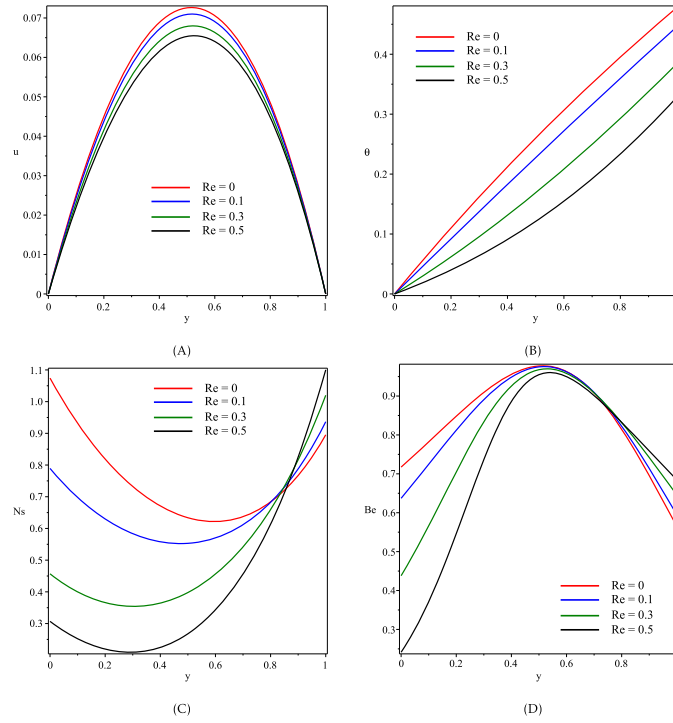


Fig. 6. Effect of varying the suction/injection Reynold number on the nanofluid (A) velocity profiles, (B) temperature profiles, (C) entropy generation rate, (D) Bejan number.

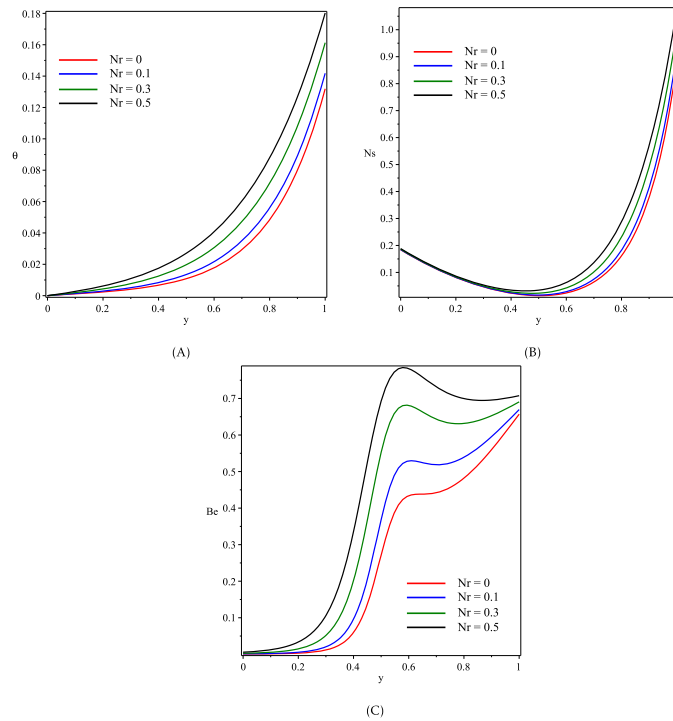


Fig. 7. Effect of varying the thermal radiation parameter on the nanofluid (A) temperature profiles, (B) entropy generation rate, (C) Bejan number.

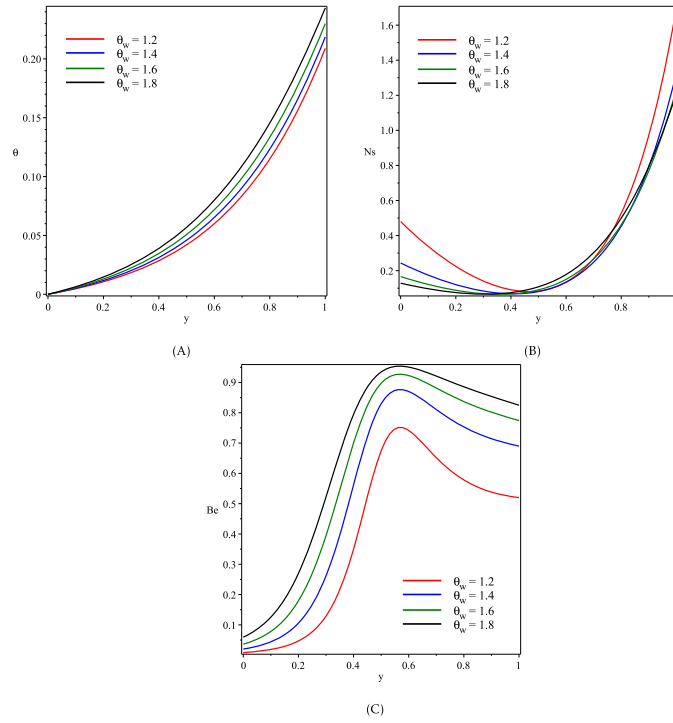


Fig. 8. Effect of varying the temperature ratio parameter on the nanofluid (A) temperature profiles, (B) entropy generation rate, (C) Bejan number.

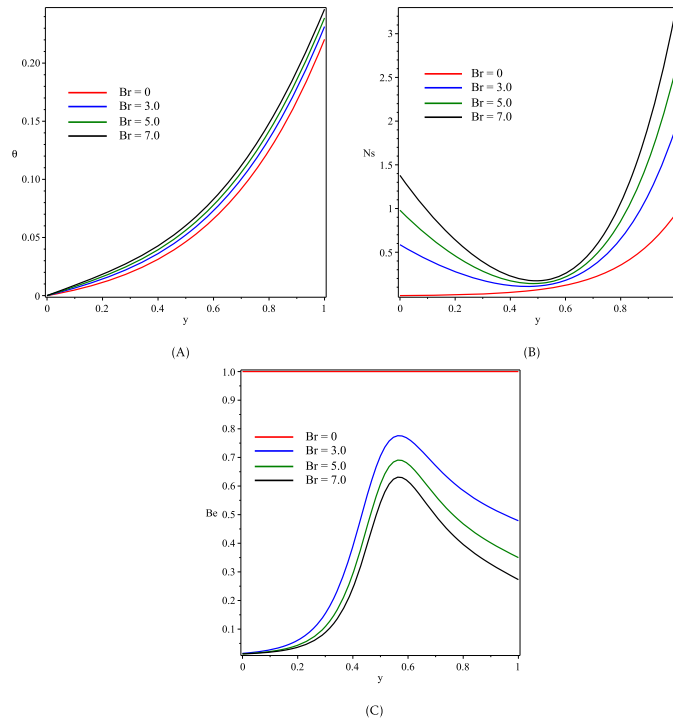


Fig. 9. Effect of varying the Brinkman number on the nanofluid (A) temperature profiles, (B) entropy generation rate, (C) Bejan number.

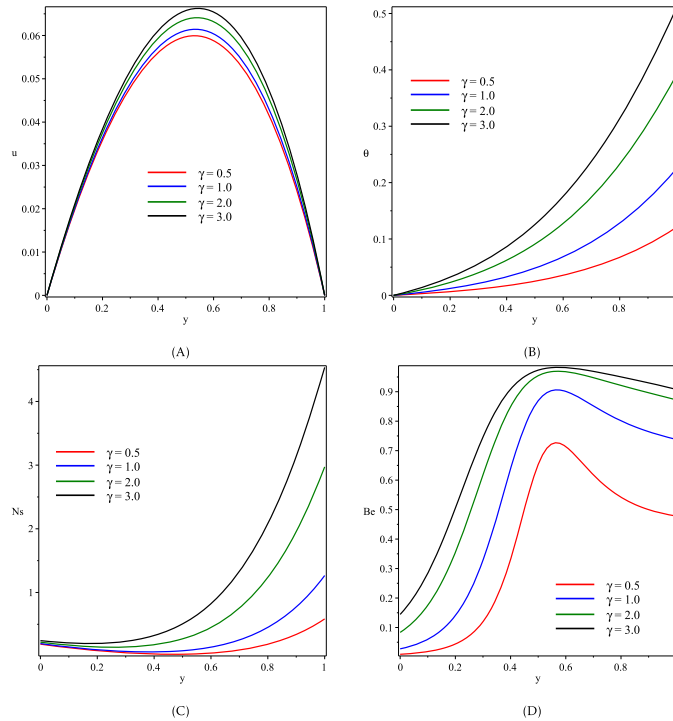


Fig. 10. Effect of varying the Biot number on the nanofluid (A) velocity profiles, (B) temperature profiles, (C) entropy generation rate, (D) Bejan number.

attained a maximum value for this case. Fig. 3B shows that the entropy generation number decreases with an increase in the fluid material parameter. This can be associated with the damping effect of the fluid material parameter on the nanofluid flow, thus, minimizing the entropy in the channel. It is easily seen from Fig. 3C that the Bejan number increases as the fluid material parameter increases.

We examined the effect of the transverse magnetic field on the nanofluid velocity, entropy generation and Bejan number. The velocity profiles, entropy generation rate and Bejan number for different values of the Hartmann number in the range $0 \leq Ha \leq 3$ are given in Fig. 4A to C. We observed that the flow in the channel decreases with an increase in the magnitude of the magnetic field intensity. Physically, this observation is correct, since, the nanofluid particles aggregate under the Lorentz dipolar forces from the transversely placed magnetic field. Interestingly, Fig. 4B shows that, the entropy generation number decreases as the Hartmann number increases close to the permeable wall, in the region $0 \leq y \leq 0.3$ and between $0.3 \leq y \leq 0.7$ the entropy generation number is an increasing function of the Hartmann number, thereafter, the entropy generation number decreases as the Hartmann number increases. The opposite trend is observed in Fig. 4C for increasing the Bejan number. Fig. 4C implies that the irreversibility due to fluid friction in the channel is higher than the heat transfer irreversibility in the region $0 \leq y \leq 0.3$ and $0.7 \leq y \leq 1$ while in the region $0.3 \leq y \leq 0.7$, the heat transfer irreversibility is higher than the irreversibility due to fluid friction.

The effect of varying the Grashof number in the range of $0 \leq Gr \leq 1.5$ on the nanofluid velocity profiles, entropy generation number and Bejan number is shown in Fig. 5A to C. We observed that the nanofluid velocity profile increases as the magnitude of the Grashof number increases as depicted in Fig. 5A. This is physically true because increasing the value of the Grashof number reduces the nanofluid dynamic viscosity. These increments lead to an increase in the volumetric thermal expansion in the channel which further enhances the nanofluid flow.

Entropy generation number increases as the Grashof number increases as seen in Fig. 5B. Fig. 5C indicates that the Bejan number decreases as the value of the Grashof number increases. This result shows that the irreversibility due to frictional forces and magnetic field dominates the irreversibility due to heat transfer in the channel.

Fig. 6A to C shows the influence of the suction/injection Reynolds number on the nanofluid velocity profiles, temperature profiles, entropy generation number and the Bejan number. The value of the suction/injection Reynolds number varies in the range $0 \leq Re \leq 0.5$. We observed that as the Reynolds number increases, both the fluid injection at the left permeable wall and the fluid suction at the right permeable wall also increase, hence the velocity profile decreases as shown in Fig. 6A. It is evident from Fig. 6B that the nanofluid temperature profiles decrease with an increase in the suction/injection Reynolds number. Within the region of $0 \leq y \leq 0.85$, both the entropy generation number and the Bejan number decrease with an increase in suction/injection Reynolds number, however, there is a change in trend close to the right permeable wall in the region of $0.85 \leq y \leq 1$ as depicted in Fig. 6C to D.

The effect of different values of the thermal radiation parameter on the nanofluid temperature profiles, entropy generation number and Bejan number are displayed in Fig. 7A to C. From Fig. 7A, the nanofluid temperature profiles are enhanced with the thermal radiation parameter. The physical reason for this observed trend is that, for a higher value of the radiation parameter, more heat is transferred to the nanofluid since the mean absorption coefficient k_m reduces with an increase in the radiation parameter. Clearly, from Fig. 7B and C, we observed that both the entropy generation number and the Bejan number increases in the channel as the values thermal radiation parameter increases. This observation may be attributed to the dominance heat irreversibility. A similar observation is seen for the behavior of the temperature ratio parameter as illustrated in Fig. 8A to C.

Fig. 9 shows the effects of varying the Brinkman number within the range of $0 \leq Br \leq 7$ on the nanofluid profiles. We observed from Fig. 9A

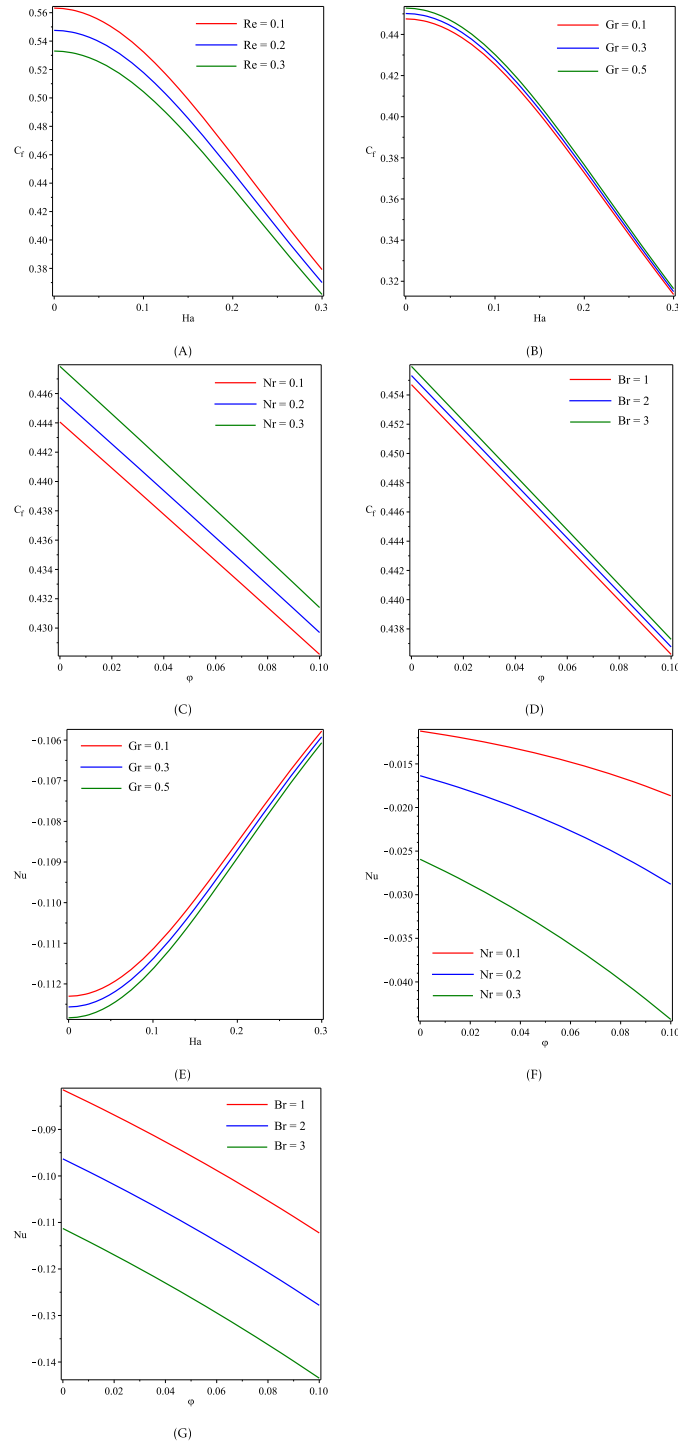


Fig. 11. (A) Effect of Reynolds number on skin friction coefficient, (B) effect of Grashof number on skin friction coefficient, (C) effect of radiation parameter on skin friction coefficient, (D) effect of Brinkman number on skin friction coefficient, (E) effect of Grashof number on Nusselt number, (F) effect of radiation parameter on Nusselt number, (G) effect of Brinkman number on Nusselt number.

that an increase in the values of the Brinkman number improves the temperature profiles. This is true, since increasing the magnitude of the Brinkman number implies an increase in the heat generated by dissipation which leads to a rise in the heat transfer rate within the channel. Fig. 9B shows the entropy generation number increases as the Brinkman number increases. Fig. 9C shows that in the absence of frictional heat irreversibility, the Bejan number is unity. Also, an increase in the Brinkman number decreases the Bejan number.

In Fig. 10, the effect of varying the Biot number on the nanofluid velocity profiles, temperature profiles, entropy generation number and Bejan number are illustrated. Fig. 10A to B shows that the nanofluid velocity profiles, as well as the temperature profiles, are enhanced with an increase in the Biot number. This is physically correct since increasing the values of the Biot number signifies an increase in the heat transfer coefficient, hence, the rate of cooling decreases while the temperature of the nanofluid within the channel rise. Both the entropy generation number and the Bejan number rises in the channel as seen in Fig. 10C to D.

The effects of various thermo-physical parameters on the skin friction and Nusselt number are illustrated in Fig. 11. We observed from these Figures that the skin friction decreases with increasing the values of Hartmann number, suction/injection Reynolds number and nanoparticle fraction volume but increases with an increase in Grashof number, thermal radiation parameter and Brinkman number. This can be attributed to a decrease or increase in nanofluid velocity gradient at the channel walls as the values of these parameters increases. Meanwhile, an increase in the Grashof number, thermal radiation parameter and Brinkman number decreases the Nusselt number due to a decrease in temperature gradient at the walls while an increase in Hartmann number and nanoparticle fraction volume increases the Nusselt number due to an increase in temperature gradient at the walls.

5. Conclusion

In this study, the entropy generation in a Powell-Eyring Al_2O_3 -water nanofluid flow in a vertical channel subjected to convective cooling has been studied. The transport equations were solved using an iterative spectral local linearization method. The entropy generation rate in the system has been analyzed using the second law of thermodynamics. In summary, the nanoparticle volume fraction and the Brinkman number are significant in minimizing the entropy generation rate in the channel. Hence, by increasing the nanoparticle volume fraction and reducing the Brinkman number the flow in channel can be optimized.

Declarations

Author contribution statement

Hammed Abiodun Ogunseye: Analyzed and interpreted the data; Wrote the paper.

Precious Sibanda: Conceived and designed the analysis.

Funding statement

This research did not receive any specific grant from funding agencies in the public, commercial, or not-for-profit sectors.

Competing interest statement

The authors declare no conflict of interest.

Additional information

No additional information is available for this paper.

References

- [1] S.U.S. Choi, Enhancing thermal conductivity of fluid with nanoparticles, developments and applications of non-Newtonian flow, in: ASME FED, vol. 231, 1995, pp. 95–105.
- [2] K.V. Wong, O. De Leon, Applications of nanofluids: current and future, *Adv. Mech. Eng.* 2 (2010) 519–659.
- [3] M. Sheikholeslami, M. Hatami, D.D. Ganji, Analytical investigation of MHD nanofluid flow in a semi-porous channel, *Powder Technol.* 246 (2013) 327–336.
- [4] J. Raza, A.M. Rohni, Z. Omar, MHD flow and heat transfer of Cu–water nanofluid in a semi porous channel with stretching walls, *Int. J. Heat Mass Transf.* 103 (2016) 336–340.
- [5] T. Hayat, M. Rashid, M. Imtiaz, A. Alsaedi, Magnetohydrodynamic (MHD) flow of Cu-water nanofluid due to a rotating disk with partial slip, *AIP Adv.* (2015).
- [6] A. Malvandi, D.D. Ganji, Brownian motion and thermophoresis effects on slip flow of alumina/water nanofluid inside a circular microchannel in the presence of a magnetic field, *Int. J. Therm. Sci.* 84 (2014) 196–206.
- [7] K. Das, P.R. Duari, P.K. Kumar, Solar radiation effects on Cu-water nanofluid flow over a stretching sheet with surface slip and temperature jump, *Arab. J. Sci. Eng.* 39 (2014) 9015–9023.
- [8] R.E. Powell, H. Eyring, Mechanisms for the relaxation theory of viscosity, *Nature* 154 (1) (1994) 427–428.
- [9] A. Tanveer, T. Hayat, F. Alsaadi, A. Alsaedi, Mixed convection peristaltic flow of Eyring-Powell nanofluid in a curved channel with compliant walls, *Comput. Biol. Med.* 82 (2017) 71–79.
- [10] W.A. Khan, I. Pop, Boundary-layer flow of a nanofluid past a stretching sheet, *Int. J. Heat Mass Transf.* 53 (11) (2010) 2477–2483.
- [11] T.M. Agbaje, S. Mondal, S.S. Motsa, P. Sibanda, A numerical study of unsteady non-Newtonian Powell-Eyring nanofluid flow over a shrinking sheet with heat generation and thermal radiation, *Alex. Eng. J.* 56 (1) (2017) 81–91.
- [12] S. Hina, MHD peristaltic transport of Eyring-Powell fluid with heat/mass transfer, wall properties and slip conditions, *J. Magn. Magn. Mater.* 404 (2016) 148–158.
- [13] T. Hayat, M.I. Khan, M. Waqas, A. Alsaedi, Effectiveness of magnetic nanoparticles in radiative flow of Eyring-Powell fluid, *J. Mol. Liq.* 231 (2017) 126–133.
- [14] A. Bejan, *Entropy Generation Minimization*, CRC, Boca Raton, 1996.
- [15] M. Pakdemirli, B.S. Yilbas, Entropy generation in a pipe due to non-Newtonian fluid flow: constant viscosity case, *Sādhanā* 31 (2006) 21–29.
- [16] S. Das, A.S. Banu, R.N. Jana, O.D. Makinde, Entropy analysis on MHD pseudo-plastic nanofluid flow through a vertical porous channel with convective heating, *Alex. Eng. J.* 54 (3) (2015) 325–337.
- [17] T.W. Ting, Y.M. Hung, N. Guo, Entropy generation of viscous dissipative nanofluid flow in thermal non-equilibrium porous media embedded in microchannels, *Int. J. Heat Mass Transf.* 81 (2015) 862–877.
- [18] G. Ibáñez, Entropy generation in MHD porous channel with hydrodynamic slip and convective boundary conditions, *Int. J. Heat Mass Transf.* 80 (2015) 274–280.
- [19] A. López, G. Ibáñez, J. Pantoja, J. Moreira, O. Lastres, Entropy generation analysis of MHD nanofluid flow in a porous vertical microchannel with nonlinear thermal radiation, slip flow and convective-radiative boundary conditions, *Int. J. Heat Mass Transf.* 107 (2017) 982–994.
- [20] O.D. Makinde, A.S. Eegunjobi, Effects of convective heating on entropy generation rate in a channel with permeable walls, *Entropy* 15 (2013) 220–233.
- [21] G. Nagaraju, S. Jangili, J.V. RamanaMurthy, O.A. Beg, A. Kadir, Second law analysis of flow in a circular pipe with uniform suction and magnetic field effects, *J. Heat Transf.* 141 (1) (2018) 012004.
- [22] M. Sheikholeslam, New computational approach for exergy and entropy analysis of nanofluid under the impact of Lorentz force through a porous media, *Comput. Methods Appl. Mech. Eng.* 344 (2019) 319–333.
- [23] S. Jangili, S.O. Adesanya, H.A. Ogunseye, R. Lebelo, Couple stress fluid flow with variable properties: a second law analysis, *Math. Methods Appl. Sci.* 42 (1) (2019) 85–98.
- [24] M.I. Afridi, M. Qasim, Entropy generation and heat transfer in boundary layer flow over a thin needle moving in a parallel stream in the presence of nonlinear Rosseland radiation, *Int. J. Therm. Sci.* 123 (2018) 117–128.
- [25] T. Hayat, F. Shaha, M.I. Khana, M. Imran Khan, A. Alsaedi, Entropy analysis for comparative study of effective Prandtl number and without effective Prandtl number via $\gamma Al_2O_3 - H_2O$ and $\gamma Al_2O_3 - C_2H_6O_2$ nanoparticles, *J. Mol. Liq.* 266 (2018) 814–823.
- [26] S.O. Adesanya, H.A. Ogunseye, J.A. Falade, R.S. Lebelo, Thermodynamic analysis for buoyancy-induced couple stress nanofluid flow with constant heat flux, *Entropy* 19 (580) (2017).
- [27] A.S. Eegunjobi, O.D. Makinde, MHD mixed convection slip flow of radiating Casson fluid with entropy generation in a channel filled with porous media, *Defect Diffus. Forum* 2017 (374) (2017) 47–66.
- [28] M. Sheikholeslami, Omid Mahian, Enhancement of PCM solidification using inorganic nanoparticles and an external magnetic field with application in energy storage systems, *J. Clean. Prod.* 215 (2019) 963–977.
- [29] C.T. Nguyen, F. Desgranges, N. Galanis, G. Roy, T. Maré, S. Boucher, H. Augue Mints, Viscosity data for Al_2O_3 -water nanofluid—hysteresis: is heat transfer enhancement using nanofluids reliable, *Int. J. Therm. Sci.* 47 (2008) 103–111.




- [30] K. Khanafer, K. Vafai, A critical synthesis of thermophysical characteristics of nanofluids, *Int. J. Heat Mass Transf.* 54 (19) (2011) 4410–4428.
- [31] S. Das, R.N. Jana, Natural convective magneto-nanofluid flow and radiative heat transfer past a moving vertical plate, *Alex. Eng. J.* 54 (1) (2015) 55–64.
- [32] S.S. Motsa, A new spectral local linearization method for nonlinear boundary layer flow problems, *J. Appl. Math.* (2013) 423628, 15 pages.
- [33] L.N. Trefethen, *Spectral Methods in MATLAB*, SIAM, 2000, p. 10.

Chapter 6

Entropy generation in an unsteady Eyring-Powell hybrid nanofluid flow over a permeable surface: A Lie group analysis

In this chapter, we extend the model investigated in Chapter 5 to the unsteady case using the novel class of hybrid nanofluids. We study the entropy generation in a viscous hybrid nanofluid described by the Eyring-Powell model. The similarity equations to the time-dependent model for the flow are obtained using the Lie group symmetry approach. The bivariate spectral quasilinearization method is used for the solution of the similarity equations. We also analyze the effect of viscous dissipation on the hybrid nanofluid flow. A comparison of the Nusselt number of a regular nanofluid and a hybrid nanofluid shows that the hybrid nanofluid has better thermal characteristics than the regular nanofluid.

Entropy generation in an unsteady Eyring-Powell hybrid nanofluid flow over a permeable surface: A Lie group analysis

Hammed Abiodun Ogunseye¹  | Yusuf Olatunji Tijani²  |
Precious Sibanda¹ 

¹School of Mathematics, Statistics and Computer Science, University of KwaZulu-Natal, Scottsville, Pietermaritzburg, South Africa

²Department of Mathematics and Applied Mathematics, Nelson Mandela University, Port Elizabeth, South Africa

Correspondence

Hammed Abiodun Ogunseye, School of Mathematics, Statistics and Computer Science, University of KwaZulu-Natal, Private Bag X01, Scottsville, Pietermaritzburg 3209, South Africa.
Email: ogunseyehammed@gmail.com

Abstract

In thermal processes, the choice of the thermofluid plays an essential role in minimizing entropy generation and thereby improving thermal efficiency. In this study, entropy generation in a viscous hybrid nanofluid described by the Eyring-Powell model is investigated. The model accounts for the effect of the nanoparticle volume fraction and viscous dissipation on an Eyring-Powell Cu-Al₂O₃/ethylene glycol nanofluid. A similarity solution to the time-dependent model is found using the Lie group symmetry technique. The bivariate spectral quasi-linearization method is used for the solution of the self-similar transport equations. We analyze the effects of the nanoparticle volume fraction, suction/injection, and viscous dissipation on the fluid properties. The skin friction and Nusselt number are determined. A comparison between the Nusselt number of a regular nanofluid and a hybrid nanofluid shows that the hybrid nanofluid has better thermal characteristics compared with the regular nanofluid. The findings show that a decrease in the nanoparticle volume fraction and Eckert number minimizes entropy generation in the system.

KEYWORDS

entropy generation, hybrid nanofluid, Lie group symmetry, Powell-Eyring model, spectral quasi-linearization method

1 | INTRODUCTION

Choi and Eastman¹ introduced the term nanofluid to describe a colloidal suspension of metallic particles with a diameter less than 10 nm in a regular fluid. Nanofluids have attracted significant theoretical and experimental studies. A review of literature on thermal properties of nanofluids can be found in Dhinesh and Valan² and the references therein. Efforts to further enhance the heat transfer rate of nanofluids have in recent years led to a new kind of nanofluid termed “hybrid nanofluid.” Hybrid nanofluids contain composite nanoparticles in a base fluid. These fluids have been reported to exhibit a better thermal characteristic than regular nanofluids, making the hybrid nanofluid a better thermofluid for industrial, engineering, and biomedical applications. Previous studies on hybrid nanofluids include those by Han et al.,³ Botha et al.,⁴ Xuan and Li,⁵ and Abbasi et al.⁶ A comprehensive review of the work so far was given by Sarkar et al.⁷

Although the heat transfer rate in a thermal system may be enhanced by using a nanofluid, the irreversibilities in the process cannot be overlooked. One of the quantitative tools used to determine the irreversibility through entropy generation is the second law of thermodynamics as proposed by Bejan. On the basis of the approach by Bejan, a number of studies on how to minimize the irreversibilities and optimize fluid flow process have been carried out by researchers in the last few decades. A comprehensive review of entropy generation in nanofluid flow was reported by Mahian et al.⁸ Qing et al.⁹ investigated entropy generation on Casson nanofluid flow past a moving surface. In 1944, Powell and Eyring¹⁰ formulated a non-Newtonian fluid model now called the Eyring-Powell fluid. Amongst many non-Newtonian fluids, the Eyring-Powell fluid is of great scientific, engineering, and biological importance. At low and high shear rate the Eyring-Powell fluid is Newtonian in nature. The effect of modified heat flux parameter on an Eyring-Powell fluid on an exponentially expanding sheet was studied by Hayat and Nadeem.¹¹ Ishaq et al.¹² studied the entropy generation on film flow of an Eyring-Powell nanofluid over an unsteady porous stretching sheet. The entropy generation in Eyring-Powell nanofluid flow in a channel was investigated by Ogunseye and Sibanda.¹³ Only a few studies are reported on the entropy generation in hybrid nanofluid flow. Among these, is the analysis done by Das et al.¹⁴ on the entropy generation in Cu-Al₂O₃/water hybrid nanofluid flow in a porous channel. Most recently, Afridi et al.¹⁵ analyzed the entropy generation in a Cu-Al₂O₃/water hybrid nanofluid flow past a curved surface. Their results showed that the hybrid nanofluid minimizes the entropy generated compared with regular nanofluid.

Ashraf et al.¹⁶ studied fluid flow over a convectively heated expanding surface using an Eyring-Powell nanofluid. The study reported that for larger values of the Brownian motion parameter, little increment is noticed in the temperature profiles, while a decrease is noticed in the concentration profiles. Kumar and Srinivas¹⁷ considered the effect of radiation and Joule heating in flow over an inclined expanding surface. Using the curved approach proposed by Sato et al.,¹⁸ Tanveer et al.¹⁹ studied the peristaltic flow of an Eyring-Powell nanofluid with compliant walls. Rehman et al.²⁰ investigated the importance of a chemical reaction, heat generation, and thermal radiation on an Eyring-Powell fluid flow in both flat and cylindrical surfaces. Malik et al.²¹ investigated mixed convection and magnetic effects on an Eyring-Powell nanofluid over a continuous surface. The scientific study of Eyring-Powell nanofluid with thermal radiation and heat generation using the multidomain bivariate spectral quasi-linearization method (MD-BSQLM) was presented by Agbaje et al.²² Recently, the flow of an Eyring-Powell nanofluid flow over an irregular expanding surface using the finite element method was investigated by Ibrahim and Gadisa.²³

To the best of our knowledge, the investigation of entropy generation in a viscous non-Newtonian hybrid nanofluid flow past a stretching permeable surface is yet to be undertaken in the literature. The aim of this study is to investigate entropy generation in the transient flow of a hybrid nanofluid described by the Eyring-Powell model past a permeable surface.

The rest of the paper is organized as follows. We present the mathematical formulation and relevant boundary conditions in Section 2. In Section 3, a similarity solution to the time-dependent model is found using the Lie group symmetry technique. In Section 4, we present the equations that describe entropy generation. In Sections 5 and 6, the bivariate spectral quasi-linearization method (BSQLM) is used to find the solution of the differential equations. A discussion of the findings in this studying is given in Section 7. The heat transfer coefficient in the hybrid nanofluid is compared with that of a regular nanofluid. We highlight the salient features of this study in Section 8.

2 | MATHEMATICAL FORMULATION

We consider the flow and heat transfer of an unsteady, incompressible, viscous non-Newtonian hybrid nanofluid, governed by the Eyring-Powell model, over a permeable stretching surface. A schematic description of the problem is given in Figure 1. The equations for the flow are derived from the conservation of mass, momentum, and energy equations. Using boundary-layer assumptions, these equations in Cartesian coordinates are (see Jalil et al²⁴ and Waini et al²⁵) as follows:

$$\frac{\partial \tilde{u}}{\partial \tilde{x}} + \frac{\partial \tilde{v}}{\partial \tilde{y}} = 0, \quad (1)$$

$$\frac{\partial \tilde{u}}{\partial \tilde{t}} + \tilde{u} \frac{\partial \tilde{u}}{\partial \tilde{x}} + \tilde{v} \frac{\partial \tilde{u}}{\partial \tilde{y}} = \left(\frac{\mu_{\text{hnf}}}{\rho_{\text{hnf}}} + \frac{1}{\rho_{\text{hnf}} \beta \gamma} \right) \frac{\partial^2 \tilde{u}}{\partial \tilde{y}^2} - \frac{1}{2 \rho_{\text{hnf}} \beta \gamma^3} \left(\frac{\partial \tilde{u}}{\partial \tilde{y}} \right)^2 \frac{\partial^2 \tilde{u}}{\partial \tilde{y}^2} + \frac{\partial \tilde{u}_e}{\partial \tilde{t}} + \tilde{u}_e \frac{\partial \tilde{u}_e}{\partial \tilde{x}}, \quad (2)$$

$$\frac{\partial \tilde{T}}{\partial \tilde{t}} + \tilde{u} \frac{\partial \tilde{T}}{\partial \tilde{x}} + \tilde{v} \frac{\partial \tilde{T}}{\partial \tilde{y}} = \frac{k_{\text{hnf}}}{(\rho C_p)_{\text{hnf}}} \frac{\partial^2 \tilde{T}}{\partial \tilde{y}^2} + \frac{1}{(\rho C_p)_{\text{hnf}}} \left[\left(\mu_{\text{hnf}} + \frac{1}{\beta \gamma} \right) \left(\frac{\partial \tilde{u}}{\partial \tilde{y}} \right)^2 - \frac{1}{6 \beta \gamma^3} \left(\frac{\partial \tilde{u}}{\partial \tilde{y}} \right)^4 \right], \quad (3)$$

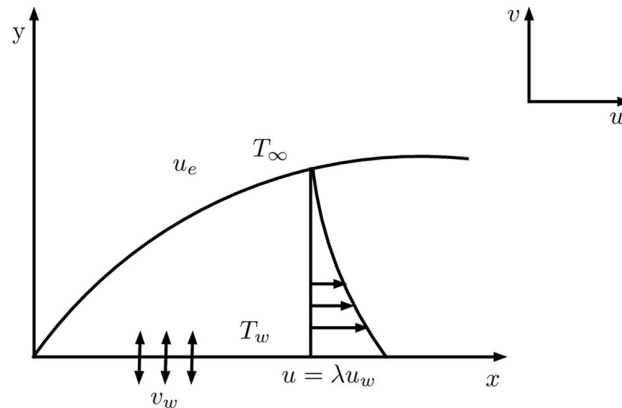


FIGURE 1 Geometry of the problem

where \tilde{x} represents the coordinate along the surface and \tilde{y} is the vertical coordinate, \tilde{t} is the time, \tilde{u} and \tilde{v} , respectively, represent the velocity components along the \tilde{x} and \tilde{y} directions, \tilde{u}_e is the free stream velocity, β and γ are the Eyring-Powell fluid parameters, and \tilde{T} is the hybrid nanofluid temperature. In addition, μ_{hnf} , ρ_{hnf} , k_{hnf} , and $(\rho C_p)_{\text{hnf}}$, respectively, are the hybrid nanofluid dynamic viscosity, density, thermal conductivity, and heat capacity. Following Devi and Devi²⁶ and Waini et al.,²⁵ these terms are evaluated using the following expressions:

$$\left. \begin{aligned} \frac{\mu_{\text{hnf}}}{\mu_f} &= \frac{1}{(1 - \phi_{s_1})^{2.5}(1 - \phi_{s_2})^{2.5}}, \\ \frac{\rho_{\text{hnf}}}{\rho_f} &= (1 - \phi_{s_2}) \left[1 - \phi_{s_1} + \phi_{s_1} \frac{\rho_{s_1}}{\rho_f} \right] + \phi_{s_2} \frac{\rho_{s_2}}{\rho_f}, \\ \frac{(\rho C_p)_{\text{hnf}}}{(\rho C_p)_f} &= (1 - \phi_{s_2}) \left[1 - \phi_{s_1} + \phi_{s_1} \frac{(\rho C_p)_{s_1}}{(\rho C_p)_f} \right] + \phi_{s_2} \frac{(\rho C_p)_{s_2}}{(\rho C_p)_f}, \\ \frac{k_{\text{hnf}}}{k_{\text{bf}}} &= \frac{k_{s_2} + 2k_{\text{bf}} - 2\phi_{s_2}(k_{\text{bf}} - k_{s_2})}{k_{s_2} + 2k_{\text{bf}} + \phi_{s_2}(k_{\text{bf}} - k_{s_2})}, \end{aligned} \right\} \quad (4)$$

where

$$\frac{k_{\text{bf}}}{k_f} = \frac{k_{s_1} + 2k_f - 2\phi_{s_1}(k_f - k_{s_1})}{k_{s_1} + 2k_f + \phi_{s_1}(k_f - k_{s_1})}.$$

In Equations (4), μ is the dynamic viscosity, ρ the density, (ρC_p) the heat capacity, and k the thermal conductivity. Also, the subscript f indicates the base fluid, hnf the hybrid nanofluid, and bf the nanofluid, while the subscripts s_1 and s_2 stand for the hybrid nanoparticles.

The hybrid nanofluid utilized in this model is a Cu-Al₂O₃/ethylene glycol. This is synthesized by adding a fixed volume fraction of the 0.1Al₂O₃(ϕ_{s_1}) nanoparticle to ethylene glycol. Different volume fractions of Cu (ϕ_{s_2}) are subsequently added. It is worth noting that, if $\phi_{s_1} = \phi_{s_2} = 0$, the model reduces to the case of ethylene glycol as the working fluid. The case of Cu/ethylene glycol nanofluid can be obtained by setting $\phi_{s_1} = 0$ and $\phi_{s_2} \neq 0$. The thermo-physical properties of ethylene glycol and the hybrid nanoparticles are presented in Table 1.

The relevant boundary conditions for the model are given as

$$\begin{aligned} \tilde{u}(\tilde{x}, 0, \tilde{t}) &= \lambda \tilde{u}_w(\tilde{x}, \tilde{t}), \quad \tilde{v}(\tilde{x}, 0, \tilde{t}) = S \tilde{v}_w(\tilde{x}, \tilde{t}), \quad \tilde{u}(\tilde{x}, \infty, \tilde{t}) = \tilde{u}_e(\tilde{x}, \tilde{t}), \\ \tilde{T}(\tilde{x}, 0, \tilde{t}) &= \tilde{T}_w(\tilde{x}, \tilde{t}), \quad \tilde{T}(\tilde{x}, \infty, \tilde{t}) = T_\infty, \end{aligned} \quad (5)$$

where $\tilde{u}_w(\tilde{x}, \tilde{t})$ is the stretching velocity, λ the stretching parameter, S the suction/injection parameter ($S > 0$ for suction and $S < 0$ for injection), $\tilde{v}_w(\tilde{x}, \tilde{t})$ the mass flux velocity, the surface temperature is denoted by $\tilde{T}_w(\tilde{x}, \tilde{t})$, and T_∞ the temperature far away from the surface.

To nondimensionalize Equations (1) to (4), we adopt the following nondimensional parameters presented by Akgül and Pakdemirli²⁷:

TABLE 1 Thermophysical properties of ethylene glycol and hybrid nanoparticles

	ρ , kg/m ³	C_p , J/kg K	k , W/m K
Ethylene glycol	1115	2430	0.253
Cu	8933	385	400
Al ₂ O ₃	3970	765	40

Source: Gholinia et al.³³ and Waini et al.²⁵

$$\begin{aligned}
u &= \frac{\tilde{u}}{U_0}, x = \frac{\tilde{x}}{L}, v = \frac{\tilde{v}}{U_0} \left(\frac{\rho_f U_0 L}{\mu_f} \right)^{\frac{1}{2}}, t = \frac{U_0 \tilde{t}}{L}, y = \frac{\tilde{y}}{L} \left(\frac{\rho_f U_0 L}{\mu_f} \right)^{\frac{1}{2}}, \\
u_e &= \frac{\tilde{u}_e}{U_0}, T = \frac{\tilde{T} - T_\infty}{T_0}, u_w = \frac{\tilde{u}_w}{U_0}, v_w = \frac{\tilde{v}_w}{U_0} \left(\frac{\rho_f U_0 L}{\mu_f} \right)^{\frac{1}{2}}, T_w = \frac{\tilde{T}_w - T_\infty}{T_0},
\end{aligned} \tag{6}$$

where U_0 , L , and T_0 are the reference velocity, characteristic length, and reference temperature, respectively.

We recall the stream function $\psi(x, y)$ defined by

$$u = \frac{\partial \psi}{\partial y} \quad \text{and} \quad v = -\frac{\partial \psi}{\partial x}. \tag{7}$$

Substituting Equations (6) and (7) into the model equations and boundary conditions reads as follows:

$$\frac{\partial^2 \psi}{\partial t \partial y} + \frac{\partial \psi}{\partial y} \frac{\partial^2 \psi}{\partial x \partial y} - \frac{\partial \psi}{\partial x} \frac{\partial^2 \psi}{\partial y^2} = \frac{1}{A_2} (A_1 + \varepsilon) \frac{\partial^3 \psi}{\partial y^3} - \frac{\varepsilon \delta}{A_2} \left(\frac{\partial^2 \psi}{\partial y^2} \right)^2 \frac{\partial^3 \psi}{\partial y^3} + \frac{\partial u_e}{\partial t} + u_e \frac{\partial u_e}{\partial x}, \tag{8}$$

$$\frac{\partial T}{\partial t} + \frac{\partial \psi}{\partial y} \frac{\partial T}{\partial x} - \frac{\partial \psi}{\partial x} \frac{\partial T}{\partial y} = \frac{1}{Pr} \frac{A_3}{A_4} \frac{\partial^2 T}{\partial y^2} + \frac{Ec}{A_4} \left[(A_1 + \varepsilon) \left(\frac{\partial^2 \psi}{\partial y^2} \right)^2 - \frac{\varepsilon \delta}{3} \left(\frac{\partial^2 \psi}{\partial y^2} \right)^4 \right], \tag{9}$$

$$\left. \begin{aligned}
\frac{\partial \psi}{\partial y} &= \lambda u_w(x, t), \frac{\partial \psi}{\partial x} = -S v_w(x, t), T = T_w(x, t) \quad \text{at} \quad y = 0, t \geq 0, \\
\frac{\partial \psi}{\partial y} &\rightarrow u_e(x, t), T \rightarrow 0 \quad \text{as} \quad y \rightarrow \infty, t \geq 0
\end{aligned} \right\} \tag{10}$$

with

$$\begin{aligned}
\varepsilon &= \frac{1}{\mu_f \beta \gamma}, \delta = \frac{U_0^3}{2\nu_f L C^2}, Pr = \frac{(\mu C_p)_f}{\kappa_f}, Ec = \frac{U_0^2}{(C_p)_f T_0}, \\
A_1 &= \frac{\mu_{hnf}}{\mu_f}, A_2 = \frac{\rho_{hnf}}{\rho_f}, A_3 = \frac{k_{hnf}}{k_f}, A_4 = \frac{(\rho C_p)_{hnf}}{(\rho C_p)_f},
\end{aligned} \tag{11}$$

where ε and δ are the Powell-Eyring parameters, Pr is the Prandtl number, and Ec is the Eckert number.

In Equation (10) we assume that the moving surface velocity, mass flux velocity, and surface temperature are defined by

$$u_w = x^m, v_w = x^n, \text{ and } T_w = x^s. \tag{12}$$

3 | SIMILARITY TRANSFORMATION USING LIE GROUP SYMMETRY

In this section, we show that Equations (8) to (10) admit scaling symmetry, then systematically reduce the number of independent variables of the given partial differential equation from three

to two. Following Pakdemirli and Yurusoy,²⁸ we introduce a one-parameter scaling group of transformation given as

$$\Gamma: t^* = te^{\zeta a_1}, x^* = xe^{\zeta a_2}, y^* = ye^{\zeta a_3}, \psi^* = \psi e^{\zeta a_4}, T^* = Te^{\zeta a_5}, u_e^* = u_e e^{\zeta a_6}. \quad (13)$$

In Equation (13), the coordinates (t, x, y, ψ, T, u_e) are transformed into the coordinates $(t^*, x^*, y^*, \psi^*, T^*, u_e^*)$, using a one point transformation and ζ is the transformation parameter. The a_i ($i = 1, \dots, 6$) are constants to be determined.

$$\begin{aligned} & e^{\zeta(a_1+a_3-a_4)} \frac{\partial^2 \psi^*}{\partial t^* \partial y^*} + e^{\zeta(a_2+2a_3-2a_4)} \left[\frac{\partial \psi^*}{\partial y^*} \frac{\partial^2 \psi^*}{\partial x^* \partial y^*} - \frac{\partial \psi^*}{\partial x^*} \frac{\partial^2 \psi^*}{\partial y^{*2}} \right] \\ &= \frac{1}{A_2} (A_1 + \varepsilon) e^{\zeta(3a_3-a_4)} \frac{\partial^3 \psi^*}{\partial y^{*3}} \frac{\varepsilon \delta}{A_2} e^{\zeta(7a_3-3a_4)} \left(\frac{\partial^2 \psi^*}{\partial y^{*2}} \right)^2 \frac{\partial^3 \psi^*}{\partial y^{*3}} + e^{\zeta(a_1-a_6)} \frac{\partial u_e^*}{\partial t^*} + e^{\zeta(a_2-2a_6)} u_e^* \frac{\partial u_e^*}{\partial t^*}, \end{aligned} \quad (14)$$

$$\begin{aligned} & e^{\zeta(a_1-a_5)} \frac{\partial T^*}{\partial t^*} + e^{\zeta(a_2+a_3-a_4-a_5)} \left[\frac{\partial \psi^*}{\partial y^*} \frac{\partial T^*}{\partial x^*} - \frac{\partial \psi^*}{\partial x^*} \frac{\partial T^*}{\partial y^*} \right] \\ &= \frac{1}{Pr} \frac{A_3}{A_4} e^{\zeta(2a_3-a_5)} \frac{\partial^2 T^*}{\partial y^{*2}} + \frac{Ec}{A_4} \left[(A_1 + \varepsilon) e^{\zeta(4a_3-2a_4)} \left(\frac{\partial^2 \psi^*}{\partial y^{*2}} \right)^2 - \frac{\varepsilon \delta}{3} e^{\zeta(8a_3-4a_4)} \left(\frac{\partial^2 \psi^*}{\partial y^{*2}} \right)^4 \right], \end{aligned} \quad (15)$$

$$e^{\zeta(a_3-a_4)} \frac{\partial \psi^*}{\partial y^*} = \lambda (x^*)^m e^{\zeta(-ma_2)}, \quad e^{\zeta(a_2-a_4)} \frac{\partial \psi^*}{\partial x^*} = -S (x^*)^n e^{\zeta(-na_2)},$$

$$e^{\zeta-a_5} T^* = (x^*)^s e^{\zeta(-sa_2)} \quad \text{at } y = 0, t \geq 0, \quad e^{\zeta(a_3-a_4)} \frac{\partial \psi^*}{\partial y^*} \longrightarrow u_e^* e^{\zeta-a_6}, \quad \theta^* \longrightarrow 0 \quad \text{as } y \longrightarrow \infty, t \geq 0. \quad (16)$$

Under the transformation Equation (13), the system Equations (14) to (16) remain invariant, if the following invariance conditions are satisfied:

$$\begin{aligned} a_1 + a_3 - a_4 &= a_2 + 2a_3 - 2a_4 = 3a_3 - a_4 = 7a_3 - 3a_4 = a_1 - a_6 = a_2 - 2a_6, \\ a_1 - a_5 &= a_2 + a_3 - a_4 - a_5 = 2a_3 - a_5 = 4a_3 - 2a_4 = 8a_3 - 4a_4, \\ a_3 - a_4 &= -ma_2, \quad a_2 - a_4 = -na_2, \quad a_5 = sa_2, \quad a_3 - a_4 = -a_6. \end{aligned} \quad (17)$$

On solving Equation (17) in terms of parameter a_2 , we obtain

$$a_1 = a_4 = a_5 = \frac{2}{3} a_2, \quad a_3 = a_6 = \frac{1}{3} a_2, \quad m = \frac{1}{3}, \quad n = -\frac{1}{3}, \quad \text{and } s = \frac{2}{3}. \quad (18)$$

Hence, the scaling group of transformation reads as follows:

$$\Gamma: t^* = te^{\frac{2}{3}\zeta a_2}, x^* = xe^{\zeta a_2}, y^* = ye^{\frac{1}{3}\zeta a_2}, \psi^* = \psi e^{\frac{2}{3}\zeta a_2}, T^* = Te^{\frac{2}{3}\zeta a_2}, u_e^* = u_e e^{\zeta \frac{1}{3} a_2}. \quad (19)$$

Expanding the exponential functions in Equation (19) by Taylor series about $\zeta = 0$ up to the first order yields

$$\begin{aligned}
t^* &= t + \frac{2}{3}\zeta ta_2, x^* = x + \zeta\alpha a_2 y^* = y + \frac{1}{3}\zeta\gamma a_2, \psi^* = \psi + \frac{2}{3}\zeta\psi a_2, \\
T^* &= T + \frac{2}{3}\zeta Ta_2, u_e^* = u_e + \frac{1}{3}\zeta u_e a_2.
\end{aligned} \tag{20}$$

In Equation (20), if we denote the differences between the transformed and original variables as a differential, and further equate each term, the following characteristic equations are obtained:

$$\frac{3dt}{2t} = \frac{dx}{x} = \frac{3dy}{y} = \frac{3d\psi}{2\psi} = \frac{3dT}{2T} = \frac{du_e}{3u_e}. \tag{21}$$

Solving Equation (21) by the method of characteristics gives the following similarity variables and functions:

$$\xi = x^{-\frac{2}{3}}t, \eta = x^{-\frac{1}{3}}y, \psi = x^{\frac{2}{3}}f(\eta, \xi), T = x^{\frac{2}{3}}\theta(\eta, \xi), u_e = c_1 x^{\frac{1}{3}}, \tag{22}$$

where c_1 is the constant of integration and will be assigned a unity value. Substituting Equations (12) and (22) into Equations (8) to (10) leads to the following similarity equations in simplified form:

$$\begin{aligned}
&\frac{1}{A_2}(A_1 + \varepsilon)\frac{\partial^3 f}{\partial \eta^3} + \frac{2}{3}f\frac{\partial^2 f}{\partial \eta^2} - \frac{\delta\varepsilon}{A_2}\left(\frac{\partial^2 f}{\partial \eta^2}\right)^2\frac{\partial^3 f}{\partial \eta^3} + \frac{1}{3}\left[1 - \left(\frac{\partial f}{\partial \eta}\right)^2\right] \\
&= \frac{\partial^2 f}{\partial \eta \partial \xi} - \frac{2}{3}\xi\left[\frac{\partial f}{\partial \eta}\frac{\partial^2 f}{\partial \eta \partial \xi} - \frac{\partial^2 f}{\partial \eta^2}\frac{\partial f}{\partial \xi}\right],
\end{aligned} \tag{23}$$

$$\begin{aligned}
&\frac{1}{Pr}\frac{A_3}{A_4}\frac{\partial^2 \theta}{\partial \eta^2} + \frac{2}{3}f\frac{\partial \theta}{\partial \eta} - \frac{2}{3}\theta\frac{\partial f}{\partial \eta} + \frac{Ec}{A_4}\left[(A_1 + \varepsilon)\left(\frac{\partial^2 f}{\partial \eta^2}\right)^2 - \frac{\delta\varepsilon}{3}\left(\frac{\partial^2 f}{\partial \eta^2}\right)^4\right] \\
&= \frac{\partial \theta}{\partial \xi} - \frac{2}{3}\xi\left[\frac{\partial f}{\partial \eta}\frac{\partial \theta}{\partial \xi} - \frac{\partial \theta}{\partial \eta}\frac{\partial f}{\partial \xi}\right],
\end{aligned} \tag{24}$$

$$f(0, \xi) = fw, \frac{\partial f}{\partial \eta}(0, \xi) = \lambda, \frac{\partial f}{\partial \eta}(\infty, \xi) \rightarrow 1, \theta(0, \xi) = 1, \theta(\infty, \xi) \rightarrow 0, \tag{25}$$

where $fw = -\frac{2}{3}S$.

The important physical quantities are the skin friction coefficient, C_f , and the Nusselt number, Nu_x . These quantities are defined as

$$C_f = \frac{\tau_w}{\rho_f U_0^2} \quad \text{and} \quad Nu_x = \frac{\tilde{x}q_w}{\kappa_f(T_f - T_\infty)}. \tag{26}$$

The wall shear stress τ_w and the wall flux q_w are expressed as

$$\tau_w = \left(\mu_{\text{hnf}} + \frac{1}{\beta\gamma}\right)\left(\frac{\partial \bar{u}}{\partial \bar{y}}\right) - \frac{1}{6\beta\gamma^3}\left(\frac{\partial \bar{u}}{\partial \bar{y}}\right)^3 \Bigg|_{\bar{y}=0} \quad \text{and} \quad q_w = -k_{\text{hnf}}\left(\frac{\partial \bar{T}}{\partial \bar{y}}\right) \Bigg|_{\bar{y}=0}. \tag{27}$$

Using Equations (6) and (22), Equation (27) in dimensionless form yields

$$(Re)^{\frac{1}{2}} C_f = (A_1 + \varepsilon) \frac{\partial^2 f}{\partial \eta^2}(0, \xi) - \frac{\varepsilon \delta}{3} \left(\frac{\partial^2 f}{\partial \eta^2}(0, \xi) \right)^3 \quad \text{and} \quad Nu_{x,x^{-\frac{1}{3}}}(Re)^{-\frac{1}{2}} = -A_3 \frac{\partial \theta}{\partial \eta}(0, \xi), \quad (28)$$

where $Re = \frac{U_0 L}{\nu_f}$ represents the local Reynolds number.

4 | ENTROPY GENERATION

In this section, we focus on the entropy generation minimization for the hybrid nanofluid flow model. The entropy generation is due to the irreversibility due to heat transfer and viscous dissipation effects within the hybrid nanofluid and the boundary surface. On the basis of the second law of thermodynamics, the local volumetric rate of entropy generation presented as (see Rashidi et al²⁹)

$$S_{\text{gen}}''' = \underbrace{\frac{k_{\text{hnf}}}{T_{\infty}^2} \left(\frac{\partial \bar{T}}{\partial \bar{y}} \right)^2}_{\text{First term}} + \frac{1}{T_{\infty}} \underbrace{\left[\left(\mu_{\text{hnf}} + \frac{1}{\beta \gamma} \right) \left(\frac{\partial \bar{u}}{\partial \bar{y}} \right)^2 - \frac{1}{6\beta \gamma^3} \left(\frac{\partial \bar{u}}{\partial \bar{y}} \right)^4 \right]}_{\text{Second term}}. \quad (29)$$

In Equation (29), the entropy generation due to heat transfer is represented by the first term while the second term explains the entropy generation due to viscous dissipation. Utilizing Equations (6) and (22), the expression for the dimensionless entropy generation number is

$$Ns = \frac{T_{\infty}^2 L^3 U_0}{T_0^2 k_f \nu_f x^{\frac{2}{3}}} S_{\text{gen}}''' = A_3 \left(\frac{\partial \theta}{\partial \eta} \right)^2 + \frac{EcPrR}{\theta_w} \left[(A_1 + \varepsilon) \left(\frac{\partial^2 f}{\partial \eta^2} \right)^2 - \frac{\delta \varepsilon}{3} \left(\frac{\partial^2 f}{\partial \eta^2} \right)^4 \right], \quad (30)$$

where $R = Rex^{-\frac{2}{3}}$ and $\theta_w = \frac{T_0}{T_{\infty}}$ are the local Reynolds number and temperature ratio, respectively. The Bejan number (Be) is defined as

$$Be = \frac{1}{1 + \Phi}, \quad (31)$$

where

$$\Phi = \frac{\frac{EcPrR}{\theta_w} \left[(A_1 + \varepsilon) \left(\frac{\partial^2 f}{\partial \eta^2} \right)^2 - \frac{\delta \varepsilon}{3} \left(\frac{\partial^2 f}{\partial \eta^2} \right)^4 \right]}{A_3 \left(\frac{\partial \theta}{\partial \eta} \right)^2}. \quad (32)$$

5 | NUMERICAL SOLUTION

Equations (23) to (25) are solved numerically using the BQSLM as described in Goqo et al.³⁰ To apply this technique, we first define the following nonlinear operators:

$$\begin{aligned}\Omega_f &= \frac{1}{A_2}(A_1 + \varepsilon)f''' + \frac{2}{3}ff'' - \frac{\delta\varepsilon}{A_2}(f'')^2f''' + \frac{1}{3}(1 - f'^2) - K + \frac{2}{3}\xi(f'K - f''P), \\ \Omega_\theta &= \frac{1}{Pr} \frac{A_3}{A_4}\theta'' + \frac{2}{3}f\theta' - \frac{2}{3}f'\theta + \frac{Ec}{A_4} \left[(A_1 + \varepsilon)(f'')^2 - \frac{\delta\varepsilon}{3}(f'')^4 \right] - Q + \frac{2}{3}\xi[f'Q - \theta'P],\end{aligned}\quad (33)$$

where prime indicates partial derivative with respect to η , $K = \frac{\partial^2 f}{\partial \eta \partial \xi}$, $P = \frac{\partial f}{\partial \xi}$, and $Q = \frac{\partial \theta}{\partial \xi}$.

Linearizing Equations (23) to (25) using the quasi-linearization method (see Bellman and Kalaba³¹) yields Equations (34) to (36):

$$c_{1,r}f_{r+1}''' + c_{2,r}f_{r+1}'' + c_{3,r}f_{r+1}' + c_{4,r}f_{r+1} + c_{5,r}K_{r+1} + c_{6,r}P_{r+1} = R_{1,r}, \quad (34)$$

$$c_{7,r}\theta_{r+1}'' + c_{8,r}\theta_{r+1}' + c_{9,r}\theta_{r+1} + c_{10,r}Q_{r+1} + c_{11,r}f_{r+1}'' + c_{12,r}f_{r+1}' + c_{13,r}f_{r+1} + c_{14,r}P_{r+1} = R_{2,r}, \quad (35)$$

$$f_{r+1}(0, \xi) = fw, f_{r+1}'(0, \xi) = \lambda, f_{r+1}'(\infty, \xi) \rightarrow 1, \theta_{r+1}(0, \xi) = 1, \theta_{r+1}(\infty, \xi) \rightarrow 0, \quad (36)$$

where

$$\left. \begin{aligned}c_{1,r} &= \frac{\partial \Omega_f}{\partial f_r'''} = \frac{1}{A_2}(A_1 + \varepsilon) - \frac{\delta\varepsilon}{A_2}(f_r'')^2, & c_{2,r} &= \frac{\partial \Omega_f}{\partial f_r''} = \frac{2}{3}f_r - \frac{2\varepsilon\delta}{A_2}f_r''f_rf_r''' - \frac{2}{3}\xi P_r, \\ c_{3,r} &= \frac{\partial \Omega_f}{\partial f_r'} = \frac{2}{3}(\xi K_r - f_r'), & c_{4,r} &= \frac{\partial \Omega_f}{\partial f_r} = \frac{2}{3}f_r'', & c_{5,r} &= \frac{\partial \Omega_f}{\partial K_r} = \frac{2}{3}\xi f_r' - 1, & c_{6,r} &= \frac{\partial \Omega_f}{\partial P_r} \\ & & & & & & & = -\frac{2}{3}\xi f_r'', \\ c_{7,r} &= \frac{\partial \Omega_\theta}{\partial \theta_r''} = \frac{1}{Pr} \frac{A_3}{A_4}, & c_{8,r} &= \frac{\partial \Omega_\theta}{\partial \theta_r'} = \frac{2}{3}(f_r - \xi P_r), & c_{9,r} &= \frac{\partial \Omega_\theta}{\partial \theta_r} = -\frac{2}{3}f_r', & c_{10,r} &= \frac{\partial \Omega_\theta}{\partial Q_r} \\ & & & & & & & = \frac{2}{3}\xi f_r' - 1, \\ c_{11,r} &= \frac{\partial \Omega_\theta}{\partial f_r''} = \frac{Ec}{A_4} \left[2(A_1 + \varepsilon)f_r'' - \frac{4\delta\varepsilon}{3}(f_r'')^3 \right], & c_{12,r} &= \frac{\partial \Omega_\theta}{\partial f_r'} = \frac{2}{3}(\xi Q_r - \theta_r), \\ c_{13,r} &= \frac{\partial \Omega_\theta}{\partial P_r} = \frac{2}{3}\xi \theta_r', & R_{1,r} &= c_{1,r}f_r''' + c_{2,r}f_r'' + c_{3,r}f_r' + c_{4,r}f_r + c_{5,r}K_r + c_{6,r}P_r - \Omega_f, \\ R_{2,r} &= c_{7,r}\theta_r'' + c_{8,r}\theta_r' + c_{9,r}\theta_r + c_{10,r}Q_r + c_{11,r}f_r'' + c_{12,r}f_r' + c_{13,r}f_r + c_{14,r}P_r - \Omega_\theta,\end{aligned}\right\} \quad (37)$$

The linearized equations are integrated using the Chebyshev spectral collocation method (CSCM). To this end, we replace the semi-infinite domain $\eta \in [0, \infty)$, with a truncated domain, $\eta \in [0, L_a]$, $L_a \in \mathbb{Z}^+$. The new domain of η and ξ is transformed to CSCM computational domain using the linear transformation:

$$\{\eta, \xi\} = \left\{ \frac{L_a}{2}(1 + p), \frac{L_b}{2}(1 + q) \right\}, \quad \forall (p, q) \in [-1, 1] \times [-1, 1]. \quad (38)$$

The collocation points are chosen to be the Chebyshev-Gauss-Lobatto nodes with N_η and N_ξ collocation points in η and ξ , respectively, expressed as

$$p_i = \cos\left(\frac{\pi i}{N_\eta}\right)\Bigg|_{i=0}^{N_\eta}, \quad q_j = \cos\left(\frac{\pi j}{N_\xi}\right)\Bigg|_{j=0}^{N_\xi}. \quad (39)$$

The unknown functions $f(\eta, \xi)$ and $\theta(\eta, \xi)$ are approximated using the bivariate Lagrange interpolation polynomials, such that the first derivatives with respect to η and ξ are defined in terms of Chebyshev differentiation matrix D (see Trefethen³²) as

$$\begin{aligned} \frac{\partial f}{\partial \eta} &= \sum_{k_1=0}^{N_\eta} D_{i,k_1} f(p_{k_1}, q_j) = \mathbf{D}f(p_i, q_j), \quad \frac{\partial^2 f}{\partial \eta^2} = \mathbf{D}^2 f(p_i, q_j), \quad \frac{\partial^3 f}{\partial \eta^3} = \mathbf{D}^3 f(p_i, q_j), \\ \frac{\partial \theta}{\partial \eta} &= \sum_{k_1=0}^{N_\eta} D_{i,k_1} \theta(p_{k_1}, q_j) = \mathbf{D}\theta(p_i, q_j), \quad \frac{\partial^2 \theta}{\partial \eta^2} = \mathbf{D}^2 \theta(p_i, q_j), \\ \frac{\partial f}{\partial \xi} &= \sum_{k_2=0}^{N_\xi} d_{j,k_2} f(p_i, q_{k_2}) = \sum_{k_2=0}^{N_\xi} \mathbf{d}_{j,k_2} f(p_i, q_{k_2}), \quad \frac{\partial \theta}{\partial \xi} = \sum_{k_2=0}^{N_\xi} d_{j,k_2} \theta(p_i, q_{k_2}) = \sum_{k_2=0}^{N_\xi} \mathbf{d}_{j,k_2} \theta(p_i, q_{k_2}), \end{aligned} \quad (40)$$

$\mathbf{D} = 2D/L_a$ and $\mathbf{d} = 2d/L_b$. Substituting Equations (39) and (40) into Equations (34) to (36) gives the BSQM scheme:

$$\begin{aligned} &\left[\text{diag}(c_{1,r})\mathbf{D}^3 + \text{diag}(c_{2,r})\mathbf{D}^2 + \text{diag}(c_{3,r})\mathbf{D} + \text{diag}(c_{4,r}) + \text{diag}(c_{5,r})\mathbf{D} \sum_{k_2=0}^{N_\xi} d_{jk_2} \right. \\ &\quad \left. + \text{diag}(c_{6,r}) \sum_{k_2=0}^{N_\xi} d_{jk_2} \right] \mathbf{F}_{r+1,j} = R_{1,r}, \end{aligned} \quad (41)$$

$$\begin{aligned} &\left[\text{diag}(c_{11,r})\mathbf{D}^2 + \text{diag}(c_{12,r})\mathbf{D} + \text{diag}(c_{13,r}) + \text{diag}(c_{14,r}) \sum_{k_2=0}^{N_\xi} d_{jk_2} \right] \\ &\quad + \left[\text{diag}(c_{7,r})\mathbf{D}^2 + \text{diag}(c_{8,r})\mathbf{D} + \text{diag}(c_{9,r}) + \text{diag}(c_{10,r}) \sum_{k_2=0}^{N_\xi} d_{jk_2} \right] \mathbf{\Theta}_{r+1,j} = R_{2,r} \end{aligned} \quad (42)$$

TABLE 2 Comparison of the BSQM results for $f''(0, 0)$ and $\theta'(0, 0)$ with Jalil et al²⁴ and Agbaje et al²² for the following values: $\varepsilon = \phi_{s_1} = \phi_{s_2} = 0$ and varying values of fw

fw	$f''(0, 0)$			$\theta'(0, 0)$		
	Jalil et al ²⁴	Agbaje et al ²²	Present	Jalil et al ²⁴	Agbaje et al ²²	Present
2	0.9251	0.9251	0.925021	1.6036	1.6036	1.603566
4	1.5030	1.5030	1.502659	2.8330	2.8333	2.833009
6	2.1233	2.1233	2.123323	4.1177	4.1177	4.117731
8	2.7627	2.7626	2.762725	5.4238	5.4238	5.423828
10	3.4116	3.4116	3.411600	6.7399	6.7399	6.739945
20	6.7069	6.7069	6.706869	13.3706	13.3706	13.370608

Abbreviation: BSQM, bivariate spectral quasi-linearization method.

TABLE 3 Nusselt number for Cu/ethylene glycol and Cu-Al₂O₃/ethylene glycol when $\varepsilon = Ec = fw = 1.0$, $\delta = 0.1$, $\lambda = 1.5$, and $Pr = 6.7$ for various values of ϕ_{s_2}

ϕ_{s_2}	Nusselt number		% Difference
	Cu/ethylene glycol	Cu-Al ₂ O ₃ /ethylene glycol	
0.005	5.099609	5.321992	4.36
0.02	5.084782	5.303393	4.30
0.04	5.065013	5.278591	4.22
0.06	5.045247	5.253799	4.13

TABLE 4 Computed results for skin friction coefficient, C_f , and Nusselt number, Nu , for Cu-Al₂O₃/ethylene glycol hybrid nanofluid for varying the parameters: ϕ_{s_2} , ε , δ , fw , λ , and Ec when $\xi = 1$

ϕ_{s_2}	ε	δ	fw	λ	Ec	C_f	Nu
0.005	1	0.1	0.5	1.5	1	-1.104099	2.568624
0.02	1	0.1	0.5	1.5	1	-1.162933	2.548472
0.04	1	0.1	0.5	1.5	1	-1.241305	2.521875
0.06	1	0.1	0.5	1.5	1	-1.320045	2.495310
0.005	0.1	0.1	0.5	1.5	1	-0.892933	2.622560
0.005	1	0.1	0.5	1.5	1	-1.104099	2.568624
0.005	2	0.1	0.5	1.5	1	-1.295975	2.528489
0.005	3	0.1	0.5	1.5	1	-1.462214	2.497262
0.005	1	0.1	0.5	1.5	1	-1.104099	2.568624
0.005	1	0.5	0.5	1.5	1	-1.100466	2.567302
0.005	1	1	0.5	1.5	1	-1.095793	2.565410
0.005	1	1.5	0.5	1.5	1	-1.090859	2.563401
0.005	1	0.1	-0.5	1.5	1	-0.862073	0.664706
0.005	1	0.1	-0.3	1.5	1	-0.907053	0.883166
0.005	1	0.1	0.3	1.5	1	-1.052357	2.039397
0.005	1	0.1	0.5	1.5	1	-1.104099	2.568624
0.005	1	0.1	0.5	0.3	1	1.210282	0.887030
0.005	1	0.1	0.5	0.5	1	0.910096	1.927190
0.005	1	0.1	0.5	1.5	1	-1.104099	2.568624
0.005	1	0.1	0.5	2	1	-2.368386	0.168083
0.005	1	0.1	0.5	1.5	0.1	-1.104110	3.348587
0.005	1	0.1	0.5	1.5	1	-1.104099	2.568624
0.005	1	0.1	0.5	1.5	1.5	-1.104109	2.135292
0.005	1	0.1	0.5	1.5	2	-1.104104	1.702098

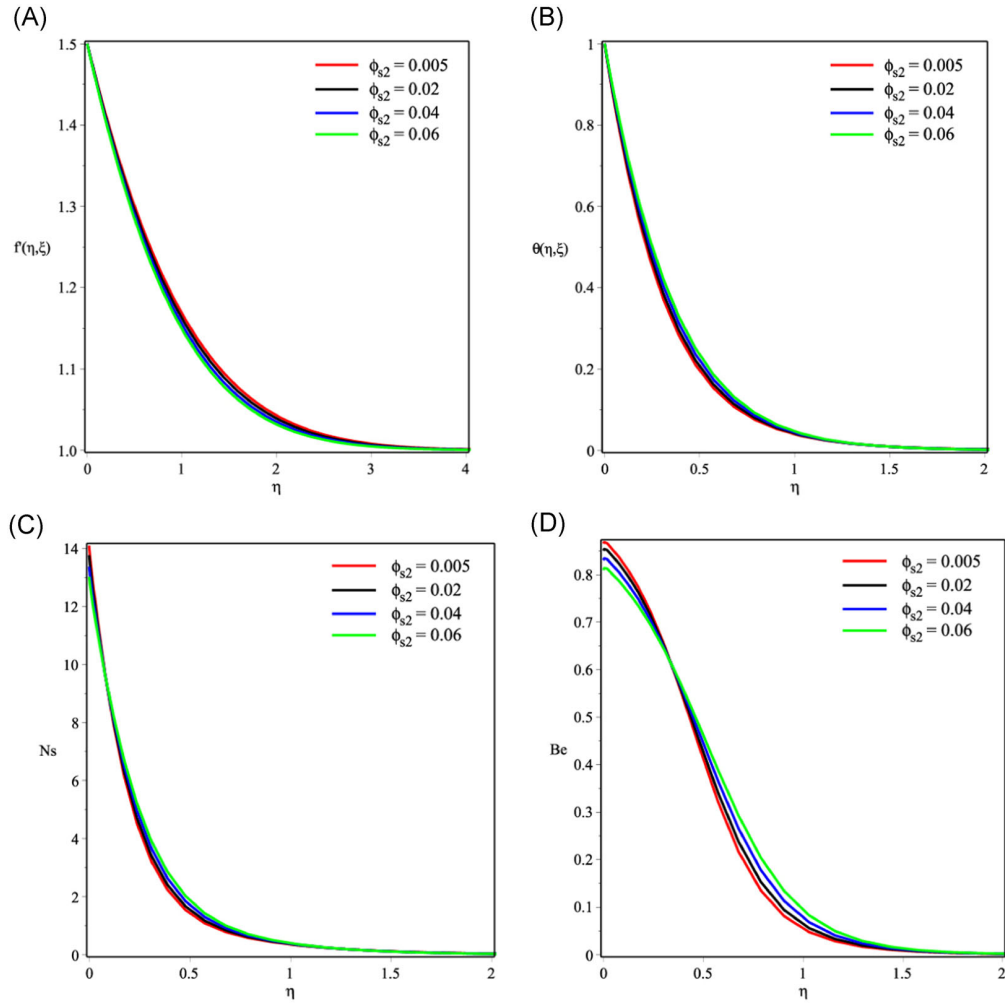


FIGURE 2 Effect of varying the nanoparticle volume fraction (ϕ_{s_2}) on the hybrid nanofluent for $\varepsilon = Ec = 1.0$, $\delta = 0.1$, $\lambda = 1.5$, $fw = 0.5$, and $Pr = 6.7$ on (A) velocity profiles, (B) temperature profiles, (C) entropy generation rate, and (D) Bejan number [Color figure can be viewed at wileyonlinelibrary.com]

with the boundary condition

$$\sum_{k_1=0}^{N_\eta} \mathbf{D}_{N_\eta, k_1} \mathbf{F}_{r+1}(p_{k_1}, q_j) = \lambda, \mathbf{F}_{r+1}(p_{N_\eta}, q_j) = fw, \sum_{k_1=0}^{N_\eta} \mathbf{D}_{0, k_1} \mathbf{F}_{r+1}(p_{k_1}, q_j) = 1, \quad (43)$$

$$\Theta_{r+1}(p_{N_\eta}, q_j) = 1, \Theta_{r+1}(p_0, q_j) = 0,$$

$\mathbf{F}_{r+1,j}$ and $\Theta_{r+1,j}$ are the solution of $f(\eta, \xi)$ and $\theta(\eta, \xi)$ evaluated at each value of ξ .

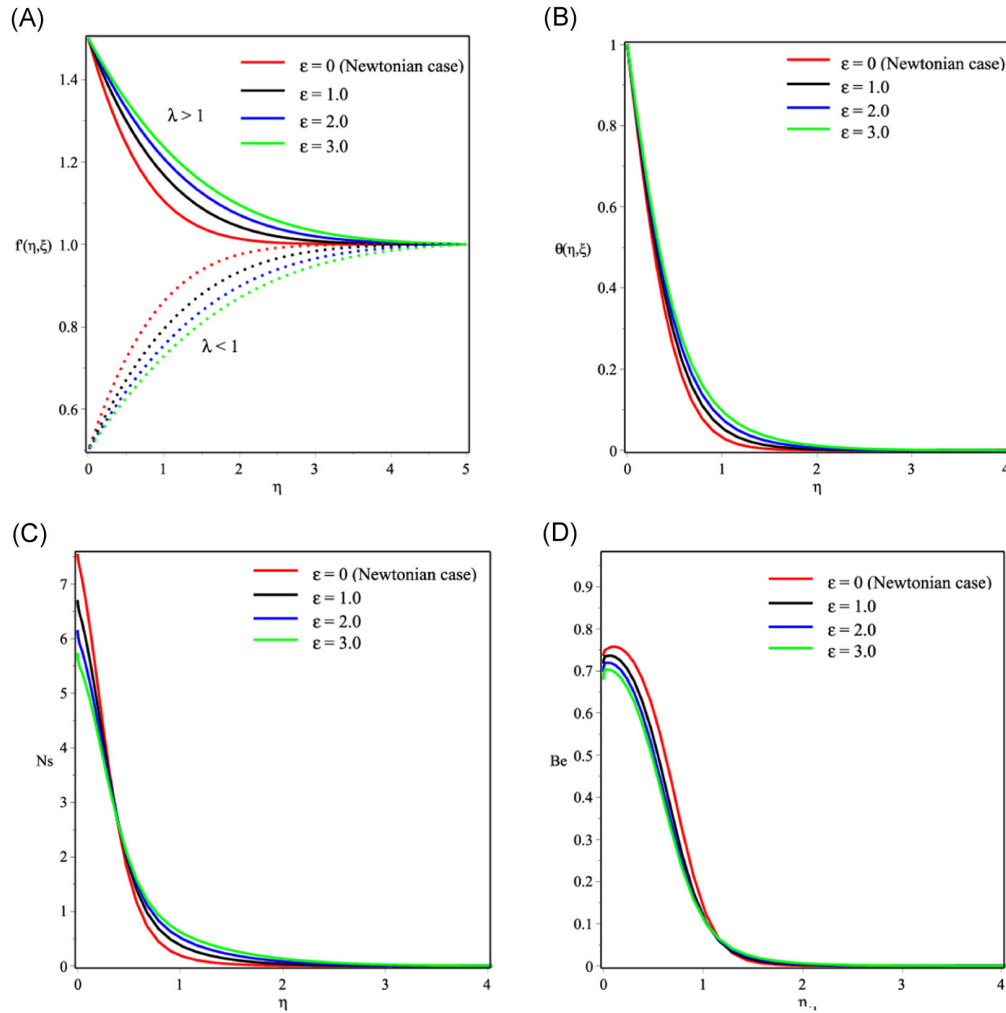


FIGURE 3 Effect of varying the Eyring-Powell fluid parameter (ϵ) on the hybrid nanofluid for $Ec = 1.0$, $\delta = 0.1$, $\lambda = 1.5$, $f_w = 0.5$, $Pr = 6.7$, and $\phi_{s_2} = 0.005$ on (A) velocity profiles, (B) temperature profiles, (C) entropy generation rate, and (D) Bejan number [Color figure can be viewed at wileyonlinelibrary.com]

6 | NUMERICAL VALIDATION

The BSQIM iterative scheme is implemented using the Maple 18 symbolic package. To validate the accuracy of the scheme, we compared the skin friction coefficient values against the results of a regular Newtonian model in the literature. In the absence of hybrid nanoparticles ($\phi_{s_1} = \phi_{s_2} = 0$), our results agree with that of Jalil et al.²⁴ and Agbaje et al.,²² see Table 2.

7 | RESULTS AND DISCUSSION

In this section, we discuss the effects of the fluid parameters: Eyring-Powell parameters, δ and ϵ , suction/injection parameter, f_w , the hybrid nanoparticle volume fractions, ϕ_{s_1} and ϕ_{s_2} , and the

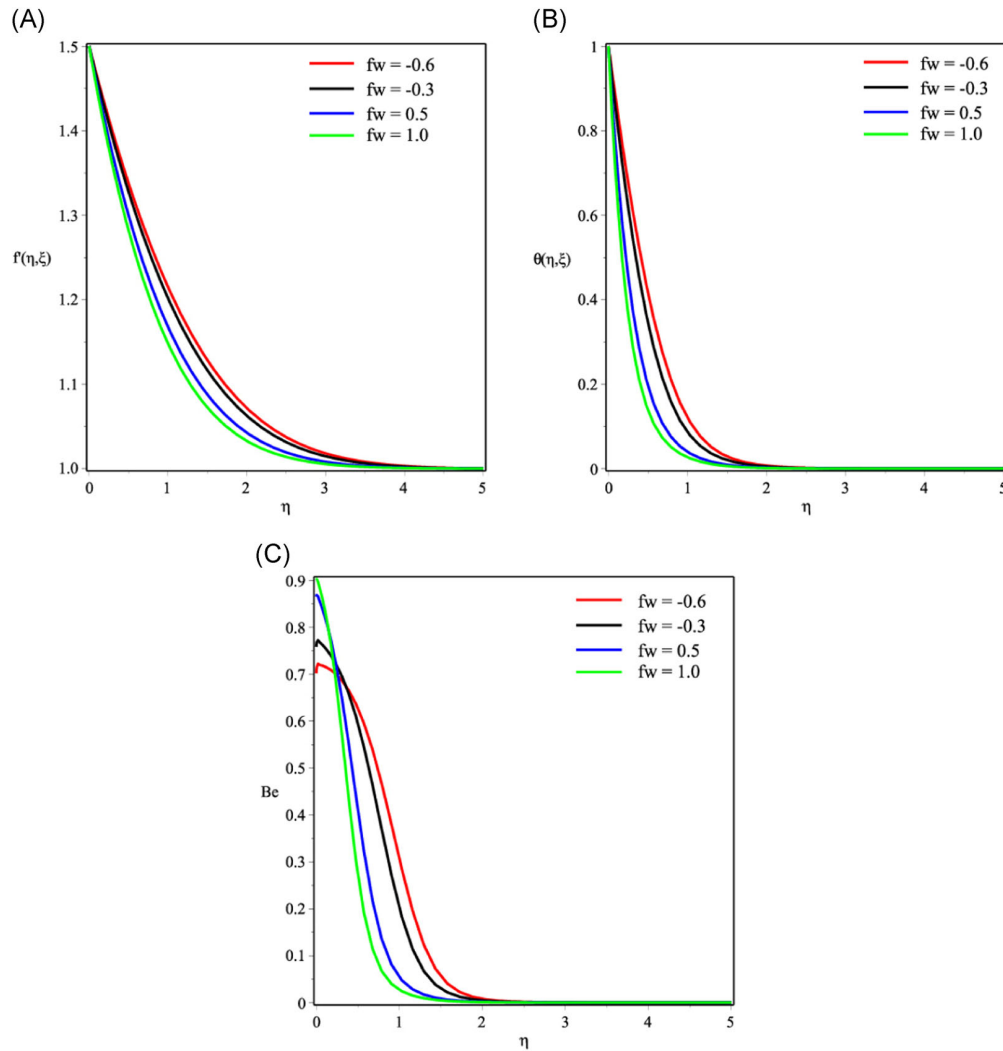


FIGURE 4 Effect of varying the suction/injection parameter (fw) on the hybrid nanofluid for $\varepsilon = Ec = 1.0$, $\delta = 0.1$, $\lambda = 1.5$, $Pr = 6.7$, and $\phi_{s_2} = 0.005$ on (A) velocity profiles, (B) temperature profiles, and (C) Bejan number [Color figure can be viewed at wileyonlinelibrary.com]

Eckert number, Ec on the hybrid nanofluid velocity profiles, $f'(\eta, \xi)$ temperature profiles, $\theta(\eta, \xi)$, entropy generation number profiles, and Bejan number profiles. In addition, we compute the skin friction and Nusselt number for different values of these parameters. Unless otherwise stated, we utilize the following parametric values (see References [24–26]): $\varepsilon = Ec = 1.0$, $\delta = 0.1$, $\lambda = 1.5$, $fw = 0.5$, $Pr = 6.7$, and $\phi_{s_2} = 0.005$.

To explore the effective thermal characteristic of the hybrid nanofluid, we compare the Nusselt number in both Cu/ethylene glycol nanofluid and Cu- Al_2O_3 /ethylene glycol hybrid nanofluid in Table 3. We observe that the heat transfer coefficient is improved by using a hybrid nanofluid.

Table 4 shows that the skin friction coefficient decreases with an increase in the nanoparticle volume fraction, ϕ_{s_2} , Eyring-Powell fluid parameter, ε , and suction/injection parameter,

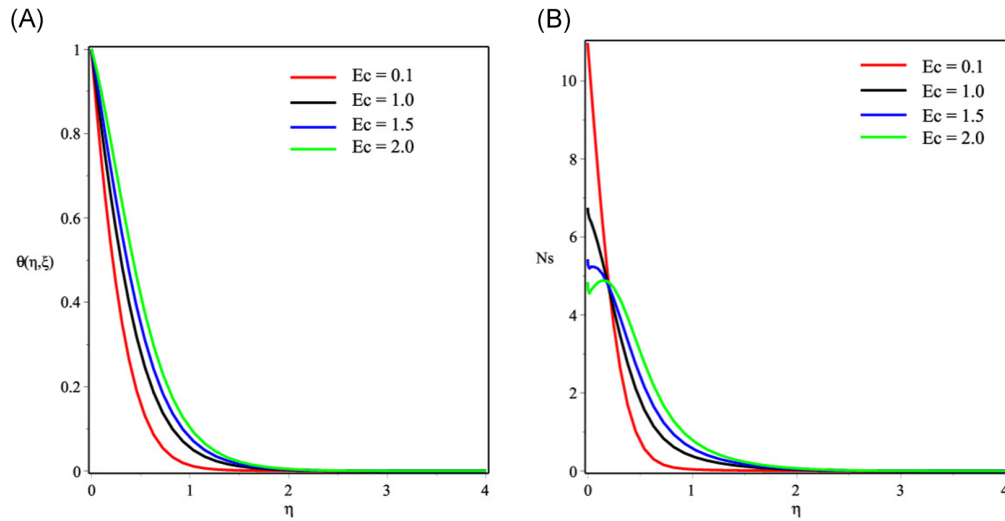


FIGURE 5 Effect of varying the Eckert number (Ec) on the hybrid nanofluid for $\varepsilon = 1.0$, $\delta = 0.1$, $\lambda = 1.5$, $fw = 0.5$, $Pr = 6.7$, and $\phi_{s_2} = 0.005$ on (A) temperature profiles and (B) entropy generation rate [Color figure can be viewed at wileyonlinelibrary.com]

fw . Also, increasing the nanoparticle volume fraction, Eyring-Powell fluid parameter (ε , δ) and Eckert number, Ec , decrease the Nusselt number, see Table 4.

The impacts of varying the nanoparticle volume fraction on the hybrid nanofluid velocity profile, temperature distribution, entropy generation number, and Bejan number profiles are displayed in Figure 2A-D. Increasing the volume fraction of the nanoparticles is observed to reduce the hybrid nanofluid velocity profiles as revealed in Figure 2A, hence, thinning the momentum boundary-layer thickness. A similar result was recorded by Devi and Devi.²⁶ The results in Figure 2B-D show that temperature distribution, entropy generation number profiles, and Bejan number profiles are enhanced with an increase in nanoparticle volume fraction. This is physically correct due to the fact that as the nanoparticle volume fraction increases, the thermal conductivity of the hybrid nanofluid is enhanced, improving the thermal distribution.

The influence of the Eyring-Powell fluid parameter, ε , on the hybrid nanofluid velocity, temperature, entropy generation number, and Bejan number profiles is presented in Figure 3A-D. Clearly, from the definition of ε , ε has an inverse relation with the fluid viscosity. Increasing ε implies decreasing the fluid viscosity. Interestingly, the hybrid nanofluid velocity profile and the momentum boundary-layer thickness increase with ε , when $\lambda > 1$ see Figure 3, and the reverse trend is observed when $\lambda < 1$. $\lambda > 1$ indicating that the stretching velocity dominates the free stream velocity. Results in Figure 3B and 3C show that the thermal boundary-layer thickness and the entropy generation number profiles also increase with ε . An increase in ε decreases the Bejan number profiles as seen in Figure 3D.

Figure 4A-C shows the effects of distinct values of the suction/injection parameter fw on the hybrid nanofluid velocity, temperature, and Bejan number profiles. Obviously, from Figure 4A, the velocity field decreases with an increase in the suction parameter ($fw > 0$) which indicates that the thickness of the momentum boundary decreases with an increase in the suction parameter. However, the opposite results were observed for injection parameter ($fw < 0$). An increase in fw decreases the temperature and Bejan number profiles as displayed in Figure 4B

and 4C. This result is physically correct for with suction the hot hybrid nanofluid is drawn closer to the surface, hence reducing the thermal boundary-layer thickness.

Finally, Figure 5A and 5B illustrates the effect of the Eckert number, Ec , on the hybrid nanofluid temperature and entropy generation number. It is observed from Figure 5A and 5B that in the temperature and entropy generation, profiles are enhanced significantly with Eckert number. Physically, increased Ec leads to heat generation in the system due to dissipation, hence increasing the temperature. The findings suggest that entropy generation can be minimized by reducing the Eckert number.

8 | CONCLUSION

We have analyzed the entropy generation in a transient Eyring-Powell hybrid nanofluid flow over a permeable surface. Similarity solutions of the model equations were obtained using the Lie group symmetry method. The computational simulations were carried out using the BSQLM. The findings of this research study include:

1. The entropy generation can be minimized using a hybrid nanofluid.
2. The irreversibility in the system can be optimized by decreasing the Eckert number.
3. Increasing the Eyring-Powell parameter ε leads to a decrease in the fluid viscosity.
4. The effects of suction to injection on the velocity profiles are in opposition.

ORCID

Hammed Abiodun Ogunseye  <http://orcid.org/0000-0003-3993-1585>

Yusuf Olatunji Tijani  <http://orcid.org/0000-0002-9127-7173>

Precious Sibanda  <http://orcid.org/0000-0003-2115-4642>

REFERENCES

1. Choi SUS, Eastman JA. Enhancing thermal conductivity of fluids with nanoparticles. In: *Proceedings of the ASME International Mechanical Engineering Congress and Exposition*. Vol. 66. Washington, DC: USDOE; 1995.
2. Dhinesh KD, Valan AA. A review on preparation, characterization, properties and applications of nanofluids. *Renew Sust Energy Rev*. 2016;60:21-40.
3. Han ZH, Yang B, Kim SH, Zachariah MR. Application of hybrid sphere/carbon nanotube particles in nanofluids. *Nanotechnology*. 2007;18:105701.
4. Botha SS, Ndungu P, Bladergroen BJ. Physicochemical properties of oil-based nanofluids containing hybrid structures of silver nanoparticles supported on silica. *Ind Eng Chem Res*. 2011;50:3071-3077.
5. Xuan Y, Li Q. Heat transfer enhancement of nanofluids. *Int J Heat Fluid Flow*. 2000;21:58-64.
6. Abbasi SM, Nemati A, Rashidi A, Arzani K. The effect of functionalisation method on the stability and the thermal conductivity of nanofluid hybrids of carbon nanotubes/gamma alumina. *Ceram Int*. 2013;39(4):3885-3891.
7. Sarkar J, Ghosh P, Adil A. A review on hybrid nanofluids: recent research, development and applications. *Renew Sust Energy Rev*. 2015;43:164-177.
8. Mahian O, Kianifar A, Kleinstreuer C, et al. A review of entropy generation in nanofluid flow. *Int J Heat Mass Transfer*. 2013;65:514-532.
9. Qing J, Bhatti MM, Abbas MA, Rashidi MM, Ali ME. Entropy generation on MHD Casson nanofluid flow over a porous stretching/shrinking surface. *Entropy*. 2016;18(4):123.
10. Powell RE, Eyring H. Mechanism for relaxation theory of viscosity. *Nature (London)*. 1944;18(154):427-428.
11. Hayat T, Nadeem S. Flow of 3D Eyring-Powell fluid by utilizing Cattaneo-Christov heat flux model and chemical processes over an exponentially stretching surface. *Results Phys*. 2018;8:397-403.

12. Ishaq M, Ali G, Shah Z, Islam S, Muhammad S. Entropy generation on nanofluid thin film flow of Eyring-Powell fluid with thermal radiation and MHD effect on an unsteady porous stretching sheet. *Entropy*. 2018;20(6):412.
13. Ogunseye HA, Sibanda P. A mathematical model for entropy generation in a Powell-Eyring nanofluid flow in a porous channel. *Heliyon*. 2019;5(5):e01662.
14. Das S, Jana RN, Makinde OD. MHD flow of Cu-Al₂O₃/water hybrid nanofluid in porous channel: analysis of entropy generation. *Defect Diffusion Forum*. 2017;377(10):45-61.
15. Afridi MI, Alkanhal TA, Qasim M, Tlili I. Entropy generation in Cu-Al₂O₃-H₂O hybrid nanofluid flow over a curved surface with thermal dissipation. *Entropy*. 2019;21(10):941.
16. Ashraf MB, Hayat T, Alsaedi A. Three-dimensional flow of Eyring-Powell nanofluid by convectively heated exponentially stretching sheet. *Eur Phys J Plus*. 2015;130. <https://doi.org/10.1140/epjp/i2015-15005-9>
17. Kumar B, Srinivas S. Unsteady hydromagnetic flow of Eyring-Powell nanofluid over an inclined permeable stretching sheet with Joule heating and thermal radiation. *J Appl Comput Mech*. 2020;6:259-270.
18. Sato H, Kawai T, Fujita T, Okabe M. Two dimensional peristaltic flow in curved channels. *Trans Jpn Soc Mech Eng B*. 2000;66:679-685.
19. Tanveer A, Hayat T, Alsaadi F, Alsaedi A. Mixed convection peristaltic flow of Eyring-Powell nanofluid in a curved channel with compliant walls. *Comput Biol Med*. 2017;82:71-79.
20. Ur Rehman K, Khan AA, Malik MY. Magneto-nanofluid numerical modelling of chemically reactive Eyring-Powell fluid flow towards both flat and cylindrical an inclined surfaces: a comparative study. *AIP Adv*. 2017;7(6):065103.
21. Malik MY, Hussain A, Sallahuddin T. Mixed convection flow of MHD Eyring-Powell nanofluid over a stretching sheet: a numerical study. *AIP Adv*. 2015;5(11):117.
22. Agbaje TM, Mondal S, Motsa SS, Sibanda P. A numerical study of unsteady non-Newtonian Powell-Eyring nanofluid flow over a shrinking sheet with heat generation and thermal radiation. *Alexandria Eng J*. 2017; 56(1):81-91.
23. Ibrahim W, Gadisa G. Finite element method solution of boundary layer flow of Powell-Eyring nanofluid over a non-linear stretching surface. *J Appl Math*. 2019. <https://doi.org/10.1155/2019/3472518>
24. Jalil M, Asghar S, Imran SM. Self similar solutions for the flow and heat transfer of Powell-Eyring fluid over a moving surface in a parallel free stream. *Int J Heat Mass Transfer*. 2013;65:73-79.
25. Waini I, Ishak A, Pop I. Hybrid nanofluid flow and heat transfer over a nonlinear permeable stretching/shrinking surface. *Int J Numer Methods Heat Fluid Flow*. 2019;29:3110-3127.
26. Devi SU, Devi SA. Heat transfer enhancement of Cu-Al₂O₃/water hybrid nanofluid flow over a stretching sheet. *J Niger Math Soc*. 2017;36:419-433.
27. Akgül MB, Pakdemirli M. Lie group analysis of a non-Newtonian fluid flow over a porous surface. *Sci Iran*. 2012;19(6):1534-1540.
28. Pakdemirli M, Yurusoy M. Similarity transformations for partial differential equations. *SIAM Rev*. 1998; 40(1):96-101.
29. Rashidi MM, Bagheri S, Momoniat E, Freidoonimehr N. Entropy analysis of convective MHD flow of third grade non-Newtonian fluid over a stretching sheet. *Ain Shams Eng J*. 2017;8(1):77-85.
30. Goqo SP, Olonijun SD, Mondal H, Sibanda P, Motsa SS. Entropy generation in MHD radiative viscous nanofluid flow over a porous wedge using the bivariate spectral quasi-linearization method. *Case Stud Therm Eng*. 2018;12:774-788.
31. Bellman RE, Kalaba RE. Quasilinearization and nonlinear boundary-value problems. Santa Monica, CA: RAND Corporation, 1965. <https://www.rand.org/pubs/reports/R438.html>
32. Trefethen LN. *Spectral Methods in MATLAB*. Vol. 10. Philadelphia: Siam; 2000.
33. Gholinia M, Gholinia S, Hosseinzadeh Kh, Ganji DD. Investigation on ethylene glycol nano fluid flow over a vertical permeable circular cylinder under effect of magnetic field. *Results Phys*. 2018;9:1525-1533.

How to cite this article: Ogunseye HA, Tijani YO, Sibanda P. Entropy generation in an unsteady Eyring-Powell hybrid nanofluid flow over a permeable surface: A Lie group analysis. *Heat Transfer*. 2020;1–17. <https://doi.org/10.1002/htj.21778>

Chapter 7

Conclusion

In this thesis, we have investigated heat transfer and entropy generation in an Eyring-Powell nanofluid for different flow geometries. The spectral quasilinearization, spectral local linearization, and bivariate spectral quasilinearization methods have been used to obtain numerical solutions of the conversion equations. We have provided an analysis of the impact on the flow of nanofluid parameters and determined the effect of these parameters on the heat transfer rate and skin friction coefficient. We have shown, among other results, that the fluid material and velocity slip parameters enhance the skin friction. In addition, an increase in thermal radiation and the temperature ratio parameter lead to increase in the Nusselt number.

In Chapter 2, we reported on the magnetohydrodynamic Eyring-Powell copper-water nanofluid flowing over a stretching vertical cylinder with mixed convective stagnation-point flow as well as heat generation, nonlinear thermal radiation, velocity and temperature slip effects. The spectral quasilinearization method was the method of solution used to handle the reduced nonlinear differential equations. Our main parameters of interest include the Eyring-Powell fluid parameter, nanoparticle volume fraction, curvature parameter, heat source parameter, thermal radiation and thermal slip parameters. We found, among other results, that the Eyring-Powell fluid parameter reduce the skin friction coefficient. Physically, this can be attributed to the inversely proportional relation between the nanofluid dynamic viscosity and the Eyring-Powell fluid parameter. Thus, the nanofluid become less viscous with increasing values of the Eyring-Powell fluid parameter, thereby reducing the skin friction coefficient. The skin friction coefficient was enhanced by increasing the nanoparticle volume fraction. In addition, the heat generation and thermal radiation parameters

both increase the heat transfer rate, while the thermal slip parameter, nanoparticle volume fraction and heat absorption parameter decrease with increased heat transfer rate.

In Chapter 3, we discussed the impact of non-Fourier heat flux with variable thermal conductivity on the heat and mass transfer of the Eyring-Powell nanofluid squeezing flow. We considered a channel flow geometry and utilized the Buongiorno nanofluid model, which accounted for the effect of Brownian motion and thermophoresis. Parametric analysis of the relevant fluid parameter was carried out using the conversion equations and the spectral local linearization method. Interestingly, the temperature profiles were enhanced with increasing values of the thermophoresis parameters and Brownian motion. Also, the thermal boundary layer thickness have a direct influence with increasing values of the thermal conductivity and relaxation parameters.

The Lie group symmetry analysis was used in Chapter 4, to investigate the boundary layer flow of Eyring-Powell nanofluid flow past a stretching surface. Based on some experimental findings, the nanofluid model was assumed to be influenced by nanoparticle size and temperature. For the partial differential equation modeling the flow and heat transfer problem, the similarity solution was obtained using Lie group symmetry analysis. An increase in the nanoparticle volume fraction, thermal radiation and temperature ratio parameters were seen to enhance the temperature profiles as well as the thermal boundary layer thickness. Furthermore, increasing the thermal radiation and temperature ratio parameters lead to increase in the Nusselt number.

It is important to analyze the entropy generation in other to determine how to minimize energy loss in fluid flow. Regarding this important attribute, in Chapter 5, we numerically analyzed using a vertical channel, the entropy production rate of a Powell-Eyring nanofluid mixed convective flow of a Cu-Al₂O₃ water. We used the efficient spectral local linearization method (SLLM) to handle the transport equations. We also shed light on the entropy generation rate using one of the laws of thermodynamics. The Brinkman number and the nanoparticle volume fraction both have a tremendous contribution to reducing the entropy production rate in the channel. We would like to point out that by reducing the Brinkman number and increasing the nanoparticle volume fraction, the flow in a channel can be optimized.

Finally, in Chapter 6, we analyzed the entropy generation using the Lie group symmetry method to obtain a similarity solutions, for unsteady Eyring-Powell hybrid nanofluid flowing over a possible leaking surface. The numerical simulations were executed using the bivariate spectral quasilinearization method. We observed that the hybrid nanofluid minimized entropy generation and by decreasing the Eckert number, the irreversibility in the system was observed to be optimized.

We believe this research should be of interest to industrial and process engineering specialists, for improving the efficiency and effectiveness of heat transfer in thermal systems. In future studies, a similar investigation will be considered for other non-Newtonian fluid models.

References

- [1] A. Nejat, E. Mirzakhali, A. Aliakbari, M. S. F. Niasar, and K. Vahidkhah, “Non-newtonian power-law fluid flow and heat transfer computation across a pair of confined elliptical cylinders in the line array,” *Journal of Non-Newtonian Fluid Mechanics*, vol. 171-172, pp. 67 – 82, 2012.
- [2] M. A. Mahmoud, “Slip velocity effect on a non-newtonian power-law fluid over a moving permeable surface with heat generation,” *Mathematical and Computer Modelling*, vol. 54, no. 5, pp. 1228 – 1237, 2011.
- [3] S. Mukhopadhyay, P. R. De, K. Bhattacharyya, and G. C. Layek, “Casson fluid flow over an unsteady stretching surface,” *Ain Shams Engineering Journal*, vol. 4, no. 4, pp. 933 – 938, 2013.
- [4] Y. Xiong, C. Bruneau, and D. Yang, “Numerical study on viscoelastic fluid flow past a rigid body,” *Applied Mathematical Modelling*, vol. 42, pp. 188 – 208, 2017.
- [5] R. E. Powell and H. Eyring, “Mechanisms for the relaxation theory of viscosity,” *Nature*, vol. 154, no. 1, pp. 427–428, 1944.
- [6] J. Rahimi, D. Ganji, M. Khaki, and K. Hosseinzadeh, “Solution of the boundary layer flow of an eyring-powell non-newtonian fluid over a linear stretching sheet by collocation method,” *Alexandria Engineering Journal*, vol. 56, no. 4, pp. 621–627, 2017.
- [7] K. Gilstrap, X. Hu, X. Lu, and X. He, “Nanotechnology for energy-based cancer therapies.” *American Journal of Cancer Research.*, vol. 1, no. 4, pp. 508—520, 2011.
- [8] S. K. Das, S. S. Choi, and H. E. Patel, “Heat transfer in nanofluids—a review,” *Heat Transfer Engineering*, vol. 27, no. 10, pp. 3–19, 2006.

- [9] T. Robert, C. Sylvain, T. O, P. Patrick, G. Andrey, L. Wei, R. Gary, P. Ravi, and T. Himanshu, “Small particles, big impacts: A review of the diverse applications of nanofluids,” *Journal of Applied Physics*, vol. 113, no. 1, p. 011301, 2013.
- [10] D. K. Devendiran and V. A. Amirtham, “A review on preparation, characterization, properties and applications of nanofluids,” *Renewable and Sustainable Energy Reviews*, vol. 60, pp. 21 – 40, 2016.
- [11] K. V. Wong and O. De Leon, “Applications of nanofluids: current and future,” *Advances in Mechanical Engineering*, vol. 2, pp. 519–659, 2010.
- [12] J. M. Munyalo and X. Zhang, “Particle size effect on thermophysical properties of nanofluid and nanofluid based phase change materials: A review,” *Journal of Molecular Liquids*, vol. 265, pp. 77 – 87, 2018.
- [13] J. J. Buongiorno, “Convective transport in nanofluids.,” *ASME. Journal of Heat Transfer.*, vol. 128, pp. 240 – 250, 2005.
- [14] R. K. Tiwari and M. K. Das, “Heat transfer augmentation in a two-sided lid-driven differentially heated square cavity utilizing nanofluids,” *International Journal of Heat and Mass Transfer*, vol. 50, no. 9, pp. 2002 –2018, 2007.
- [15] W. Khan and I. Pop, “Boundary-layer flow of a nanofluid past a stretching sheet,” *International Journal of Heat and Mass Transfer*, vol. 53, pp. 2477–2483, 2010.
- [16] N. Bachok, A. Ishak, and I. Pop, “Stagnation-point flow over a stretching/shrinking sheet in a nanofluid,” *Nanoscale Research Letters*, vol. 6, no. 1, p. 623, 2011.
- [17] D. Pal and G. Mandal, “Influence of thermal radiation on mixed convection heat and mass transfer stagnation-point flow in nanofluids over stretching/shrinking sheet in a porous medium with chemical reaction,” *Nuclear Engineering and Design*, vol. 273, pp. 644 – 652, 2014.

- [18] O. Makinde and A. Aziz, "Boundary layer flow of a nanofluid past a stretching sheet with a convective boundary condition," *International Journal of Thermal Sciences*, vol. 50, no. 7, pp. 1326 – 1332, 2011.
- [19] A. Noghrehabadi and A. Behseresht, "Flow and heat transfer affected by variable properties of nanofluids in natural-convection over a vertical cone in porous media," *Computers & Fluids*, vol. 88, pp. 313 – 325, 2013.
- [20] K. Das, N. Acharya, and P. K. Kundu, "Influence of variable fluid properties on nanofluid flow over a wedge with surface slip," *Arabian Journal for Science and Engineering*, vol. 43, no. 1, pp. 2119—2131, 2018.
- [21] H. S. Masoud, A. R. Moghadassi, and D. E. Henneke, "A new dimensionless group model for determining the viscosity of nanofluids," *Journal of Thermal Analysis and Calorimetry*, vol. 100, no. 3, pp. 873–877, 2010.
- [22] S. Hassani, R. Saidur, S. Mekhilef, and A. Hepbasli, "A new correlation for predicting the thermal conductivity of nanofluids; using dimensional analysis," *International Journal of Heat and Mass Transfer*, vol. 90, pp. 121 – 130, 2015.
- [23] R. S. Vajjha and D. K. Das, "Experimental determination of thermal conductivity of three nanofluids and development of new correlations," *International Journal of Heat and Mass Transfer*, vol. 52, no. 21, pp. 4675– 4682, 2009.
- [24] Y. Xuan and Q. Li, "Heat transfer enhancement of nanofluid.," *International Journal of Heat and Fluid Flow*, vol. 21, no. 1, pp. 58 – 64, 2000.
- [25] S. S. Botha, P. Ndungu, and B. J. Bladergroen, "Physicochemical properties of oil-based nanofluids containing hybrid structures of silver nanoparticles supported on silica.," *Industrial & Engineering Chemistry Research*, vol. 50, no. 6, pp. 3071 – 3077, 2011.
- [26] S. M. Abbasi, A. Nemati, A. Rashidi, and K. Arzani, "The effect of functionalisation method on the stability and the thermal conductivity of nanofluid hybrids of carbon nanotubes/gamma alumina.," *Ceramics International*, vol. 39, no. 4, pp. 3885 – 3891, 2013.

- [27] Z. H. Han, B. Yang, S. H. Kim, and M. R. Zachariah, "Application of hybrid sphere/carbon nanotube particles in nanofluids," *Nanotechnology*, vol. 18, no. 10, p. 105701, 2007.
- [28] J. Sarkar, P. Ghosh, and A. Adil, "A review on hybrid nanofluids: Recent research, development and applications," *Renewable and Sustainable Energy Reviews*, no. 43, pp. 164 – 177, 2015.
- [29] H. Yoon and A. Ghajar, "A note on the powell-eyring fluid model," *International Communications in Heat and Mass Transfer*, vol. 14, no. 4, pp. 381 – 390, 1987.
- [30] T. Javed, N. Ali, Z. Abbas, and M. Sajid, "Flow of an eyring-powell non-newtonian fluid over a stretching sheet," *Chemical Engineering Communications*, vol. 200, no. 3, pp. 327–336, 2013.
- [31] T. Hayat, Z. Iqbal, M. Qasim, and S. Obaidat, "Steady flow of an eyring powell fluid over a moving surface with convective boundary conditions," *International Journal of Heat and Mass Transfer*, vol. 55, no. 7, pp. 1817 – 1822, 2012.
- [32] N. S. Akbar, A. Ebaid, and Z. Khan, "Numerical analysis of magnetic field effects on eyring-powell fluid flow towards a stretching sheet," *Journal of Magnetism and Magnetic Materials*, vol. 382, pp. 355 – 358, 2015.
- [33] M. Y. Malik, I. Khan, A. Hussain, and T. Salahuddin, "Mixed convection flow of mhd eyring-powell nanofluid over a stretching sheet: a numerical study," *AIP Advances.*, vol. 5, pp. 117 – 118, 2015.
- [34] I. Khan, M. Khan, M. Y. Malik, T. Salahuddin, and Shafquatullah, "Mixed convection flow of eyring-powell nanofluid over a cone and plate with chemical reactive species," *Results in Physics*, vol. 7, pp. 3716–3722, 2017.
- [35] A. Tanveer, T. Hayat, F. Alsaadi, and A. Alsaedi, "Mixed convection peristaltic flow of eyring-powell nanofluid in a curved channel with compliant walls," *Computers in Biology and Medicine*, vol. 82, pp. 71 – 79, 2017.

- [36] T. Agbaje, S. Mondal, S. Motsa, and P. Sibanda, “A numerical study of unsteady non-newtonian powell-eyring nanofluid flow over a shrinking sheet with heat generation and thermal radiation,” *Alexandria Engineering Journal*, vol. 56, no. 1, pp. 81 – 91, 2017.
- [37] S. Hina, “Mhd peristaltic transport of eyring–powell fluid with heat/mass transfer, wall properties and slip conditions,” *Journal of Magnetism and Magnetic Materials*, vol. 404, pp. 148 – 158, 2016.
- [38] T. Hayat, M. Ijaz Khan, M. Waqas, and A. Alsaedi, “Effectiveness of magnetic nanoparticles in radiative flow of eyring-powell fluid,” *Journal of Molecular Liquids*, vol. 231, pp. 126 – 133, 2017.
- [39] A. Bejan, *Entropy generation minimization*. CRC Press Boca Raton, 1996.
- [40] A. Bejan, *Entropy Generation through Heat and Fluid Flow*. Wiley, New York, 1982.
- [41] M. Pakdemirli and B. Yilbas, “Entropy generation in a pipe due to non-newtonian fluid flow: Constant viscosity case,” *Sadhana*, vol. 31, pp. 21—29, 2006.
- [42] S. Das, A. Banu, R. Jana, and O. Makinde, “Entropy analysis on mhd pseudo-plastic nanofluid flow through a vertical porous channel with convective heating,” *Alexandria Engineering Journal*, vol. 54, no. 3, pp. 325 – 337, 2015.
- [43] S. Jangili, S. O. Adesanya, H. A. Ogunseye, and R. Lebelo, “Couple stress fluid flow with variable properties: A second law analysis,” *Mathematical Methods in the Applied Sciences*, vol. 42, no. 1, pp. 85–98, 2019.
- [44] W. T. Tiew, M. H. Yew, and G. Ningqun, “Entropy generation of viscous dissipative nanofluid flow in thermal non-equilibrium porous media embedded in microchannels,” *International Journal of Heat and Mass Transfer*, vol. 81, pp. 862 – 877, 2015.
- [45] G. Ibáñez, “Entropy generation in mhd porous channel with hydrodynamic slip and convective boundary conditions,” *International Journal of Heat and Mass Transfer*, vol. 80, pp. 274 – 280, 2015.

- [46] A. López, G. Ibáñez, J. Pantoja, J. Moreira, and O. Lastre, “Entropy generation analysis of mhd nanofluid flow in a porous vertical microchannel with nonlinear thermal radiation, slip flow and convective-radiative boundary conditions,” *International Journal of Heat and Mass Transfer*, vol. 107, pp. 982 – 994, 2017.
- [47] O. D. Makinde and A. S. Eegunjobi, “Effects of convective heating on entropy generation rate in a channel with permeable walls,” *Entropy*, vol. 1, pp. 220–233, 2013.
- [48] G. Nagaraju, S. Jangili, J. V. Ramana Murthy, O. A. Bég, and A. Kadir, “Second Law Analysis of Flow in a Circular Pipe With Uniform Suction and Magnetic Field Effects,” *Journal of Heat Transfer*, vol. 141, no. 1, 2018. 012004.
- [49] M. Ishaq, G. Ali, Z. Shah, S. Islam, and S. Muhammad, “Entropy generation on nanofluid thin film flow of eyring–powell fluid with thermal radiation and mhd effect on an unsteady porous stretching sheet,” *Entropy*, vol. 20, no. 6, 2018.
- [50] S. Das, R. N. Jana, and O. D. Makinde, “Mhd flow of cu-al₂o₃/water hybrid nanofluid in porous channel: Analysis of entropy generation,” *Defect and Diffusion Forum*, vol. 377, pp. 42–61, 10 2017.
- [51] M. I. Afridi, a. M. Q. T. A. Alkanhal, and I. Tlili, “Entropy generation in cu-al₂o₃-h₂o hybrid nanofluid flow over a curved surface with thermal dissipation,” *Entropy*, vol. 21, no. 10, 2019.
- [52] P. Olver, *Applications of Lie Groups to Differential Equations, Graduate Texts in Mathematics*. 2nd Edition, Springer-Verlag, Berlin, 1993.
- [53] G. Bluman and S. Kumei, *Symmetries and Differential Equations*. Springer, New York, 1974.
- [54] J. Argyris and M. Haase, “An engineer’s guide to soliton phenomena: Application of the Finite element method,” *Computer Methods in Applied Mechanics and Engineering*, vol. 61, no. 1, pp. 71–122, 1987.

- [55] M. Jalil and S. Asghar., “Flow and heat transfer of powell–eyring fluid over a stretching surface: A Lie group analysis,” *Journal of Fluids Engineering*, vol. 135, no. 12, pp. 121201–121206, 2013.
- [56] A. A. Afify, “Similarity solution in MHD: effects of thermal diffusion and diffusion thermo on free convective heat and mass transfer over a stretching surface considering suction or injection,” *Communications in Nonlinear Science and Numerical Simulation*, vol. 14, no. 5, pp. 2202–2214, 2009.
- [57] T. Cebeci and P. Bradshaw, “Finite-difference solution of boundary-layer equations,” in *Physical and Computational Aspects of Convective Heat Transfer*, pp. 385–428, Springer, 1984.
- [58] A. Asaithambi, “A second-order Finite-difference method for the Falkner–Skan equation,” *Applied Mathematics and Computation*, vol. 156, no. 3, pp. 779–786, 2004.
- [59] S. S. Motsa, P. G. Dlamini, and M. Khumalo, “Spectral relaxation method and spectral quasi-linearization method for solving unsteady boundary layer flow problems,” *Advances in Mathematical Physics*, vol. Article ID 341964, 12 pages, 2014.
- [60] S. Motsa, V. Magagula, and P. Sibanda, “A bivariate Chebyshev spectral collocation quasilinearization method for nonlinear evolution parabolic equations,” *The Scientific World Journal*, vol. 2014, Article ID 581987, 2014.
- [61] I. S. Oyelakin, S. Mondal, and P. Sibanda, “Unsteady casson nanofluid flow over a stretching sheet with thermal radiation, convective and slip boundary conditions,” *Alexandria Engineering Journal*, vol. 55, no. 2, pp. 1025 – 1035, 2016.
- [62] R. E. Bellman and R. E. Kalaba, “Quasilinearization and nonlinear boundary-value problems,” 1965.
- [63] M. Dhlamini, H. Mondal, P. Sibanda, and S. Motsa, “Spectral quasi-linearization methods for powell–eyring mhd flow over a nonlinear stretching surface,” *Journal of Nanofluids*, vol. 7, no. 5, pp. 917–927, 2018.

- [64] C. RamReddy and T. Pradeepa, “Spectral quasi-linearisation method for nonlinear thermal convection flow of a micropolar fluid under convective boundary condition,” *Nonlinear Engineering*, vol. 5, no. 3, 2016.
- [65] C. Canuto, T. A. Zang, M. Y. Hussaini, and A. Quarteroni, *Spectral methods in fluid dynamics*. New York: Springer Verlag, 1988.
- [66] M. Javidi, “Spectral collocation method for the solution of the generalized burger–fisher equation,” *Applied Mathematics and Computation*, vol. 174, no. 1, pp. 345–352, 2006.
- [67] W. Ibrahim, “Spectral quasilinearization method for solution of convective heating condition,” *Engineering Transactions*, vol. 68, no. 1, 2020.
- [68] S. S. Motsa and P. Sibanda, “Spectral method based numerical solutions of partial differential equations. sixth annual workshop on computational applied mathematics and mathematical modelling in fluid flow,” *University of Kwazulu-Natal, Pietermaritzburg, South Africa*, July, 1–7, 2013.
- [69] C. Canuto, M. Y. Hussaini, A. Quarteroni, and T. A. Zang, *Spectral Methods: Evolution to Complex Geometries and Applications to Fluid Dynamics (Scientific Computation)*. Springer-Verlag New York, Inc., 2007.
- [70] C. Canuto, M. Y. Hussaini, A. Quarteroni, and A. Thomas Jr, *Spectral methods in fluid dynamics*. Springer Science & Business Media, 2012.
- [71] S. S. Motsa, “A new spectral local linearization method for nonlinear boundary layer flow problems,” *Journal of Applied Mathematics*, vol. 2013, Article ID 423628, 2013.
- [72] H. Sithole, H. Mondal, and P. Sibanda, “Entropy generation in a second grade magnetohydrodynamic nanofluid flow over a convectively heated stretching sheet with nonlinear thermal radiation and viscous dissipation,” *Results in Physics*, vol. 9, pp. 1077 – 1085, 2018.